Universitat de Girona

FRONT SPREADING IN POPULATION DYNAMIC MODELS.
THEORY AND APPLICATION TO THE NEOLITHIC TRANSITION

Neus ISERN SARDÓ

Dipòsit legal: GI-115-2012
http://hdl.handle.net/1xxxxxx

Universitat de Girona

THESIS

FRONT SPREADING IN POPULATION DYNAMICS MODELS. THEORY AND APPLICATION TO THE NEOLITHIC TRANSITION.

NEUS ISERN SARDÓ

2011

Universitat de Girona

THESIS

FRONT SPREADING IN POPULATION DYNAMICS MODELS. THEORY AND APPLICATION TO THE NEOLITHIC TRANSITION.

NEUS ISERN SARDÓ

2011

PROGRAMA OFICIAL DE POSTGRAU (POP) EN CIÈNCIES EXPERIMENTALS I SOSTENIBILITAT

Supervisor:
JOAQUIM FORT VIADER

Thesis submitted for the degree of Doctor of Philosophy by the University of Girona

This Ph.D. thesis has been prepared as a collection of papers, in agreement with the regulations of the University of Girona. This thesis includes three original papers that have been published in peer-reviewed journals, and a paper that has not been yet published at the moment of preparing this thesis. The four papers have been published in (or submitted to) journals with impact factors within the first quartile, according to the 2009 Journal Citation Reports (JCR), for the subject categories *Physics, Multidisciplinary* and *Physics, Mathematical*.

The complete references of the papers comprised in this thesis and the impact factor of the journals are

Isern N, Fort J, Pérez-Losada, J. Realistic dispersion kernels applied to cohabitation reaction-dispersion equations. J Stat Mech - Theor Exp 2008; 2008: P10012. (Impact Factor 2.67, journal 4 of 47, Quartile 1, category *Physics, Mathematical*)

Isern N, Fort J. Time-delayed reaction-diffusion fronts. Phys Rev E 2009; 80: 057103. (Impact Factor 2.4, journal 5 of 47, Quartile 1, category *Physics, Mathematical*)

Isern N, Fort J. Anisotropic dispersion, space competition and the slowdown of the Neolithic transition. New J Phys 2010; 12: 123002. (Impact Factor 3.312, journal 12 of 71, Quartile 1, category *Physics, Multidisciplinary*)

Isern N, Fort J. Cohabitation effect on the slowdown of the Neolithic expansion. Europhys Lett *Submitted*. (Impact Factor 2.893, journal 14 of 71, Quartile 1, category *Physics, Multidisciplinary*)

Abstract

The transition from the Mesolithic (last hunter-gatherers) culture to the Neolithic (farmers) is one of the most important socioeconomic changes in human history. It took place in Europe from about 9000 to 5000 years ago. This thesis presents population dynamics models that can be applied to predict the rate of spread of the Neolithic transition across the European continent from the Near East.

The first models in this thesis provide results that can be compared to the average rate of expansion of the Neolithic transition in Europe at a continental scale. In chapter 3, we develop population dynamics models with explicit dispersion probability distributions as a function of distance (kernels). We derive expression for the front speed when using discrete approximations to real population dispersive patterns (obtaining reasonable results) as well as for the Gauss and the Laplace distributions (obtaining that they sometimes overestimate the speed).

In chapter 4, we derive a new time-delayed reaction-diffusion equation, now taking proper care of the reproduction process as opposed to previous derivations. This new result yields speeds about a 10% slower than previous models when applied to the Neolithic transition, but still consistent with the average estimations for the expansion of the Neolithic in Europe.

Chapters 5 and 6 deal with a regional variability: the slowdown of the Neolithic front when reaching the North of Europe. This slowdown is measured by the analysis of an interpolation map of early Neolithic dates. We develop simple reaction-diffusion models that can predict the measured speeds in terms of the non-homogeneous distribution of pre-Neolithic (Mesolithic) population in Europe, which were present in higher densities at the North of the continent. Such models can explain the observed speeds.

In this thesis we apply both cohabitation and non-cohabitation models, obtaining speeds up to 38% faster for cohabitation models. Cohabitation models are more realistic for human populations (they model the cohabitation between parents and children until adulthood of the later). The regional study in this thesis provides an example in which cohabitation models clearly perform better than non-cohabitation models (chapter 6).

Resum

La transició del mesolític (darrers caçadors-recol·lectors) al neolític (agricultors) és un dels canvis socioeconòmics més importants en la història de la humanitat. Aquest canvi va tenir lloc a Europa fa entre 9000 i 5000 anys. Aquesta tesi presenta models de dinàmica de poblacions que es poden aplicar a la transició del neolític per tal de predir-ne la velocitat d'expansió des de l'orient proper i a través de tot el continent europeu.

Els primers models inclosos en aquesta tesi proporcionen prediccions de la velocitat mitjana d'expansió del neolític a Europa a escala continental. Al capítol 3, desenvolupem models de dinàmica poblacional incloent expressions explícites de la distribució de la probabilitat de dipersió en funció de la distància (*kernel*). Derivem expressions per a la velocitat del front usant aproximacions discretes als patrons de dispersió de poblacions humanes reals (pels que obtenim resultats raonables) així com les distribucions de Gauss i Laplace (pels que obtenim en alguns casos velocitats poc realistes i massa ràpides).

Al capítol 4 desmotrem una nova equació de reacció-difusió amb retard temporal tractant, en aquest cas, el terme de reacció de manera adequada, a diferència que en demostracions anteriors. Amb aquest nou resultat s'obtenen velocitats entorn d'un 10% més lentes que en models previs de retard temporal, tot i que són encara coherents amb el rang mitjà estimat per l'expansió del neolític a Europa.

Els capítols 5 i 6 fan referència a una variabilitat regional: la disminució del ritme d'expansió del front neolític al nord d'Europa. La mesura d'aquest alentiment es realitza per mitjà de l'anàlisis d'un mapa d'interpolació de dates d'arribada del neolític inicial. Desenvolupem models de reacció-difusió senzills que tenen en compte la distribució no homogènia de poblacions preneolítiques (mesolítiques) a Europa, les quals eren presents amb majors densitats al nord del continent. Aquests models poden predir les velocitats mesurades.

En aquesta tesi apliquem models tant de cohabitació com de no cohabitació, i obtenim que els models de cohabitació prediuen velocitats fins a un 38% més ràpides. Els models de cohabitació són més realistes per poblacions humanes (modelitzen la cohabitació entre pares i fills fins que els darrers arriben a l'edat adulta). L'estudi regional portat a terme en aquesta tesi presenta un cas en què els models de cohabitació clarament dónen resultats millors (capítol 6).

Acknowledgements

Contents

List of Figures

List of Tables

Chapter 1

Introduction

The Neolithic transition, the change from hunter-gathering economics to farming, is a crucial process in human history that has been subject of numerous studies, not only from archaeological or anthropological perspectives, but also by means of mathematical and computational models.

This Ph.D. thesis comprises four papers on modeling applied to the spread of the Neolithic transition in Europe. These publications aim to be a contribution to better understand the Neolithisation process of the European continent by analyzing the importance and effect on the spreading front of applying realistic dispersion kernels (chapter 3), using cohabitation models (chapters 3 and 6) or assuming anisotropic distributions of pre-Neolithic populations (chapters 5 and 6), as well as by improving the derivation of a time-delayed model for the Neolithic expansion (chapter 4).

The following sections in this introduction give a brief overview on the Neolithic transition and some previous population dynamics models, as well as a summary of the studies included in this thesis.

1.1 The Neolithic transition in Europe

The transition from hunter-gathering economics (Mesolithic) to farming economics (Neolithic) is known as the Neolithic transition. This transition is one of the most important changes in human history because it meant not only the beginning of animal and plant domestication, but also a global socioeconomic change from the foraging subsistence led by human beings for several million years. The new farming technologies provided reliable food resources which allowed human populations to grow in number.[1] Hence, settlements became larger, with the appearance of the first cities, and more complex social structures and belief systems also appeared [1].

The appearance of agricultural economics took place at least in seven independent regions of the world between 10000 and 4500 years ago and spread across most of the planet [1]. About 10000 years ago, the first agricultural economies appeared at the Near

---

[1]The carrying capacity, maximum number of individuals that the environment can sustain, increased with farming societies due to the increase in reliable food resources and storage capability.
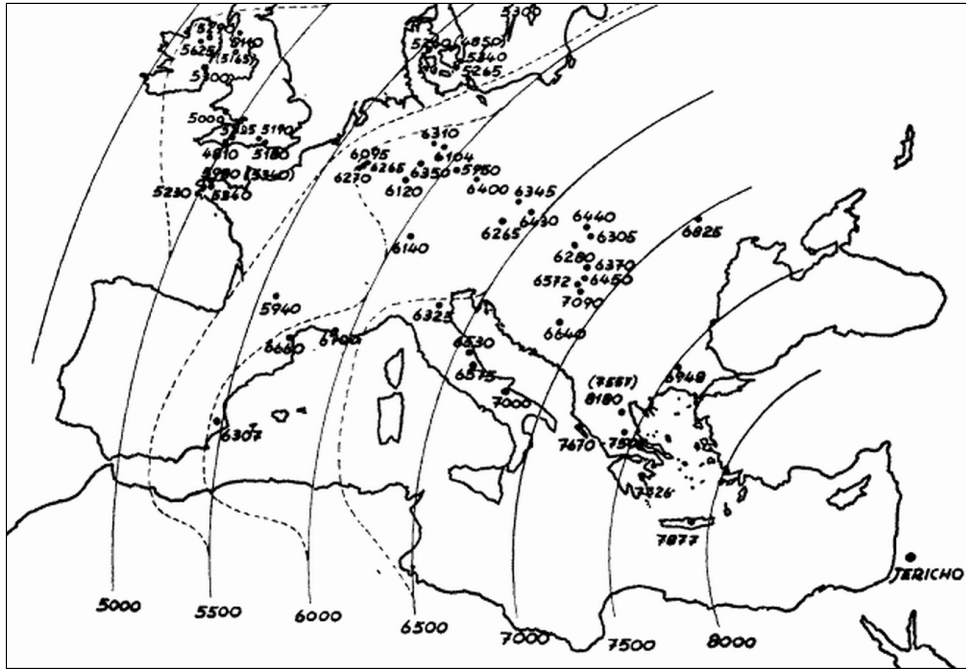
Figure 1.1: Map of radiocarbon dates analyzed by Ammerman and Cavalli-Sforza [6]. The arcs show the expected positions for a constant rate expansion from Jericho. Dates are in years Before Present (BP).[2]

East, at the Fertile Crescent, and spread gradually all over the European continent.

The idea that the Neolithic transition penetrated Europe from the Near East was first introduced by Childe in 1925 [2, 3], who proposed a demic expansion due to demographic pressure, with farmers from the Near East migrating and colonizing Europe. This idea was consistent with the first attempt to analyze spatiotemporal patterns of Neolithic radiocarbon dates realized by Clark in 1965 [4, 5]. Clark classified the available radiocarbon dates from Europe and the Near East in three time intervals and represented them on a map. The obtained map gave a rough picture of the trend that verified the hypotheses of a Neolithic expansion from the Near East.

In 1971, Ammerman and Cavalli-Sforza [6] led the first quantitative analysis of the spread of farming in Europe. Using the available radiocarbon dates from 53 settlements, they fitted a linear regression curve to dates and distances (great-circle distances) for five possible origins. All sources gave a relatively high correlation coefficient ($R > 0.8$) with the highest value obtained for Jericho, which was chosen as the most probable source. This analysis suggested a rate of spread of the Neolithic in Europe of about 1km/yr on average ($c = 1.0 \pm 0.2$km/yr [3] [7]) with minor variations in some parts of

---

[2]The time scale years BP, or Before Present, is a time scale used in archaeology that uses year 1950 as origin.

[3]The observed speed range is calculated from the archaeological data by performing two linear regressions: one of distances versus dates and one of dates versus distances [7], and combining both slopes and their errors.

2

the continent. Figure 1.1 shows the map of radiocarbon dates analyzed by Ammerman and Cavalli-Sforza and the expected positions of the front with Jericho as source of the expanding wave.

More recently, in 2003, Gkiasta et al. [8] performed a similar analysis, now using 510 radiocarbon dates, and obtaining a rate of spread of 1.3km/yr. However, this analysis assumed Jericho as origin of the spread, instead of searching for the most probable source (i.e., that with the highest correlation coefficient) and did not compute an error range.

In 2005 Pinhasi et al. [9] did perform a more complete analysis with a database of 735 early Neolithic sites from Europe and the Near East. They used 35 possible origins (10 real sites and 25 hypothetical locations) and fitted linear regression curves to age and distance, with distances calculated both as great-circle and shortest-path distances. This analysis yielded a highly probable source region (centers with $R > 0.8$) and a range for the spreading speed of the Neolithic in Europe of $0.6 - 1.3$km/yr (95% confidence level)[4]. Thus, these results are consistent with the initial analysis undertaken by Ammerman and Cavalli-Sforza [6] and imply that a constant spread rate is a good approximation at the continental scale.

1.2 Previous population dynamics models for the Neolithic spread

Since the first mathematical model proposed by Ammerman and Cavalli-Sforza in 1973 [10] to describe the expansion of the Neolithic transition in Europe, the modeling of this process has been tackled in numerous studies. Previous population dynamics models applied to the Neolithic expansion include time-delayed models [7, 11], dispersion along waterways [12], cohabitation and non-cohabitation models [13, 14], settlement formation [15] and models for interacting populations [14, 16]. The following points present some previous population dynamics models that are directly related to the models included in this Ph.D. thesis.

1.2.1 Fisher's model

The first attempt to model the Neolithic transition mathematically was undertaken by Ammerman and Cavalli-Sforza [10, 17]. Their observations of a steady rate of spread [6] were consistent with a population wave of advance generated when a population with local migratory activity undergoes an increase in population number. On this account, they applied to the Neolithic transition the wave of advance model initially proposed by Fisher [18] to predict the spread of advantageous genes, and later applied by Skellam [19] to population spread (biological invasions). Similar models have been applied to the propagation of combustion flames [20].

---

[4]See footnote 3.

Fisher's model assumes a logistic population growth and a random migratory process. The logistic growth model describes a growth process that is exponential, with an initial growth rate a, for low values of the population density $p(x, y, t)$, and that is self-limiting for large densities, with a maximum possible density $p_{\max}$. Then, the rate of change of the population size when undergoing a logistic growth is [21]

$$\left.\frac{\partial p}{\partial t}\right|_{growth} = ap\left(1 - \frac{p}{p_{\max}}\right). \tag{1.1}$$

On the other hand, the migratory process can be described in terms of the mobility, or mean squared displacement per unit time, $m = \langle \Delta^2 \rangle / T$, where Δ is the displacement of an individual during a time interval T (usually, a generation) and the symbols $\langle ... \rangle$ denote average. Then, if the migration takes place in a $2-$dimensional space, the diffusion coefficient is $D = \langle \Delta^2 \rangle / 4T$.[5]

According to Fisher, these two assumptions (logistic growth and local migratory diffusion) yield the following reaction-diffusion equation for the population density $p(x, y, t)$,

$$\frac{\partial p}{\partial t} = D\left(\frac{\partial^2 p}{\partial x^2} + \frac{\partial^2 p}{\partial y^2}\right) + ap\left(1 - \frac{p}{p_{\max}}\right), \tag{1.2}$$

with the first term on the right describing the diffusive process and the last term being the logistic growth equation. Front solutions to Fisher's equation (1.2) describe population invasions expanding at a steady rate given by (see section 2.3.1)

$$c_{Fisher} = 2\sqrt{aD}. \tag{1.3}$$

In their study, Ammerman and Cavalli-Sforza [17] estimated the values of a and D from anthropological data.

1.2.2 A time-delayed model

Fisher's model considers a continuous migration in time (in the sense that there is no delay between the end of an individual's migration and the beginning of the migration of their children). However, in sedentary farming societies children usually stay with their parents at the place of birth until they reach adulthood and can migrate to create their own family. Thus, there is a time delay between birth and migration that Fisher's equation does not consider.

Fort and Méndez [7] studied the effect of a time delay on reaction-diffusion systems (that would otherwise led to Fisher's model) by incorporating second-order terms. In this way, in reference [7] it was argued that then, equation (1.2) is generalized into

$$\frac{\partial p}{\partial t} + \frac{T}{2}\frac{\partial^2 p}{\partial t^2} = D\left(\frac{\partial^2 p}{\partial x^2} + \frac{\partial^2 p}{\partial y^2}\right) + F + \frac{T}{2}\frac{\partial F}{\partial t}, \tag{1.4}$$

---

[5]In fact, Ammerman and Cavalli-Sforza [17] approximated the diffusion coefficient D to the mobility m, instead of the more correct expression for a $2-$dimensional dispersion $D = m/4$.

where F is the time derivative of $p(x, y, t)$ due to reproduction, which can be described by the logistic growth equation (1.1). This time-delayed reaction-diffusion equation yields a front speed that is significantly slower than Fisher's wave of advance, as expected because of the effect of the time delay,

$$c_{HRD} = \frac{2\sqrt{aD}}{1 + a\frac{T}{2}}. \tag{1.5}$$

T is the time delay between two migrations (here referred to as the generation time, see also section 2.1.3) and the subindex HRD stands for hyperbolic reaction-diffusion, which is the mathematical type to which the differential equation (1.4) belongs. In reference [7], the diffusion coefficient D was already estimated as $D = \langle \Delta^2 \rangle / 4T$ (see footnote 5), which corresponds to a diffusion in a 2-dimensional space. Note that equation (1.5) becomes Fisher's speed (1.3) when the time delay is negligible, that is, for $T \ll 1/a$.

1.2.3 Cohabitation and non-cohabitation models

Both Fisher's and the generalized time-delayed model can be obtained by assuming that the population density $p(x, y, t)$ follows an evolution equation such as [7]

$$p(x, y, t+T) - p(x, y, t) = \iint p(x - \Delta_x, y - \Delta_y, t)\, \phi(x, y; \Delta, \theta)\, \mathrm{d}\Delta_x \mathrm{d}\Delta_y - p(x, y, t)$$
$$+ R\left[p(x, y, t)\right], \tag{1.6}$$

which gives the variation in population density during a generation time T (left-hand side) in terms of the population dispersal (first two terms on the right-hand side) and population growth (last term). The integral term on the right-hand side of equation (1.6) gives the final population density after the dispersion process, and the dispersion kernel $\phi(x, y; \Delta, \theta)$ gives the probability that an individual initially at position $(x - \Delta_x, y - \Delta_y)$ moves to (x, y) after a generation time T, with $\Delta = \sqrt{\Delta_x^2 + \Delta_y^2}$ and $\theta = \tan^{-1}(\Delta_y/\Delta_x)$. Note that when $\Delta = 0$ (or $\Delta_x = \Delta_y = 0$) the kernel $\phi(x, y; \Delta, \theta)$ gives the persistency (p_0) or probability of staying at the initial place. The last term in equation (1.6) is the reproduction function $R\left[p(x, y, t)\right]$ which gives the increase in population density due to population growth (births minus deaths).[6] For isotropic kernels, Fisher's equation (1.2) is obtained by Taylor expanding equation (1.6) up to first-order in time and second-order in space, whereas the HRD equation (1.4) was obtained by including also second order terms in time [7].

Recently it has been argued that the evolution equation (1.6) may not be the most realistic way to represent human behavior, as it implies that newborn children stay at their birthplace (last term) whereas parents migrate away from them (first term on

---

[6]The definition of the reproduction function $R\left[p(x, y, t)\right]$ here and in chapter 6 is not exactly the same as the function $R_T[p]$ in chapter 3. $R[p]$ represents the net increase in population density, while in chapter 3, $R_T[p]$ gives the final population number after the growth process (initial population plus increase). Therefore, $R[p] = R_T[p] - p$.

the right). Thus, an equation modeling the cohabitation between parents and children, until adulthood of the latter, would be a more realistic framework. Such a cohabitation equation can be written as [13]

$$p\left(x, y, t+T\right) - p\left(x, y, t\right) = \iint p\left(x - \Delta_x, y - \Delta_y, t\right) \phi\left(x, y; \Delta, \theta\right) \mathrm{d}\Delta_x \mathrm{d}\Delta_y - p\left(x, y, t\right)$$

$$+ R\left[\iint p\left(x - \Delta_x, y - \Delta_y, t\right) \phi\left(x, y; \Delta, \theta\right) \mathrm{d}\Delta_x \mathrm{d}\Delta_y\right]. \quad (1.7)$$

Cohabitation models lead to faster speeds, with substantial corrections to non-cohabitation models [13], because in a cohabitation model the whole population (parents and children) can disperse whereas in a non-cohabitation model only the parent population does migrate. Further discussion and comparison between cohabitation and non-cohabitation models when applied to the Neolithic is shown in the papers presented in chapters 3 and 6, as well as in the general discussion in chapter 7.

1.3 Population dynamics models in this thesis

1.3.1 Realistic dispersion kernels

Most models on the Neolithic spread, such as Fisher's and the HRD models described before, include the dispersion of populations simply as a parameter, namely, the diffusion coefficient D. Chapter 3 presents a study of the effect on the front speed of using complex dispersion kernels based on observational data and mathematical functions. Chapter 3 aims to check the compatibility of the results from using realistic data with the observed front speed, as well as to assess the validity of using the diffusion coefficient D as an approximation to the dispersion process.

In chapter 3, front speeds are computed using dispersive data from six human populations. The kernels studied are (i) a simple model with dispersion to a single distance, (ii) a continuous approximation using Gauss and Laplace distributions, and (iii) a discrete approximation to the recorded data using a sum of Dirac deltas. Moreover, all of the kernels are applied in both cohabitation and non-cohabitation models. Thus, this analysis yields a wide range of values for the front speed, but it is interesting that most of the results lie within the observed range of speeds for the Neolithic transition, or are at least marginally consistent with the observed speeds.

Chapter 3 also includes comparison between analytic results and numerical simulations. Analytic results are calculated from integrodifference equations, such as (1.6) and (1.7), by applying continuous-space and discrete-space random walks [see sections 2.2.1 and 2.2.2], and verified with reactive random walk simulations [see section 2.2.3] (with both deterministic and stochastic dispersal processes).

1.3.2 New time-delayed equation

When carefully Taylor expanding up to second order in time and space the non-cohabitation model in chapter 3, the differential equation obtained does not yield the

time-delayed result (1.5) but a new time-delayed speed. Chapter 4 introduces and compares this new time-delayed equation with the HRD equation.

The reaction-diffusion equation derived in chapter 4 is rather similar to the HRD equation (1.4), but the difference lies in how the reactive terms are treated. The model derived in chapter 4 takes care of the fact that, if F is the time derivative due to reproduction, then the second order term [last term in equation (1.4)] must also relate only to the reproduction process. So, taking proper care of the effect of the time delay T in the population growth process, the speed of the spreading front is (see chapter 4)

$$c_{time\text{-}delayed} = \frac{2\sqrt{aD\left(1 + aT/2\right)}}{1 + aT}.$$ (1.8)

When applied to the Neolithic transition, this new time-delayed speed yields slower speeds than the HRD equation when using realistic parameters for the Neolithic transition (see chapter 4).

1.3.3 Models for the slowdown of the Neolithic expansion

All of the models introduced up to this point study the Neolithic spread as an homogeneous process taking place in an isotropic space. Even though from a global point of view this is consistent with observations, as noted in the previous sections, there are also some regional variabilities worth studying. Chapters 5 and 6 tackle the observed slowdown of the Neolithic spreading front as higher latitudes were reached. Chapter 5 focuses on how the non-homogeneous distribution of Mesolithic populations (with higher densities at northern regions) can explain the observed decrease in the rate of spread. Chapter 6 applies the modified growth function and anisotropic dispersion kernel derived in chapter 5 to cohabitation models, obtaining a better agreement with observations.

The main premise in these models is that the presence of another population (Mesolithic population) using the same space and resources will reduce the available space for the Neolithic invaders, and thus, there will be an effect on the spreading front. On the one hand, the dispersion kernel is constructed so that the Neolithic populations have a higher probability to move to the directions where the presence of Mesolithic individuals is lower (more free space). On the other hand, the reduction of available space due to the Mesolithic populations must also be included in the population growth equation, because the logistic equation (1.1) is only a single-population model.[7]

These modifications on the reaction and diffusion processes lead to fronts that slow down at regions where the density of Mesolithic populations increases, in accordance with observations (chapter 5). Furthermore, when improving the initial model by introducing the cohabitation effect (chapter 6), the results can also explain the absolute values of the measured Neolithic front speeds.

---

[7]Single-population models do not consider the effect of the interaction with other populations.

Chapter 2

Materials and methods

In order to make this Ph.D. thesis as much self-contained as possible, this chapter contains a discussion on some empirical data for which a detailed explanation does not appear in the papers included in the next chapters. This chapter also contains details on the analytical and numerical methods applied in the following chapters to calculate the front speeds for each model. The population dynamics models contained in this Ph.D. thesis are described by two kind of equations: integrodifference equations and differential equations. As these two kinds of equations require quite different techniques to calculate the front speed, the analytical and numerical methods are also classified according to which kind of equation they are appropriate to solve.

2.1 Empirical data

2.1.1 Initial growth rate a

For a population following a logistic growth, the initial growth rate a indicates the rate of growth when the population number is low, i.e., when the increase in population is approximately exponential (see equation (1.1) and figure 2.1). This parameter can be estimated from data on the evolution of the population number for human populations established in a previously unpopulated space. Birdsell [22] reported this kind of data for two populations: (i) the colony settled in the Pitcairn Island (about 4000 miles west of Chile), which remained essentially closed during the period $1790-1856$, (ii) and the isolated populations inhabiting the islands of the Furneaux group in the Bass Strait (between Australia and Tasmania) during the period $1820-1945$. Birdsell noted that when plotting these data against the elapsed time (in terms of τ intervals for each population, with τ the mean age of parents at the birth of their *first* child) the results fitted almost the same exponential curve, with the population number doubling approximately every time interval τ. Fitting the data for the Pitcairn Island to an exponential curve, with age at the birth of the first child $\tau = 20$ yr [22], yields $a = (0.037\,44 \pm 0.001\,49)$ yr^{-1}. On the other hand, using $\tau = 25$ yr [22] for the Bass Strait
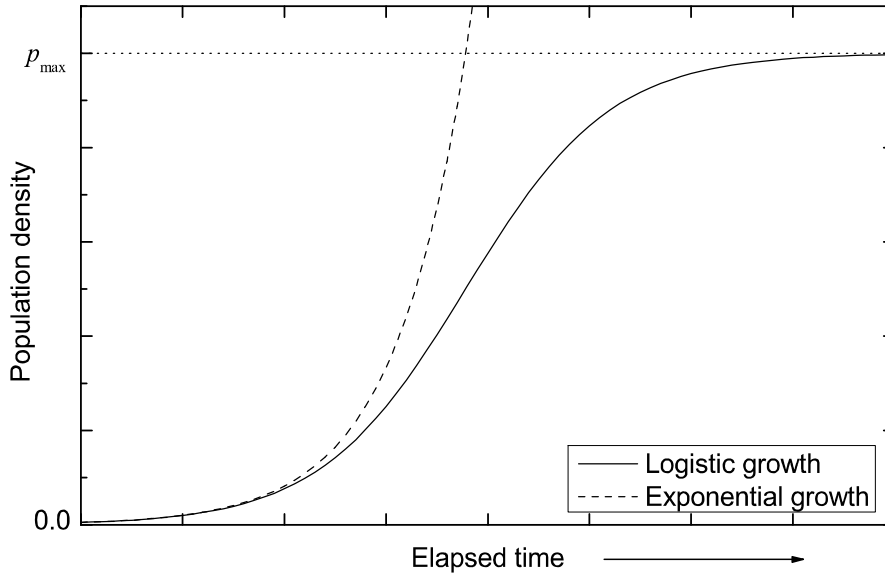
Figure 2.1: Comparison between logistic and exponential growth curves with the same initial growth rate a. At low values of population density both models behave in a similar way.

islands we obtain $a = (0.026\,26 \pm 0.000\,52)$ yr^{-1}.[1]

The initial growth rate can also be estimated from the Tristan da Cunha islands (in the middle of the South Atlantic Ocean). There are records on the population number for these islands from the first colonization in 1817 reported by Roberts [23], however, they experienced two main episodes of emigration, thus not the whole range of the data is usable. Fitting the values for the period 1892–1946 to an exponential curve with $\tau = 24.5$ yr [22] leads to $a = (0.025\,79 \pm 0.000\,33)$ yr^{-1} (see footnote 1). Although immigration from Europe took place, from 1885 the island became nearly isolated [22], and this value of a similar to the ones quoted above seems to indicate that the effect of immigration may have been indeed negligible.

The evolution of the population number of the United States during the period 1790–1910 analyzed by Lotka [24] is another useful source. Lotka fitted these data to a logistic growth, which yields an initial growth rate $a = (0.031\,35 \pm 0.000\,63)$ yr^{-1} (see footnote 1), for an average age at the first child's birth of $\tau = 25$ yr [7, 17]. The increase in population in the United States also includes immigration together with internal growth, but again the obtained range is consistent with those calculated above, so in this case immigration does not lead to a substantially higher value of a (two possible reason for this are that the effect of immigration was not strong enough, or that the mortality rate was higher than in the other three example above).

Even though these four populations yield similar values of the initial growth rate a, a better way to compare and analyze them is in terms of the age at the birth of the first

---

[1]We have performed all fits to obtain paramer a in this chapter without fixing the inital value of the population number, as this first datum is not more reliable than the rest of the set.

9

child τ as in the analysis led by Birdsell, because in this way the curves almost overlap [22]. When expressed in terms of τ, the initial growth rates calculated above become $a = (0.749 \pm 0.030)$ gen^{-1} for Pitcairn, $a = (0.657 \pm 0.013)$ gen^{-1} for the Bass Strait, $a = (0.631 \pm 0.008)$ gen^{-1} for Tristan da Cunha and $a = (0.784 \pm 0.016)$ gen^{-1} for the United States. Then, the 80% confidence level range is $a = (0.705 \pm 0.122)$ gen^{-1}. Assuming for the mean age at the birth of the first child the characteristic value $\tau = 25$ yr [7, 17], this yields $a = (0.028 \pm 0.005)$ yr^{-1} which is the range applied in the following chapters.[2,3]

2.1.2 Mobility m

The mobility of a population is the mean squared displacement per generation, $m = \langle \Delta^2 \rangle / T$, where the displacement Δ corresponds to the distance between a person's birthplace and his/her children's birthplace, T is the time difference between the migration of parents and their children (averaged over all children) and $\langle ... \rangle$ denotes average. Data on mobility patterns for primitive farming cultures are scarce, but using data for present farming or hunter-gathering populations may lead to rather different results [25]. The only data on mobility of primitive farmers known to us corresponds to the Majangir people, a population of shifting agriculturalist in Ethiopia, collected by Stauder [26]. Ammerman and Cavalli-Sforza obtained the mean squared displacement per generation for three groups (Gilishi 10-19 year-old age group, Gilishi 20-29 and Shiri 10-19) with values $m_1 = 1115.7$ km^2/gen, $m_2 = 1325.6$ km^2/gen and $m_3 = 2153.0$ km^2/gen [17].[4] They selected these groups because according to Stauder [26] their mobility corresponds to one generation, as older age groups were chased away from their earlier territory by raids of foreign tribes. Thus, the mean mobility that will be applied in this thesis is $m = 1531$ km^2/gen ($933 - 2129$ km^2/gen at 80% confidence level).

An approximation to the mobility is sometimes obtained from mating distances (distance between birthplaces of the two parents). This is the case for the data for Issocongos (preindustrial agriculturalists, $m = 404$ km^2/gen) [27][5], Yanomamo [28] (preindustrial horticulturists, $m = 1728$ km^2/gen) and modern Parma Valley [27][6] populations ($m = 508$ km^2/gen) used in chapter 3 together with the three Majangir populations mentioned above (see footnote 4). Even though the values of mobility obtained from mating distances will differ from the real mobility value, this kind of

---

[2]In reference [7] the range $a = (0.032 \pm 0.003)$ yr^{-1} was obtained in a similar way using only data from Pitcairn and Bass Strait Islands, and fixing the initial value when fitting, as opposed to the procedure here (see footnote 1).

[3]The initial growth rates for the four populations that appear in chapter 3 can be obtained from the results in gen^{-1} units calculated here by dividing them by 25 yr, i.e., they are normalized to a standard value $\tau = 25$ yr.

[4]Note that these mobilities are slightly different than those in table 3.1 for the same populations ($m_1 = 1003$ km^2/yr, $m_2 = 1210$ km^2/yr and $m_3 = 2197$ km^2/yr). In chapter 3, instead of using directly the mobilities in reference [17] (p. 155), they are calculated using the dispersal data in reference [26]. In this way, the mobility values are consistent with the discrete kernel (3.25).

[5]Mating distances for Issocongos is obtained from figure 8.16.B in this reference.

[6]Mating distances for modern Parma Valley populations is calculated from data on table 8.7 in this reference.

data is useful in chapter 3 when studying the sensitivity of the front speed on the dispersion kernel.

2.1.3 Time between migrations T (generation time)

The time interval between two successive migrations can be (as a first approximation) assumed to be a generation time, defined as the mean age difference between parents and one of their children, not necessarily the eldest (this later quantity corresponds to τ in section 2.1.1). The value of the generation time T has been calculated in reference [11] using data for preindustrial agriculturalists, the Majangir people in Ethiopia, collected by Stauder [26]. Table 5 (in page 58) in Stauder's book [26] gives the age distribution of unmarried people, which allows to estimate the age at which people leave their parents. According to these data, the number of people leaving a domestic group are $N_1 = 44$, $N_2 = 49$, $N_3 = 2$ and $N_4 = 1$, at mean ages $a_1 = 19$ yr, $a_2 = 27.5$ yr, $a_3 = 37.5$ yr and $a_4 = 47.5$ yr.[7] These values lead to a mean age when leaving a domestic group $\langle a \rangle \simeq 24$ yr [11].[8]

Then, since the mean number of children per family for preindustrial agriculturalists is about 6.5 [29] and the average birth interval is about 2.5 yr [17, p. 66], the mean time interval between migration and the birth of a child is about 8 yr. Hence, the value of generation time to be used in the models is $T = 32$ yr ($29\text{--}35$ yr at 80% confidence level [9]).

2.1.4 Early Neolithic dates and measurement of the local speed

Chapters 5 and 6 study the slowdown of the Neolithic spreading front when Northern regions were reached. The variation of the speed value with distance is obtained from the analysis of an interpolation map for early Neolithic dates.

The data on early Neolithic sites used is obtained from the database published by Pinhasi et al. [9] in 2005 (see a sample in table 2.1), which contains data on 765 early Neolithic dates. The main fields contained in this database, in terms of the analysis of the front speed, are the geographic coordinates, Latitude and Longitude, and the calibrated dates (field CAL C14 BP in table 2.1) in years BP.[9] The calibrated dates were calculated from the uncalibrated radiocarbon dates (UNCAL 14 BP) using Oxcal 2004 software (www.oxcal.de). The database also contains information on the Site name, location (Country), Period, lab code for the dated sample (Lab Number), and

---

[7]When calculating T in this reference (note [24]) there is a typographic mistake: where it says $a_1 \simeq 15$yr, it should say $a_1 \simeq 19$yr.

[8]Note that a mean age when leaving a domestic group $\langle a \rangle \simeq 24$yr is consistent with a mean age at the birth of the first child $\tau = 25$yr [7, 17], if adding about 1yr between the migration and the birth of the child.

[9]The time scale years BP, or Before Present, is a time scale used in archaeology that uses year 1950 as origin.

Latitude	Longitude	Site name	Country	Period	Lab Number	Uncal C14 BP	Uncal C14_SD	CAL C14 BP	CAL C14_SD
38,3700	34,2500	Asikli Höyük	Turkey	Aceramic	GrN-19116	8920	50	10047	101
36,7830	34,5670	Yumuktepe	Turkey	Pottery Neolithic	Rome-467	7920	90	8787	147
38,2800	34,5700	Kaletepe	Turkey	Aceramic	GifA-100396	9030	80	10122	128
47,8200	13,4500	See am Mondsee	Austria	LBK		4820	82	5531	100
48,6000	15,0833	Guttenbrunn	Austria	LBK	Bln-2227	5935	50	6759	64
48,7000	15,5667	Poigen	Austria	LBK	H-2121/1552	6017	90	6866	114
48,6700	15,6300	Frauenhofen	Austria	Stichbandkeramik	KN-2566	6290	65	7181	96
48,6333	15,6833	Mold	Austria	LBK	Bln-58	5990	160	6853	205
48,7000	15,8600	Pulkau	Austria	LBK	Bln-83	6215	100	7099	126
48,1000	16,2800	Brunn am Gebirge	Austria	LBK	ETH-11148	6785	75	7637	55
48,7500	16,4700	Schletz	Austria	LBK	ETH-13289	6175	65	7073	98
47,5000	16,5000	Unterpullendorf	Austria	Early painted Ware	VRI-42	6130	140	7001	178
47,5000	16,5000	Frankenau	Austria	LBK	VRI-207	5660	100	6464	113
47,6000	16,5500	Neckenmarkt	Austria	LBK	OxA-1536	6210	80	7104	106
47,9500	16,8300	Winden am See	Austria	LBK	Bln-55	5940	100	6773	121
50,5800	3,6800	Blicquy, Couture de la	Belgium	LBK	Hv-9271	6705	165	7575	135
50,6100	3,7500	Irchonwelz	Belgium	Blicquy Group	Bln-2531	6030	60	6867	81
50,8000	5,0500	Wange	Belgium	Late LBK	Lv-1116	6310	75	7207	106
50,6500	5,1800	Darion	Belgium	LBK	Lv-1579	6240	100	7126	123
50,6500	5,2000	Omal	Belgium	LBK	Hv-9285	6505	105	7412	97

Table 2.1: Sample of the early Neolithic radiocarbon dates database published by Pinhasi et al. [9]. The database contains data on 765 early Neolithic sites.

statistical deviations of the calibrated and uncalibrated dates (Uncal C14_SD and CAL C14_SD)[10].

The analysis of the database to measure the front speed has been performed using ArcGIS 9.3 software. This software allows us to represent all the data on a map and interpolate the dates to obtain an isochron map; the selected region of study is a rectangular area 1300 km long comprised between the Balkans and the North Sea (see figure 5.1 in chapter 5). The front speeds are estimated by computing the area comprised between two isochrones (separated 250 yr) within the region of study. From the value of each area, and the width of the studied region (about 400 km), one can calculate the mean distance covered by the spreading front during a 250-year period, and thus estimate the mean speed during this period.

In order to plot the speed of the spreading front as a function of the distance (e.g., figure 5.3), the values for the distances are computed from the position of the centroid of each of the studied areas (i.e., the areas between isochrones separated 250 yr).

2.2 Fronts from integrodifference equations

Integrodifference equations are widely used in mathematical biology to model the dispersal and growth of populations. They are integral recurrence relations, discrete in time, such as equations (1.6) and (1.7) in chapter 1. In chapter 3, in order to include the effect of using the full kernel, the speed of range expansion has to be obtained from the analysis of these integrodifference equations. This front speed can be calculated analytically by applying continuous-space random walks (CSRW) and discrete-space random

---

[10]The original database published by Pinhasi et al. [9] contains a larger number of fields related to the calculus in their work but that are not necessary for the analyses performed in this thesis.

walks (DSRW), or numerically by computing reactive random walk simulations. We summarize these three methods in turn.

2.2.1 Continuous-space random walks (CSRW)

When searching for the front speed using analytical methods there are three main assumptions. First, as the population density p at the leading edge of the front is very low, the equation describing the dynamics there can be linearized (in terms of p). This linearization affects mainly the growth process which becomes exponential (see figure 2.1). The second assumption is that for $t \to \infty$ and $r \to \infty$, the front can be considered approximately planar at the local scale. Thus, the local velocity can be assumed parallel to the radial axis (for example x) and the speed along the perpendicular direction (y) will be negligible. Finally, the following *ansatz* is made for the solution at large values of the coordinate $z = (x - ct)$ moving with the front ($z \to \infty$), $p = \bar{p} \exp{(-\lambda z)}$. Therefore

$$
\begin{aligned}
p\left(x, y, t+T\right) &= p\left(x, y, t\right) \mathrm{e}^{\lambda c T}, \\
p\left(x + \Delta_x, y + \Delta_y, t\right) &= p\left(x, y, t\right) \mathrm{e}^{-\lambda \Delta_x}.
\end{aligned}
\tag{2.1}
$$

Applying these relations to an integrodifference equation leads to a complex equation for the front speed c depending on the unknown parameter λ, which can be solved if applying the usual assumption [30] that the minimum speed is, in fact, that of the front. This is called the marginal stability or linear analysis assumption. For example, for the cohabitation equation (1.7) with the solution to the logistic growth (1.1),

$$
\begin{aligned}
R\left[p\left(x, y, t\right)\right] &= \frac{p\left(x, y, t\right) p_{\max} \mathrm{e}^{aT}}{p_{\max} + p(x, y, t)(\mathrm{e}^{aT} - 1)} - p\left(x, y, t\right) \\
&\simeq p\left(x, y, t\right)\left(\mathrm{e}^{aT} - 1\right),
\end{aligned}
\tag{2.2}
$$

the front speed is

$$
c = \min_{\lambda > 0} \frac{\ln\left[\mathrm{e}^{aT} \iint \mathrm{e}^{-\lambda \Delta_x} \phi\left(x, y; \Delta, \theta\right) \mathrm{d}\Delta_x \mathrm{d}\Delta_y\right]}{\lambda T}.
\tag{2.3}
$$

If the integral $\iint \mathrm{e}^{-\lambda \Delta_x} \phi\left(x, y; \Delta, \theta\right) \mathrm{d}\Delta_x \mathrm{d}\Delta_y$ has an explicit solution, it is possible to obtain an explicit expression for the front speed (for example, with the Gauss or Laplace distributions, as shown in section 3.4). Otherwise, the minimum has to be obtained numerically. The validity of equations such as (2.3) can be checked by means of the methods in the two subsections below.

2.2.2 Discrete-space random walks (DSRW)

The previous method considers the space as a continuous, in the sense that individuals can move to any point in space, but when performing numerical simulations, the space is necessarily discrete. Using discrete-space random walks provides analytical results
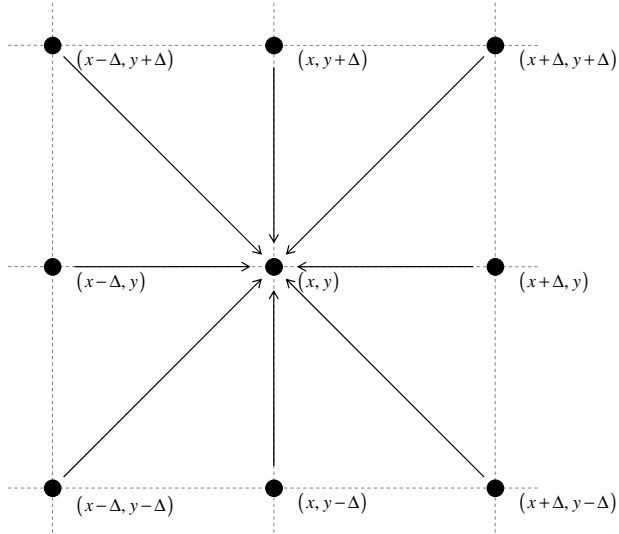
Figure 2.2: Diagram of the discretized dispersion kernel with jump from the eight nearest neighbors. Corresponds to the single-distance jump isotropic kernel.

for a dispersion process taking place in a discrete space, that are directly comparable with the simulations.

The discretization of space is taken into account by discretizing the integral

$$\iint p\left(x - \Delta_x, y - \Delta_y, t\right) \phi\left(x, y; \Delta, \theta\right) \mathrm{d}\Delta_x \mathrm{d}\Delta_y \tag{2.4}$$

from the integrodifference equation (e.g., equation (1.6) or (1.7)), according to the approximation used in the numerical simulation. For example, for the very simple case in which only jumps from the eight nearest neighbors are included, (2.4) is replaced by

$$\frac{1}{8}[p\left(x + \Delta, y + \Delta, t\right) + p\left(x + \Delta, y, t\right) + p\left(x + \Delta, y - \Delta, t\right) + p\left(x, y - \Delta, t\right)$$
$$+ p\left(x - \Delta, y - \Delta, t\right) + p\left(x - \Delta, y, t\right) + p\left(x - \Delta, y + \Delta, t\right) + p\left(x, y + \Delta, t\right)] \tag{2.5}$$

for isotropic kernels (see figure 2.2). Then, the front speed is calculated by the same mathematical analysis applied before, i.e., assuming low densities, planar fronts and $p \simeq \bar{p} \exp\left(-\lambda z\right)$, with $z = \left(x - ct\right)$.

2.2.3 Reactive random walk simulations

This kind of numerical simulations follow the evolution of the population density in time and space. A 2−dimensional grid must be defined, with each node being a potential settlement. Before performing the simulation, the initial conditions must be fixed (typically $p = p_{\max}$ at the center and $p = 0$ elsewhere). Then, the evolution of the population density for each time interval T is computed according to the following steps:

Dispersion For *each* node, the initial population is redistributed according to the dispersion kernel $\phi(x, y; \Delta, \theta)$, but approximated to a discrete grid. For example, if the population can either stay with probability p_0 or disperse to the eight nearest neighbors, a fraction p_0 of the initial population at point (x, y) would remain in the same position, and each of the eight nearest neighbors could be assigned a fraction $p_1 = (1 - p_0)/8$ of the initial population at (x, y) (see figure 2.2).[11]
The redistribution of the population can be performed in a deterministic way, as in the example above, or following an stochastic process. The latter procedure means that each individual initially at (x, y) is assigned a destination according to a random function (see section 3.6).

Reaction The increase in population number due to the reaction (i.e., net reproduction) process is computed with the solution to the logistic growth equation (1.1), namely

$$p(x, y, t + T) = \frac{p(x, y, y)\, p_{\max} \mathrm{e}^{aT}}{p_{\max} + p(x, y, t)(\mathrm{e}^{aT} - 1)} \tag{2.6}$$

for each node of the grid.

The front speed is obtained from linear regression of the position of successive fronts (defined, e.g., as $p = p_{\max}/10$) when the time is $t \gg T$.

2.3   Fronts from differential equations

In chapters 4, 5 and 6, the evolution of the population is modeled using reaction-diffusion differential equations. Differential equations [such as (1.2) and (1.4) in chapter 1] require a different analysis and, specially, different numerical techniques than integrodifference equations [such as equations (1.6) and (1.7) in chapter 1]. The front speed for differential equations can be obtained from linear and variational analysis, or from numerical integration.

2.3.1   Linear analysis (lower bound)

The three main assumptions made in the analysis of integrodifference equations also apply when dealing with differential equations: (i) the population density is low at the leading edge of the front, so the differential equation can be linearized in terms of the population density $p(x, y, t)$, e.g. Fisher's equation (1.2) becomes

$$\frac{\partial p}{\partial t} \simeq D \left(\frac{\partial^2 p}{\partial x^2} + \frac{\partial^2 p}{\partial y^2} \right) + ap \;, \tag{2.7}$$

(ii) fronts can be considered approximately planar for $t \to \infty$ and $r \to \infty$; and (iii) $p(z) \simeq \bar{p} \exp(-\lambda z)$, with $z = (x - ct)$. With differential equations, however, the

---

[11]This example corresponds to the *Simplified model* presented in section 3.5.1 (chapter 3).

necessary relations, obtained from (iii), are the following

$$\frac{\partial p}{\partial t} = \lambda c\, p\,(x,y,t)\,, \qquad\qquad \frac{\partial^2 p}{\partial t^2} = (\lambda c)^2\; p\,(x,y,t)\,,$$

$$\frac{\partial p}{\partial x} = -\lambda\, p\,(x,y,t)\,, \qquad\qquad \frac{\partial^2 p}{\partial x^2} = (-\lambda)^2\; p\,(x,y,t)\,. \tag{2.8}$$

Applying these relations to the differential equation describing the model (e.g., the linearized Fisher's equation (2.7)) leads to a quadratic equation in terms of the parameter λ. As λ is a real value, the discriminant from the quadratic equation must be non-negative, and from this condition follows a lower bound for the front speed (e.g., $c > 2\sqrt{aD}$ for equation (2.7), which leads to Fisher's speed (1.3) when combined with the upper bound explained below).

2.3.2   Variational analysis (upper bound)

Even though according to marginal stability hypothesis the asymptotic velocity of spreading fronts generically approaches the minimal velocity (which can be obtained from the linear analysis above), this hypothesis does not hold for all reaction-diffusion systems. Benguria and Depassier [31] described a variational analysis leading to an upper bound for parabolic reaction-diffusion equations, that Méndez et al. [32] generalized to hyperbolic reaction-diffusion equations. This is the variational analysis that will be used in the following chapters to find an upper bound for the front speed of the proposed reaction-diffusion models.

As usual, the front profile is assumed to be planar and that it depends only on $z = (x - ct)$, thus the following relations can be applied to the differential equation,

$$\frac{\partial p}{\partial t} = -c\frac{\partial p}{\partial z}, \qquad\qquad \frac{\partial^2 p}{\partial t^2} = c^2\frac{\partial^2 p}{\partial z^2},$$

$$\frac{\partial p}{\partial x} = \frac{\partial p}{\partial z}, \qquad\qquad \frac{\partial^2 p}{\partial x^2} = \frac{\partial^2 p}{\partial z^2}, \tag{2.9}$$

and, as the analysis is performed in the phase space, it is convenient to define $n\,(p) \equiv -\partial p/\partial z$, with $n\,(0) = n\,(p_{\max}) = 0$, and $n\,(p) > 0$ for a front with $c > 0$ and $p \in (0, p_{\max})$.

Let $g\,(p)$ be an arbitrary positive function, with $h\,(p) = -g'\,(p)$ also positive. Multiplying the differential equation by g/n and integrating leads to an integral variational principle for the speed of fronts [e.g., equation (4.16) in chapter 4], after integrating by parts and applying that for $r, s > 0$, $(r + s) \geq 2\sqrt{rs}$ (the latter inequality follows directly from the Pythagorean theorem). From this variational principle it is possible to find an upper bound for the front speed (e.g., $c < 2\sqrt{aD}$ for equation (2.7), which leads to Fisher's speed when combined with the lower bound above).

More detail on this variational analysis is given in chapter 4, section 4.2, where the analysis is described step-by-step for a second-order reaction-diffusion equation.

In the three reaction-diffusion equations studied (chapters 4, 5 and 6), the lower and upper bounds coincide, so the calculated speed is the exact front speed for each system.

2.3.3   Numerical integration: finite-difference method

Differential equations can be solved numerically. However, before performing numerical integrations it is convenient to work with dimensionless variables, so that the results can be applied to systems with any parameter values. For this purpose, time and space variables are rescaled as follows

$$
\begin{aligned}
t^* &= t\,k \\
x^* &= x\sqrt{\frac{k}{D}}
\end{aligned}
\tag{2.10}
$$

where $1/k$ is the characteristic time of the reactive process [32]; for example, for the logistic case $k = a$, the initial growth rate. Then, for example, the dimensionless form of Fisher's equation (1.2) is

$$
\frac{\partial p}{\partial t^*} = \left(\frac{\partial^2 p}{\partial x^{*2}} + \frac{\partial^2 p}{\partial y^{*2}} \right) + p\left(1 - \frac{p}{p_{\max}} \right).
\tag{2.11}
$$

In order to numerically solve a differential equation, such as equation (2.11), the time and space derivatives are finite differenced according to the *fully implicit* or *backward time* differencing scheme [33][12]

$$
\begin{aligned}
\frac{\partial p}{\partial t^*} &\simeq \frac{p_j^{n+1} - p_j^n}{\Delta t^*}, & \frac{\partial^2 p}{\partial t^{*2}} &\simeq \frac{p_j^{n+1} - 2p_j^n + p_j^{n-1}}{\left(\Delta t^*\right)^2}, \\
\frac{\partial p}{\partial x^*} &\simeq \frac{p_{j+1}^{n+1} - p_j^{n+1}}{\Delta x^*}, & \frac{\partial^2 p}{\partial x^{*2}} &\simeq \frac{p_{j+1}^{n+1} - 2p_j^{n+1} + p_{j-1}^{n+1}}{\left(\Delta x^*\right)^2},
\end{aligned}
\tag{2.12}
$$

where the superscripts denote the time and the subscripts the space point at which p is evaluated. The fully implicit differencing scheme is an unconditionally stable scheme that leads to results that are first-order accurate in time. In contrast, the explicit scheme (i.e., using the time instant n instead of $n+1$ in the spatial derivatives) is also first-order accurate in time but requires the use of very short time steps Δt^* in order to be stable, and this means that the number of steps necessary to obtain results is usually prohibitive [33].[13]   When applied to a reaction-diffusion equation, the fully implicit differencing scheme yields, in general, a set of linear equations for each time step $n+1$ such as

$$
\alpha_j p_{j-1}^{n+1} + \beta_j p_j^{n+1} + \gamma_j p_{j+1}^{n+1} = r_j, \qquad j = 1, 2 ... J - 1,
\tag{2.13}
$$

---

[12]See section 16.6 and chapter 19 in this reference for further details on finite-difference methods. The *fully implicit* scheme is described in section 19.2 in this reference.

[13]The explicit scheme was applied to solve reaction-diffusion-advection equations modeling the Neolithic transition by Davison [34] but using parallel computing.

with α_j, β_j and γ_j the coefficients for p_{j-1}^{n+1}, p_j^{n+1} and p_{j+1}^{n+1}, respectively; and r_j a function of p_j^n for reaction-diffusion equations without the derivative $\partial^2 p/\partial t^{*2}$ (parabolic equations), or function of p_j^n and p_j^{n-1} for reaction-diffusion equations with first and second time derivatives (2.12) (hyperbolic equations). J is given by $J = L^*/\Delta x^*$, with $L^* = L\sqrt{k/D}$ the dimensionless system size, and usually the system considered is a square with side L. The set of linear equations (2.13), together with Dirichlet boundary conditions $p_0^n = p_{\max}$ and $p_J^n = 0$ (for all n), conform a tridiagonal system that can be easily solved by using the Tridag routine in Fortran [33][14], provided that the initial conditions p_j^0 (and p_j^{-1} for hyperbolic equations, e.g. $p_j^{-1} = p_j^0$ for $j = 1, 2...J-1$) are implemented so that they have compact support, in order to obtain a travelling wavefront that is independent of them [21]. For example, appropriate initial conditions are such that

$$\begin{cases} p_j^0 = p_{\max}, & \text{for } j \leq j_{ic} \\ p_j^0 = 0, & \text{for } j \geq j_{ic} + 1 \end{cases}, \tag{2.14}$$

assuming p_j^0 continuous between j_{ic} and $j_{ic} + 1$. In the model described in chapter 4, when performing the numerical integration, j_{ic} was chosen $j_{ic} = J/6$. Biologically, the range $j \leq j_{ic}$ is that initially occupied by the population.

---

[14]The Tridag routine code can be found in section 4.2 in this reference.

Chapter 3

Realistic dispersion kernels applied to cohabitation reaction-dispersion equations [*J Stat Mech - Theor Exp 2008; 2008: P10012*]

This chapter is an exact transcription of the contents of the following paper (please, find a copy of the published version in appendix A):

Abstract We develop front spreading models for several jump distance probability distributions (dispersion kernels). We derive expressions for a cohabitation model (cohabitation of parents and children) and a non-cohabitation model, and apply them to the Neolithic using data from real human populations. The speeds we obtain are consistent with observations of the Neolithic transition. The correction due to the cohabitation effect is up to 38%.

3.1   Introduction

In systems where dispersion and reaction process coexist, front spreading may be observed. A front can be defined as a moving profile connecting an initial, unstable state with a final, stable state. For example, in population dynamics the final state corresponds to the maximum population density that can be supported by the environment, whereas in combustion flames it corresponds to the burned state.

Previous work on front spreading includes analytical calculation of front speeds for (i) reaction terms such that linear analysis is appropriate (pulled fronts), as well as for the non-linear case (pushed fronts) [35], (ii) sequential reaction and dispersion [36], (iii) dispersal kernel effects leading to the breakdown of classical diffusion [37], (iv) biased random walks [12, 38], (v) age-structured systems [13, 39], (vi) distributed delays [11, 40], etc. (For a recent review see [41]).

Front propagation models have been extensively applied to study physical and biological systems including population dispersals [12], combustion flames [42], Taylor-Couette and Rayleigh-Bénard experiments [35], viral infections [43], tumor growth [44], etc.

In most studies on human population dynamics, the velocity of fronts has been calculated with Fisher's equation ($c_{\text{Fisher}} = \sqrt{2aD}$, where a is the initial growth rate and D the diffusion coefficient) or, more recently, with the HRD (hyperbolic reaction-diffusion) equation [7, 45]. In the HRD model, it is assumed that (i) each individual (or particle) rests for a time interval T between successive jumps, and (ii) the duration of jumps is negligible compared to the rest time T. This leads to the front speed (for the detailed derivation, see [7])

$$c_{\text{HRD}} = \frac{2\sqrt{aD}}{1 + (aT/2)}. \tag{3.1}$$

Fisher's speed ($c_{\text{Fisher}} = \sqrt{2aD}$) is recovered for $T \ll 1/a$, so it is valid only if the rest time T is negligible.

Fisher's and HRD equations include the dispersion just as a parameter, namely the diffusion coefficient ($D = \langle \Delta^2 \rangle / 4T$, where $\langle \Delta^2 \rangle$ is the mean squared displacement of jumps). In this work, we study the effect of using the whole dispersion kernel (distribution of the dispersal probability on jump distance Δ) on front speeds. We tackle this problem not only from hypothetical distributions, but also using data from real human populations in order to obtain more realistic results and compare them to the observed front speed of the Neolithic transition in Europe.

Results depending on the full kernel have to be obtained from an integrodifferential* evolution equation for the population density, rather than a differential equation [7]. In previous work, we have already used integrodifferential† evolution equations for population dynamics models in order to study persistency effects on front speeds [13], fronts from biased random walks [38] and fronts for interacting species [14]. However, realistic dispersion distributions obtained from observed human populations have not been applied before. In section 3.2 we present two possible evolution equations (a cohabitation model and a non-cohabitation one). Then we obtain analytical and numerical results for the front speed for both evolution equations. In section 3.3 we consider several-distance dispersion kernels in 2D, while in section 3.4 we apply Laplace and Gauss 2D kernels. These results are applied to the Neolithic transition in Europe in section 3.5

---

*In the published version of this work (Appendix A) there is a typographical error in this sentence; the right word is integrodifference, rather than integrodifferential.

†See footnote *.

using real dispersion data from six human populations. In section 3.6 we describe a stochastic model which we compare with the deterministic results. Finally, in section 3.7 we present our conclusions.

3.2   Evolution equations

In order to study the effect of the dispersion kernel on front speeds, we need an integrodifferential[‡] evolution equation for the population density $p(x, y, t)$. A possible expression for the evolution equation is [13, 14, 38],

$$p(x, y, t + T) = \int_{-\infty}^{+\infty} \int_{-\infty}^{+\infty} p(x + \Delta_x, y + \Delta_y, t)\phi(\Delta_x, \Delta_y) \, \mathrm{d}\Delta_x \, \mathrm{d}\Delta_y$$
$$+ R_T\left[p(x, y, t)\right] - p(x, y, t). \tag{3.2}$$

The first term in equation (3.2) is the dispersal term, where the probability $\phi(\Delta_x, \Delta_y)$ is the dispersion kernel, and gives the probability per unit area that an individual initially placed at $(x+\Delta_x, y+\Delta_y)$ moves to (x, y) during a time interval T of one generation [7].

$R_T\left[p(x, y, t)\right]$ in equation (3.2) is the solution of the logistic growth equation, widely used in population dynamics [21],

$$R_T\left[p(x, y, t)\right] = \frac{p(x, y, t) \, p_{\max} \, \mathrm{e}^{aT}}{p_{\max} + p(x, y, t) \, (\mathrm{e}^{aT} - 1)}, \tag{3.3}$$

where $p_{\max}$ is the carrying capacity. Equation (3.3) gives the final population density, due to population growth, after a time interval T from the initial value $p(x, y, t)$. So, the last two terms in equation (3.2), $R_T\left[p(x, y, t)\right] - p(x, y, t)$, correspond to the net growth (natality-mortality balance) during T.

However, according to equation (3.2), after a generation new individuals appear due to reproduction at (x, y) while parents have moved to $(x - \Delta_x, y - \Delta_y)$, i.e., parents leave their children behind when the former migrate. But this is not realistic for human populations; thus we use a more realistic evolution equation [13, 14, 38],

$$p(x, y, t + T) = R_T\left[\int_{-\infty}^{+\infty} \int_{-\infty}^{+\infty} p(x + \Delta_x, y + \Delta_y, t)\phi(\Delta_x, \Delta_y) \, \mathrm{d}\Delta_x \, \mathrm{d}\Delta_y\right]. \tag{3.4}$$

The difference between equation (3.2) and equation (3.4) is a very important point. It is thus shown in figure 3.1 for the 1D case and a population at a single position at $t = 0$ (figure 3.1(a)). For equation (3.4), figure 3.1(b), the initial population migrates (full columns) and the population growth (hatched columns) takes place at the destination position. On the other hand, for equation (3.2), figure 3.1(c), population growth (hatched column) takes place only at the initial position x due to the whole initial population, while part of this initial population has already migrated (full columns). So, from now on, equation (3.2) and its results will be named as non-cohabitation (NCohab), since parents migrate leaving their children behind, and equation (3.4) and its results will be named as cohabitation (Cohab).

[‡]See footnote ∗.
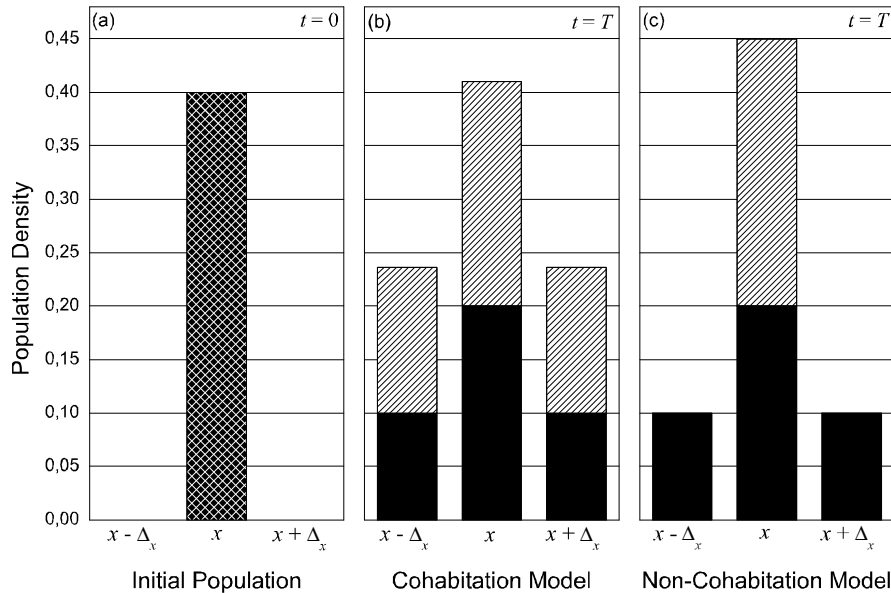
Figure 3.1: Comparison of cohabitation (equation (3.4)) and non-cohabitation (equation (3.2)) model in 1D. Initially the population is at a single position $p(x, t = 0)$ (a). In (b) and (c) full columns correspond to the dispersed population (parents) and hatched columns to the population growth (children). ($p_0 = 0.5$, $\phi\left(\Delta_x\right) = \delta\left(x \pm \Delta_x\right)$, $a = 0.028 \text{ yr}^{-1}$, $T = 32$ yr)

3.3 Several-distances dispersion model

For real populations, the migrated distances per generation are usually continually distributed. But available data are recorded in intervals, so here we consider a discrete approximation with a kernel that allows dispersion to multiple discrete distances. Therefore, assuming an isotropic kernel, the linear distribution of probability can be expressed as a sum of Dirac deltas[1]

$$\varphi\left(\Delta\right) = 2\pi\Delta\phi\left(\Delta\right) = \sum\nolimits_{i=0}^{n} p_i\delta(\Delta - r_i), \tag{3.5}$$

where p_i is the probability for the individuals to move a distance $r_i = i \cdot d$, for $i = 0, 1, 2..., n$, with d the width of the intervals used when recording the data.

Below we search the front speed using analytical methods (CSRW, DSRW) and numerical simulations.

3.3.1 Continuous-space random-walks (CSRW)

In order to find an analytical expression for the front speed, we apply some simplifications to the evolution equation. Firstly, as the population density at the leading edge

---

[1]The linear distribution of probability, $\varphi\left(\Delta\right)$, is the integration over the azimuthal coordinate θ of the 2D kernel, $\phi(\Delta)$. For an isotropic kernel, $i.e.$, independent of θ, the relation between both distributions is $\varphi\left(\Delta\right) = 2\pi\Delta\phi\left(\Delta\right)$.

of the front is low, equation (3.3) can be linearized there, becoming

$$R_T\left[p(x,y,t)\right] = p(x,y,t)\,\mathrm{e}^{aT}. \tag{3.6}$$

Moreover, since we have assumed an isotropic kernel, the front is azimuthally symmetric, so it can be considered approximately planar for $t \to \infty$ and $r \to \infty$. Then, choosing x-axis as parallel to the local velocity of the front, $c \equiv |c_x|$, we look for constant-shape solutions with the form $p = \bar{p}\exp[-\lambda\,(x - ct)]$. Applying these simplifications to cohabitation equation (3.4), it may be rewritten as

$$\mathrm{e}^{\lambda cT} = \mathrm{e}^{aT} \int_{-\infty}^{+\infty} \int_{-\infty}^{+\infty} \mathrm{e}^{-\lambda\Delta_x}\phi(\Delta_x, \Delta_y)\,\mathrm{d}\Delta_x\,\mathrm{d}\Delta_y\ . \tag{3.7}$$

Finally, changing the coordinate system to polar coordinates, i.e., defining $\Delta \equiv \sqrt{\Delta_x^2 + \Delta_y^2}$ and $\theta \equiv \tan^{-1}\left(\Delta_y/\Delta_x\right)$, and using equation (3.5), we find an expression for the front velocity[2],

$$c_{\mathrm{Cohab}} = \min_{\lambda > 0} \frac{\ln\left[\mathrm{e}^{aT}\sum_{i=0}^{n} p_i I_o(\lambda id)\right]}{\lambda T}, \tag{3.8}$$

where $I_0\left(\lambda id\right)$ is the modified Bessel function of the first kind and order zero,

$$I_0\left(\lambda id\right) = \frac{1}{2\pi}\int_0^{2\pi}\exp\left(\lambda id\cos\theta\right)\mathrm{d}\theta. \tag{3.9}$$

Applying the same steps to the non-cohabitation equation (3.2), we obtain the expression for the front velocity (see footnote 2),

$$c_{\mathrm{NCohab}} = \min_{\lambda > 0} \frac{\ln\left[\left(\mathrm{e}^{aT} - 1\right) + \sum_{i=0}^{n} p_i I_o(\lambda id)\right]}{\lambda T}. \tag{3.10}$$

3.3.2 Reactive random walk simulations

Random walk numerical simulations follow the evolution of the population density in space and time. We consider a 2D grid of 3000×3000 nodes, with the initial condition $p\left(x = 0, y = 0, t = 0\right) = 1$, and $p\left(x, y, t = 0\right) = 0$ at every other node (x, y). The evolution of the population is computed by repeating the following steps at each time interval ($T = 1$ generation):

(i) We apply the dispersion kernel (3.5), but as the grid is Cartesian, the density is in fact distributed into the four edges of n squares of side $2r_i = 2id$.[3] Thus, to each of the $8i$ nodes of the i-square corresponds a fraction $(p_i/8i)$ from the initial population.

(ii) The final population at each node is computed applying the population growth equation (3.3) to the result of step (i) (in the case of equation (3.4)) or applying equation (3.3) to the initial population and adding the result to that of step (i) (in the case of equation (3.2)).

---

[2]The value of d for CSRW is related to the mean squared displacement by $\left\langle\Delta^2\right\rangle = \sum_{i=0}^{n} p_i\left(id\right)^2$.

[3]The value of d for DSRW (and numerical simulations) is related with the mean squared displacement by the approximation $\left\langle\Delta^2\right\rangle = \sum_{i=0}^{n}\left(p_i/8i\right)\sum_{j=-i}^{i-1} 4[(id)^2 + (jd)^2]$.

3.3.3 Discrete-space random walks (DSRW)

In the CSRW approach (section 3.3.1) we consider a continuous space. But the simulation grid (section 3.3.2) is necessarily discrete, and this in fact modifies the kernel shape. Thus, the results from these two methods may be different. Therefore, here we suppose a discrete space in order to reproduce analytically the results obtained from the numerical simulations.

We first discretize equation (3.4) so that the kernel is square shaped as in the simulations. The dispersion term, namely

$$\int_{-\infty}^{+\infty} \int_{-\infty}^{+\infty} p(x + \Delta_x, y + \Delta_y, t)\phi(\Delta_x, \Delta_y)\mathrm{d}\Delta_x\mathrm{d}\Delta_y, \tag{3.11}$$

as a result of the discretization, becomes

$$p_0\, p(x, y, t) + \sum_{i=1}^{n} \frac{p_i}{8i} \left\{ \sum_{j=-i}^{i} [p(x + r_i, y + r_j, t) + p(x - r_i, y + r_j, t)] \right.$$
$$\left. + \sum_{j=-i+1}^{i-1} [p(x + r_j, y + r_i, t) + p(x + r_j, y - r_i, t)] \right\}. \tag{3.12}$$

Applying now the same simplifications as with the CSRW (section 3.3.1) we obtain that the expression for the front speed is (see footnote 3)

$$c_{\text{Cohab}} = \min_{\lambda > 0} \frac{\ln\left[\mathrm{e}^{aT}\ \Psi(\lambda d)\right]}{\lambda T}, \tag{3.13}$$

where

$$\Psi(\lambda d) \equiv p_0 + \sum_{i=1}^{n} \frac{p_i}{4i} \left[1 + \sum_{j=1}^{i-1} 2\cosh(\lambda j d) + (2i + 1)\cosh(\lambda i d)\right]. \tag{3.14}$$

Following the same method as above we find that the speed expression for the non-cohabitation equation (3.2) is (see footnote 3)

$$c_{\text{NCohab}} = \min_{\lambda > 0} \frac{\ln\left[\left(\mathrm{e}^{aT} - 1\right) + \Psi(\lambda d)\right]}{\lambda T}. \tag{3.15}$$

3.4 Continuous dispersion models

In this section, instead of a multiple Dirac delta for the kernel (section 3.3), we consider isotropic continuous probability distributions in 2D.

In order to find analytical results we apply the same simplifications than in section 3.3: linearization of the growth equation and assumption of constant-shape front

solutions $p = \bar{p} \exp[-\lambda (x - ct)]$. In this way, using again polar coordinates as in the CSRW, we obtain the following general expression for the cohabitation equation (3.4):

$$c_{\text{Cohab}} = \min_{\lambda > 0} \frac{\ln \left[e^{aT} \int_0^{+\infty} \varphi (\Delta) I_0 (\lambda \Delta) \, d\Delta \right]}{\lambda T}, \tag{3.16}$$

where, as in equation (3.5), $\varphi (\Delta) = 2\pi \Delta \phi (\Delta)$ (see footnote 1).

The exact solution for this expression can be obtained from the value of λ that satisfies $dc_{\text{Cohab}}/d\lambda = 0$. Thus λ is to be calculated from the relation

$$\tilde{\varphi} (\lambda) \ln \left[e^{aT} \tilde{\varphi} (\lambda) \right] = \lambda \tilde{\varphi}' (\lambda), \tag{3.17}$$

where we have defined $\tilde{\varphi} (\lambda) \equiv \int_0^{+\infty} \varphi (\Delta) I_0 (\lambda \Delta) \, d\Delta$ and $\tilde{\varphi}' (\lambda) \equiv d\tilde{\varphi} (\lambda) / d\lambda$.

Applying the same steps to the non-cohabitation equation (3.2), we obtain the expression

$$\beta + \tilde{\varphi} (\lambda) \ln [\beta + \tilde{\varphi} (\lambda)] = \lambda \tilde{\varphi}' (\lambda), \tag{3.18}$$

where we have introduced $\beta \equiv e^{aT} - 1$.

Some important kernels that have been widely applied to population dispersal are the Gauss and Laplace distributions [46]–[48]. These two kernels will also allow us to derive explicit equations for the front speed. In contrast to previous work in 1D [37, 48, 49], here we consider a 2D space, as necessary for application to the Neolithic transition (section 3.5).

3.4.1 Gauss distribution

The Gauss lineal probability distribution is $\varphi (\Delta) = (2\Delta/\alpha^2) \, e^{-(\Delta/\alpha)^2}$, so we obtain that

$$\tilde{\varphi} (\lambda) = e^{\alpha^2 \lambda^2 / 4}. \tag{3.19}$$

For the cohabitation equation (3.4), using equation (3.19) into equation (3.17) we obtain the exact result,

$$c_{\text{Cohab}} = \alpha \sqrt{\frac{a}{T}}. \tag{3.20}$$

For the non-cohabitation equation (3.2), an exact solution cannot be found, but expanding equation (3.18) up to second order in $\alpha\lambda$ ($\alpha\lambda \ll 1$), we obtain the following explicit result:

$$c_{\text{NCohab}} = \frac{\alpha}{2T} \sqrt{\frac{1 + \beta \ln(1 + \beta)}{(1 + \beta) \ln(1 + \beta)}} \times \ln \left[(1 + \beta)^{(1+\beta)/[1+\beta \ln(1+\beta)]} + \beta \right]. \tag{3.21}$$

3.4.2 Laplace distribution

The Laplace linear probability distribution can be expressed as $\varphi(\Delta) = (\Delta/\alpha^2)\,e^{-\Delta/\alpha}$, so we have that

$$\tilde{\varphi}(\lambda) = 1/(1 - \alpha^2\lambda^2)^{3/2}. \tag{3.22}$$

The second order approximation in $\alpha\lambda$ ($\alpha\lambda \ll 1$) for the front speed for the cohabitation equation, i.e., when using equation (3.22) into equation (3.17), is

$$c_{\mathrm{Cohab}} = \frac{\alpha}{T}\sqrt{1 + \frac{3}{2aT}}\left(aT + \frac{3}{2}\ln\left[1 + \frac{2aT}{3}\right]\right). \tag{3.23}$$

For the non-cohabitation equation, the second-order expansion in $\alpha\lambda$ ($\alpha\lambda \ll 1$) for equation (3.18) leads to the expression

$$c_{\mathrm{NCohab}} = \frac{\alpha}{T}\sqrt{\frac{\frac{3}{2} + \left(1 + \frac{5}{2}\beta\right)\ln(1+\beta)}{(1+\beta)\ln(1+\beta)}}$$
$$\times \ln\left[\left(\frac{1 + \left(\frac{2}{3} + \frac{5}{3}\beta\right)\ln(1+\beta)}{(1+\beta)\ln(1+\beta)}\right)^{3/2} + \beta\right]. \tag{3.24}$$

3.5 Application to the Neolithic Transition

We apply the results from sections 3.3 and 3.4 to the Neolithic transition, i.e., the transition from hunter-gatherer to agricultural economics (the corresponding front speed has been measured from archaeological data on the first arrival of farmer populations [9]). We study two cases: (i) a simple approximation with single-distance dispersion (migration to nearest neighbors), and (ii) a more realistic case using mobility data from real populations (using both discrete and continuous kernels).

The generation time we apply in all cases is $T = 32$ yr, which was estimated in reference [11][4] as the mean age of the parents when a child is born (not necessarily the first one).

The range of values for the initial growth rate a that we use at the rest of the paper has been estimated from data of four human populations (Pitcairn [22], Bass Strait [22] and Tristan da Cunha [23] Islands, and the United States population during the nineteenth century [24]). Fits to exponential growth of the population data from the three islands yield $a = 0.029\,95 \pm 0.001\,19$ yr^{-1} for Pitcairn, $a = 0.026\,26 \pm 0.000\,52$ yr^{-1} for Bass Strait and $a = 0.025\,27 \pm 0.000\,32$ yr^{-1} for Tristan da Cunha. The growth rate calculated from the same logistic equation as was used by Lotka [24] for the US is $a = 0.031\,35 \pm 0.000\,63$ yr^{-1}. These four values yield the range $a = 0.028 \pm 0.005$ yr^{-1} (80% confidence level). For populations colonizing a new habitat prior to the existence of the modern health and medicine [50], we are not aware of any population number time series leading to higher values of a.

---

[4]For the estimation of the generation time $T = 32$ yr, see note [24] in this reference.

Population	$\langle\Delta^2\rangle$ (km^2)	p_0	$v_{\min\ \text{Cohab}}$ (km yr^{-1})	$v_{\max\ \text{Cohab}}$ (km yr^{-1})	$v_{\min\ \text{NCohab}}$ (km yr^{-1})	$v_{\max\ \text{NCohab}}$ (km yr^{-1})
A Gilishi15 [26]	1003	0.54	0.850	1.010	0.659	0.734
B Gilishi25 [26]	1210	0.40	0.899	1.055	0.693	0.764
C Shiri15 [26]	2197	0.19	1.161	1.335	0.891	0.967
D Yanomamo [28]	1728	0.19	0.926	1.066	0.711	0.772
E Issocongos [27]	404	0.41	0.521	0.612	0.402	0.443
F Parma [27]	508	0.77	0.674	0.825	0.533	0.611

Table 3.1: Front speeds for the simplified model. The front speeds have been computed for the six human populations with the cohabitation equation (3.4) and the non-cohabitation one (3.2), using the values of the parameters $\langle\Delta^2\rangle$ and p_0 from the present table, and the extreme values of the range $a = 0.028 \pm 0.005$ yr^{-1} ($v_{\min}$ and $v_{\max}$).

3.5.1 Simplified model

Here we analyze a simplified model in which individuals can either stay at the initial position, with a persistency (probability of resting) p_0, or migrate to a single distance d, determined by the values of persistency p_0 and the mean-squared displacement (mobility) $\langle\Delta^2\rangle$ (see footnotes 2 and 3).

In table 3.1 we present the parameter values and computed speeds for four preindustrial farmer populations (Gilishi15 [26], Gilishi25 [26], Shiri15 [26] and Issocongos [27][5]), the Yanomamo [28] (who are horticulturists), and the modern populations in the Parma Valley [27][6] already considered by Ammerman and Cavalli-Sforza [17]. The values for the front speed have been calculated for both the cohabitation equation (3.4) and the non-cohabitation one (3.2), using the CSRW (section 3.3.1) and the minimum and maximum values of the range $a = 0.028 \pm 0.005$ yr^{-1}, obtained above.

In figure 3.2 we present results for both evolution equations (3.2) and (3.4), obtained with the three methods (CSRW, DSRW and simulations), the mean mobility value of populations A, B and C ($\langle\Delta^2\rangle = 1531$ km^2), and two values of the persistency: (i) an extreme case with all individuals migrating, $p_0 = 0.0$ and (ii) a more realistic value, $p_0 = 0.5$ [13]. Front speed values in figure 3.2 have been computed over a large range of a, and note that in all cases the speed increases and tends to a maximum for large values of a (discrete methods saturate at this speed) which corresponds precisely to d km/gen. We can understand this limit intuitively as follows. Since this is a single-distance dispersion model, d is the distance individuals move along the x direction when they migrate, and thus, d km/gen must be the maximum possible speed.[7].

From figure 3.2 it can be seen that the speeds from the non-cohabitation equation (3.2) are always lower than those from the cohabitation equation (3.4); up to 34% lower when comparing results from the CSRW (full and dashed curves in figure 3.2).

---

[5]Data for the Issocongos has been obtained from Figure 8.16.B in this reference.

[6]Data for Parma populations is obtained from Table 8.7 in this reference.

[7]The value of d is calculated differently for the CSRW case (see footnote 2) or the DSRW case and simulations (see footnote 3). Thus the speed limits obtained are different for continuous-space or discrete-space random-walks (figure 3.2).

Figure 3.2: Front speeds for single-distance dispersion kernels. The speeds for the cohabitation equation (3.4), the non-cohabitation equation (3.2) and the HRD equation (3.1), have been computed using the mobility value $\langle \Delta^2 \rangle = 1531$ km^2 and persistencies $p_0 = 0.0$ and $p_0 = 0.5$. The hatched area corresponds to the observed ranges for a and c.

This was to be expected because according to equation (3.2) just the parent generation can disperse, whereas using equation (3.4) it is the whole population that can migrate (parents and children); see figure 3.1.

Comparing the results from the two values of the persistency in figure 3.2, we find that the front speed increases with the persistency, as it could be expected[8] for populations with the same mobility value. We can also see this effect on table 3.1, where populations E and F have similar mobilities but population F has a higher persistency and thus a higher front speed. On the other hand, in table 3.1 we can also observe how for populations with the same persistency (C and D) a higher mobility (and thus, a higher diffusion coefficient $D = \langle \Delta^2 \rangle / 4T$) yields a higher speed.

The 95%-confidence-level speed for the Neolithic transition in Europe is currently estimated as $0.6 - 1.3$ km yr^{-1} [9]. In figure 3.2, the hatched box delimits this range for the initial growth rate range obtained above ($0.023 - 0.033$ yr^{-1}). Thus, although we obtain different speed values for each model, they all lie within the observed for the speed of the Neolithic transition. However, from table 3.1, we see that whereas for

---

[8]Front speed increases with persistency because the jump distance d has been calculated from the same value of the diffusion coefficient $D = \langle \Delta^2 \rangle / 4T$; so a larger probability of staying implies that those who migrate have to move a larger distance d (see footnotes 2 and 3). Therefore, the front speed increases. This effect cannot be predicted by equation (3.1) (full line and triangles at figure 3.2), for example, as it only depends on D.
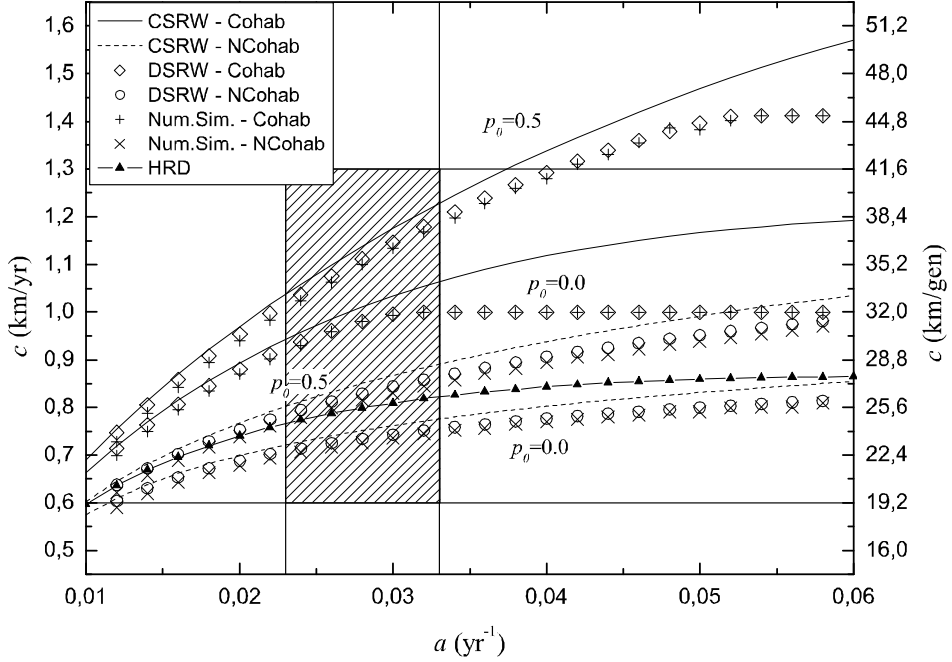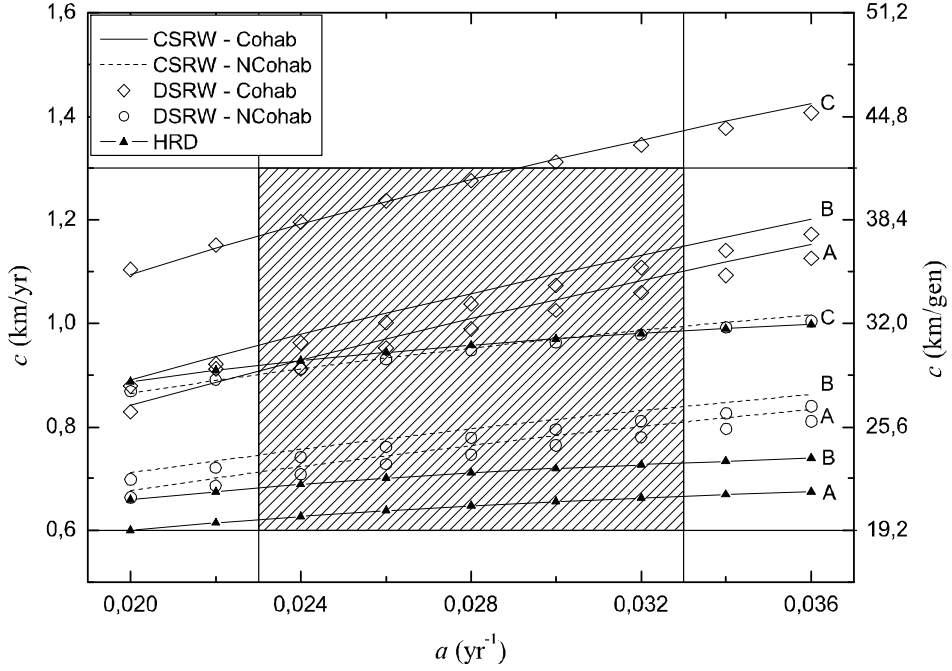
Figure 3.3: Front speeds for three real human dispersal kernels. The speeds for the cohabitation equation (3.4) and the non-cohabitation equation (3.2) are computed using kernel (3.25) (results for each population are labeled). The results for equation (3.1) are calculated from the value of D for each population obtained from kernels (3.25) (see table 3.1). The hatched area corresponds to the observed ranges for a and c.

the cohabitation equation (3.4) the calculated speeds are consistent with the observed range, for populations with low mobilities (E and F) the non-cohabitation equation (3.2) yields lower front speeds than the observed range for the Neolithic transition (up to 33% lower for population E).

3.5.2   Several-distances Dirac deltas model

Now we use the dispersion kernels obtained from real dispersion data of the six populations studied above. Firstly, we consider the dispersion kernels for three of these populations (namely, A, B and C in table 3.1),

$$
\begin{aligned}
P_A &= \{0.54;\ 0.17;\ 0.04;\ 0.25\}\,, \\
P_B &= \{0.40;\ 0.17;\ 0.17;\ 0.26\}\,, \\
P_C &= \{0.19;\ 0.07;\ 0.22;\ 0.52\}\,,
\end{aligned}
\tag{3.25}
$$

where the values correspond to the probabilities p_i for distances $\{2.4;\ 14.5;\ 36.2;\ 60.4\}$ km.[9] For the sake of clarity, in figure 3.3 we show the results only for these

---

[9]These values are the mean of each interval from Stauder's data [26] according to the calculation of mobility by Ammerman and Cavalli-Sforza [17]. The distances correspond to $d = 2.4$ km and $i = \{1;\ 6;\ 15;\ 25\}$ in the kernel expression (3.5).

Population	$v_{\text{min Cohab}}$ (km yr^{-1})	$v_{\text{max Cohab}}$ (km yr^{-1})	$v_{\text{min NCohab}}$ (km yr^{-1})	$v_{\text{max NCohab}}$ (km yr^{-1})
A Gilishi15 [26]	0.908	1.101	0.712	0.810
B Gilishi25 [26]	0.957	1.150	0.746	0.840
C Shiri15 [26]	1.196	1.397	0.920	1.011
D Yanomamo [28]	1.179	1.435	0.927	1.062
E Issocongos [27]	0.737	0.940	0.608	0.737
F Parma [27]	0.800	1.008	0.651	0.774

Table 3.2: Front speeds for the Dirac deltas model. The front speeds have been computed for the six human populations with the cohabitation equation (3.4) and the non-cohabitation one (3.2), using the dispersion kernels from the text (section 3.5.2 and the extreme values of the range $a = 0.028 \pm 0.005$ yr^{-1} (v_{min} and v_{max}).

three populations (computed with the results from sections 3.3.1 and 3.3.3). Here it is seen that the speeds obtained using the full kernel are consistent with the observed range (hatched area), and that again results from equation (3.2) are lower than those from equation (3.4) ($22\% - 28\%$ lower), for the same reasons given at the previous subsection.

In table 3.2 we present the front speed values computed with the cohabitation and non-cohabitation models (using the CSRW) for all six populations and the range $a = 0.028 \pm 0.005$ yr^{-1} obtained above. The dispersion kernels used for populations D, E and F are

$$P_D = \{0.19;\ 0.54;\ 0.17;\ 0.04;\ 0.04;\ 0.02\} \tag{3.26}$$

for distances $\{5.0;\ 30.0;\ 50.0;\ 70.0;\ 90.0;\ 110.0\}$ km,

$$P_E = \{0.42;\ 0.23;\ 0.18;\ 0.08;\ 0.07;\ 0.02;\ 0.01;\ 0.01\} \tag{3.27}$$

for distances $\{2.3;\ 7.3;\ 15;\ 25;\ 35;\ 45;\ 55;\ 100\}$ km and

$$P_F = \{0.77;\ 0.04;\ 0.04;\ 0.03;\ 0.03;\ 0.01;\ 0.01;\ 0.02;\ 0.05\} \tag{3.28}$$

for distances $\{1.3;\ 4.5;\ 9.5;\ 16.5;\ 25.5;\ 36.5;\ 49.5;\ 64.4;\ 81.5\}$ km.

Comparing results from tables 3.1 and 3.2 we see that, in all cases, the front speed is faster when using the full kernel. The jump distance d used in the previous section will always be lower than the longer possible distance of the kernel, and when individuals have a certain probability of moving further, the front speed increases. Thus, the correction introduced by using the full kernel will be more important for those populations with a certain probability of migrating to distances much higher than the value of d calculated from $\langle \Delta^2 \rangle$. For example, for populations D and E, the corrections introduced by applying the full kernel are of approximately 30% and 48% respectively for the cohabitation equation (34% and 59% for the non-cohabitation equation). For both populations, individuals can move to large distances (110 km and 100 km respectively), while for the simplified model the dispersion distance d is about 41 km for population D and about 26 km for population E (see footnote 2).

On the other hand, we can see that the values of front speed for population C in tables 3.1 and 3.2 are approximately the same. It can be explained mathematically

because for these populations, the characteristic dispersal distance for the simplified model, $d \simeq 51$ km (see footnote 2), is similar to the maximum dispersed distance, 60 km. But it can also be explained qualitatively from the dispersion kernel (3.25), as for this population over 50% of individuals move to a single, long-range distance. Thus, this kernel behaves approximately as if the whole population could either not move or migrate just to a single-distance (as the simplified model studied in the previous section). This is also the reason why in figure 3.3 we see that there is a good agreement between the results from the non-cohabitation equation (3.2) and the HRD equation (3.1) for population C (figure 3.2 shows that equation (3.1) is a good approximation to the non-cohabitation model in this case[10]), while for A and B the difference is up to 20%.

Here we have shown that, if a population has a strong long-range dispersal component, then (i) its predicted speeds are faster, and (ii) the HRD equation (3.1) is a good approximation to the exact non-cohabitation model (3.2).

Referring to the speed values obtained, with the exception of populations C and D for equation (3.4) and large values of the growth rate a, they are all within the range of observed speed for the Neolithic transition ($0.6 - 1.3$ km yr^{-1} [9]). But even the speeds for populations C and D are marginally consistent with the observed range. Therefore, we conclude that the application of realistic human kernels to reaction-dispersion equations yields front speeds which are consistent with the values obtained from archaeological data. It is important to note that the whole kernel is necessary, because the single-distance model yielded speeds slower than the observed range for populations E and F (table 3.1).

3.5.3 Several-distances continuous model

Now we apply Laplace and Gauss probability distributions. For the sake of brevity, we consider the populations A, B and C from previous subsections. We calculate the value of the parameter α for both distributions from the mobility $\langle \Delta^2 \rangle$ of each population ($\alpha^2 = \langle \Delta^2 \rangle$ for the 2D Gauss distribution, and $\alpha^2 = \langle \Delta^2 \rangle /6$ for the 2D Laplace distribution).

Comparing the results obtained from the Gauss and Laplace distributions, in figure 3.4 we can see that the speed for Laplace distribution is always faster. This is due to the fact that, for the same value of $\langle \Delta^2 \rangle$, the Laplace distribution has higher values of probability at large distances than the Gauss distribution.

In figure 3.4 we also see that, whereas the difference between speeds from the Laplace distribution and kernel (3.25) for populations A and B is lower than a 12%, for population C results from Laplace distribution are about a 30% faster. For the Gauss distribution, we see that the difference from the speeds obtained with the Dirac deltas kernel (3.25) is also larger for population C. This is due to the fact that for population C the distribution maximum is displaced to larger distances than for the other two

---

[10]HRD equation (3.1) was deduced [7] from an analogous equation to equation (3.2), and thus it is an approximation to it.
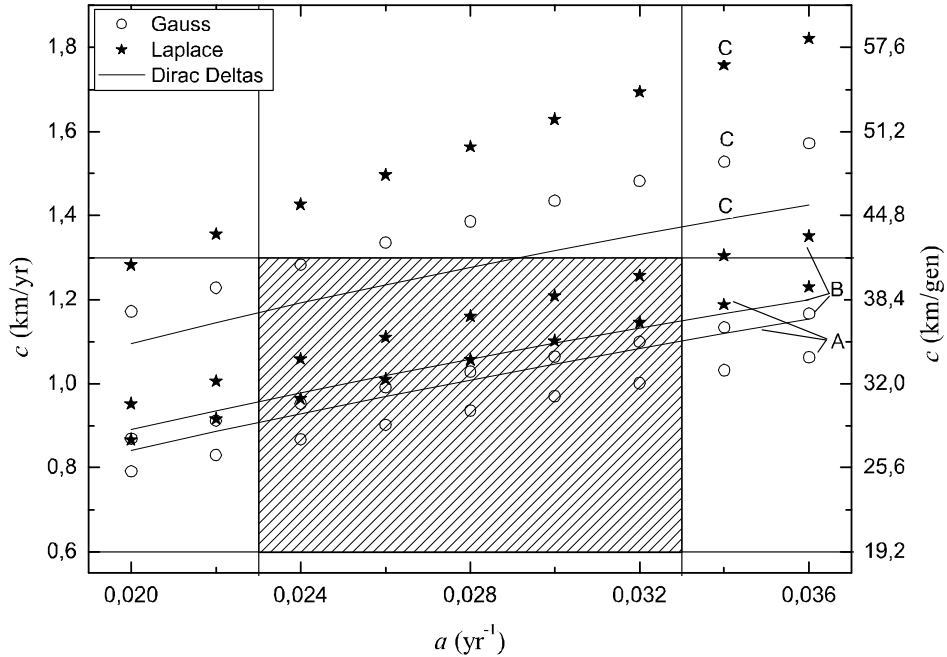
Figure 3.4: Front speeds from continuous probability distributions. Speeds obtained from the Gauss and Laplace cohabitation equations (3.20) and (3.23), using the mobility values for each population obtained from kernels (3.25) (see table 3.1). Dirac deltas correspond to the speeds from CSRW and cohabitation equation in figure 3.3. The hatched area corresponds to the observed ranges for a and c.

populations and thus, there is a larger probability tail for population C.[11]

Here we have shown that, in the absence of a long-range dispersal component, discrete and continuous kernels lead to similar speeds (figure 3.4, populations A and B). However, long-range dispersal can make continuous kernels grossly overestimate the front speed (figure 3.4, population C).

3.6   Stochastic model

In the previous sections, all the results for the front speed have been obtained from deterministic models. Even the numerical simulations correspond to the deterministic equations, and differ from the results of the CSRW (section 3.3.1) due to the discretization of space.

However, population dynamics is a stochastic process that could introduce corrections to the deterministic front propagation [51]. In this section we describe a stochastic model that we apply to the simplified model studied in section 3.5.1. We perform the numerical simulations repeating the following steps for each time interval (T):

---

[11]For population C, the tail probability for distances beyond the range considered in equation (3.25) is about a 40% (twice higher than for populations A and B).
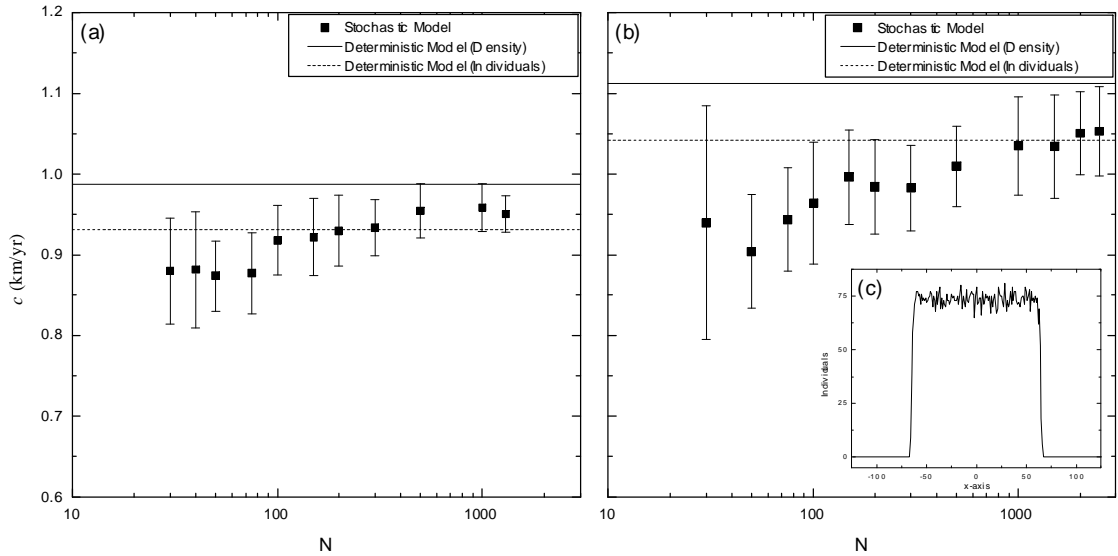
Figure 3.5: Front speeds for the stochastic model. Front speeds for (a) $p_0 = 0.0$ and (b) $p_0 = 0.5$ are represented for different values of N (maximum number of individuals per cell), and compared with the deterministic model (solid and dashed lines). (c) shows a front profile for $N = 75$ individuals.($a = 0.028$ yr^{-1})

(i) For the dispersion process, we first assign *to each individual* a random value n in the interval $[0, 1)$, so if $n < p_0$ the individual stays, and otherwise it migrates. Here, as in the simplified model (section 3.5.1) individuals can only migrate to the eight nearest neighbors on a square with equal probability. So each individual who can migrate is assigned randomly an integer value between 0 and 7 (each corresponding to one of the eight possible final positions). Finally, the position of each individuals is changed according to this random value.

(ii) The reaction process is computed as in section 3.3.2, but since here we are dealing with individuals (instead of population densities) the final value is converted to an integer (by simply truncating the computed number).

In figure 3.5 we show the stochastic results obtained for different values of the number of individuals per cell N (and $a = 0.028$ yr^{-1}). The error bars give the standard deviation of 16 simulations. In order to compare the results from the stochastic model with the deterministic simulations, we have used that the value of carrying capacity for the Neolithic is $p_{max} = 1.28$ hab km^{-2} following reference [52]. This value of p_{max} corresponds to $N = 1306$ individuals per cell when $d = 31.95$ km ($p_0 = 0.0$) (see footnote 3), or to $N = 2613$ individuals per cell when $d = 45.19$ km ($p_0 = 0.5$) (see footnote 3). When the number of individuals per cell reaches the carrying capacity for the Neolithic the results for front speed from the stochastic model are very close to the deterministic ones (full horizontal line in figure 3.5); they are about 3% slower then the deterministic speed when $p_0 = 0.0$ and about 5% slower when $p_0 = 0.5$. Nevertheless, this difference is not only due to the randomness of the process, but also to the effect of using a discrete number of individuals (instead of a continuous population density).

As shown in the figure, when performing simulations with the deterministic model but with a discrete number of individuals (dashed horizontal lines) the front speed obtained is slower than when using population densities; and we see that for large N the results from the stochastic model lie between the results from the two deterministic simulations.

3.7   Concluding remarks

In this paper we have developed discrete and continuous models for reaction-dispersion systems with dispersion kernels. We have applied these models to the Neolithic transition using dispersion data sets from real human populations. Other authors [40, 53] have previously studied the Neolithic transition using data from real populations assuming that each individual is either a non-disperser or a disperser, with the same distance for all dispersers. However, here we have used full kernel expressions and, for the first time, we have applied them to a cohabitation evolution equation, equation (3.4).

The cohabitation equation, equation (3.4), is more realistic for human populations since they do not leave their children behind when migrating as it happens with equation (3.2) (figure 1). Since equation (3.4) implies that more population migrates per generation time, the front speeds are faster than those from equation (3.2). For real populations, this difference is very important: up to 38% faster for the populations studied (table 3.2). However, the front speeds are still consistent with the observed range for the Neolithic transition ($0.6-1.3$ km yr^{-1} [9]). In the simplified model ignoring the kernel shape (table 3.1) this is no longer true for some populations (E and F). Thus, the whole kernel is essential when modeling human dispersals.

We also have provided new explicit equations for the front speed for the Gauss and Laplace 2D distributions and the cohabitation model (3.4) (section 3.4).

Acknowledgments

Chapter 4

Time-delayed reaction-diffusion fronts [*Phys Rev E 2009; 80: 057103*]

This chapter is an exact transcription of the contents of the following paper (please, find a copy of the published version in appendix A):

Isern N, Fort J. Time-delayed reaction-diffusion fronts. Phys Rev E 2009; 80: 057103.

Abstract A time-delayed second-order approximation for the front speed in reaction-dispersion systems was obtained by Fort and Méndez [Phys. Rev. Lett. **82**, 867 (1999)]. Here we show that taking proper care of the effect of the time delay on the reactive process yields a different evolution equation and, therefore, an alternate equation for the front speed. We apply the new equation to the Neolithic transition. For this application the new equation yields speeds about 10% slower than the previous one.

4.1   Introduction

Reaction-diffusion systems have been applied to many complex biological and physical systems such as population dispersals [12], viral infections [43], chemical reaction processes [54], combustion flames [42], etc. In reference [7] a time-delayed model for the front speed was presented including terms up to second order. However, here we will show that there was an error in the mathematical derivation, and we will derive and analyze the behavior of the correct time-delayed equation for the front speed.

In biological systems, variations in the population number density, p, are due to two processes: population growth (reproduction minus deaths) and migration (dispersion). The variation due to population growth can be expressed as a Taylor series,

$$[p\,(x,y,t+T) - p\,(x,y,t)]_g = T\,\frac{\partial p}{\partial t}\bigg|_g + \frac{T^2}{2}\,\frac{\partial^2 p}{\partial t^2}\bigg|_g + \cdots$$

$$= TF + \frac{T^2}{2}\,\frac{\partial F}{\partial t}\bigg|_g + \cdots \qquad (4.1)$$

where the subindex g denotes growth, we have introduced the growth function as $F\,(p) = \frac{\partial p}{\partial t}\big|_g$, and T is the time delay (one generation in most applications [7]). As usual, we assume that $F\,(p) > 0$.

On the other hand, for the migration (dispersion) we will define the dispersion kernel $\phi\,(\Delta_x,\Delta_y)$ which gives the probability per unit area that an individual initially placed at $(x+\Delta_x,y+\Delta_y)$ has moved to (x,y) after a time interval T. Thus, the variation in population number density due to migration can be expressed as [7]

$$[p\,(x,y,t+T) - p\,(x,y,t)]_m = \iint p\,(x+\Delta_x,y+\Delta_y,t)\,\phi\,(\Delta_x,\Delta_y)\,\mathrm{d}\Delta_x\mathrm{d}\Delta_y$$

$$- p\,(x,y,t)\,. \qquad (4.2)$$

In a system involving the two processes (population growth and migration), the total variation in population density during a time interval T can be expressed as the sum of both contributions,

$$p\,(x,y,t+T) - p\,(x,y,t) = \iint p\,(x+\Delta_x,y+\Delta_y,t)\,\phi\,(\Delta_x,\Delta_y)\,\mathrm{d}\Delta_x\mathrm{d}\Delta_y - p\,(x,y,t)$$

$$+ TF + \frac{T^2}{2}\,\frac{\partial F}{\partial t}\bigg|_g + \cdots \qquad (4.3)$$

We assume that the kernel is isotropic, i.e., $\phi\,(\Delta_x,\Delta_y) = \phi\,(\Delta)$, with $\Delta = \sqrt{\Delta_x^2 + \Delta_y^2}$, and we Taylor-expand equation (4.3) up to second order in time and space, thus, obtaining the following reaction-diffusion equation:

$$\frac{\partial p}{\partial t} + \frac{T}{2}\frac{\partial^2 p}{\partial t^2} = D\left(\frac{\partial^2 p}{\partial x^2} + \frac{\partial^2 p}{\partial y^2}\right) + F + \frac{T}{2}\,\frac{\partial F}{\partial t}\bigg|_g\,, \qquad (4.4)$$

where D is the diffusion coefficient $D = \frac{\langle \Delta^2 \rangle}{4T} = \frac{\langle \Delta_x^2 \rangle}{2T} = \frac{\langle \Delta_y^2 \rangle}{2T}$.

Since $F\,(p)$ depends only on the population density p, then the last term in equation (4.4) can be written as

$$\frac{T}{2}\,\frac{\partial F}{\partial t}\bigg|_g = \frac{T}{2}\,\frac{\mathrm{d}F}{\mathrm{d}p}\,\frac{\partial p}{\partial t}\bigg|_g = \frac{T}{2}F'F\,. \qquad (4.5)$$

In addition, as the density at the leading edge of the front is low, $p \approx 0$, we have that $F(p) \approx pF'(0)$ and $F'(p) \approx F'(0)$. Therefore, for $p \approx 0$ equation (4.4) may be rewritten as

$$\frac{\partial p}{\partial t} + \frac{T}{2}\frac{\partial^2 p}{\partial t^2} = D\left(\frac{\partial^2 p}{\partial x^2} + \frac{\partial^2 p}{\partial y^2}\right) + pF'(0) + \frac{T}{2}pF'(0)F(0), ^* \qquad (4.6)$$

We now assume that for $t \to \infty$ and $r \to \infty$ the front can be considered locally planar. Thus, choosing the x axis parallel to the local speed of the front, $c \equiv |c_x|$, we can look for constant-shape solutions with the form $p = \bar{p}\exp[\lambda(x - ct)]$. Applying this *ansatz* to equation (4.6) we see that the value of λ can be obtained from

$$\lambda = \frac{-c \pm \sqrt{c^2 - 4\left(D - \frac{T}{2}c^2\right)F'(0)\left[1 + \frac{T}{2}F'(0)\right]}}{2\left(D - \frac{T}{2}c^2\right)}. \qquad (4.7)$$

As λ has to be real, we obtain a lower bound for the front speed

$$c \geqslant \frac{2\sqrt{DF'(0)\left[1 + \frac{T}{2}F'(0)\right]}}{1 + TF'(0)}. \qquad (4.8)$$

However, the result obtained in reference [7] was the so-called HRD speed, namely

$$c_{HRD} \geqslant \frac{2\sqrt{DF'(0)}}{1 + \frac{T}{2}F'(0)}, \qquad (4.9)$$

which is different from equation (4.8).

The reason of this difference is the following. Here we have used equation (4.5), which allows us to rewrite equation (4.4) as

$$\frac{\partial p}{\partial t} + \frac{T}{2}\frac{\partial^2 p}{\partial t^2} = D\left(\frac{\partial^2 p}{\partial x^2} + \frac{\partial^2 p}{\partial y^2}\right) + F(p) + \frac{T}{2}\frac{\mathrm{d}F}{\mathrm{d}p}F. \qquad (4.10)$$

In contrast, in reference [7] the following equation was used:

$$\frac{\partial p}{\partial t} + \frac{T}{2}\frac{\partial^2 p}{\partial t^2} = D\left(\frac{\partial^2 p}{\partial x^2} + \frac{\partial^2 p}{\partial y^2}\right) + F(p) + \frac{T}{2}\frac{\mathrm{d}F}{\mathrm{d}p}\frac{\partial p}{\partial t}. \qquad (4.11)$$

We can see that the last term is different. The reason is that in reference [7] the subindex g was omitted in the last term in equation (4.4). Therefore, in reference [7], the last term in equation (4.4) was not written as in equation (4.5) but as follows:

$$\frac{T}{2}\frac{\partial F}{\partial t} = \frac{T}{2}\frac{\mathrm{d}F}{\mathrm{d}p}\frac{\partial p}{\partial t} = \frac{T}{2}F'\frac{\partial p}{\partial t}, \qquad (4.12)$$

---

*In the published version of this work (Appendix A) there is a typographical error in this equation; in the correct version the last term should be $(T/2)\,pF'(0)\,F'(0)$.

37

and thus leading to equation (4.11) instead of (4.10). This is why in reference [7], speed (4.9) was obtained instead of equation (4.8). However, the derivation above clearly shows that equation (4.8) is the right result. In this Brief Report, we will apply variational analysis and show that equation (4.8) is not only a lower bound but the exact speed (section 4.2). We will also analyze the difference between the new equation (4.8) and the HRD speed (4.9) by applying both equations to the Neolithic transition (section 4.3). In section 4.4 we present our conclusions.

4.2 Variational analysis. Upper bound

Equation (4.8) is just a lower bound for the speed of front solutions to the new differential equation (4.4) [or equation (4.10)]. In order to find an upper bound, we apply variational analysis [31] to equation (4.10). As mentioned above, we assume that the fronts have a profile $p(z) = p(x - ct)$ travelling with a speed $c > 0$, so all of the derivatives in equation (4.10) can be expressed in terms of z. We also assume that the population number density $p > 0$ cannot attain values above some value $p_{\max}$, the so-called saturation density. Then, defining $n(p) = -p_z$ and assuming that $n(0) = n(p_{\max}) = 0$ and $n > 0$ in $(0, \ p_{\max})$, the differential equation (4.10) can be rewritten as

$$\left(D - c^2 \frac{T}{2} \right) n \frac{\partial n}{\partial p} - cn + F \left(1 + \frac{T}{2} F' \right) = 0. \tag{4.13}$$

Now, introducing an arbitrary function $g(p)$ such that $g(p) > 0$ and $h(p) = -g'(p) > 0$, we multiply equation (4.13) by $g(p)/n(p)$. Integrating the resulting expression by parts, we obtain

$$c \int_0^{p_{\max}} g \mathrm{d}p = \int_0^{p_{\max}} \left[\left(D - \frac{T}{2} c^2 \right) h \ n + \frac{g}{n} F \left(1 + \frac{T}{2} F' \right) \right] \mathrm{d}p, \tag{4.14}$$

Now, we can eliminate $n(p)$ from equation (4.14) applying that for any positive numbers r and s, it follows from $(r - s)^2 \geq 0$ that $(r + s) \geq 2\sqrt{rs}$. Let us assume that the condition

$$1 + \frac{T}{2} F'(p) > 0 \tag{4.15}$$

holds for all $p \in (0, \ p_{\max})$. As $g(p)$, $h(p)$, $n(p)$, $F(p)$ and $\left(D - \frac{T}{2} c^2 \right)$ are positive[1], we may choose $r \equiv \left(D - \frac{T}{2} c^2 \right) hn$ and $s \equiv \frac{g}{n} F \left(1 + \frac{T}{2} F' \right)$ into $(r + s) \geq 2\sqrt{rs}$ and use equation (4.14) to get the following restriction,

$$\frac{c}{\sqrt{\left(D - \frac{T}{2} c^2 \right)}} \geqslant \frac{2 \int_0^{p_{\max}} \sqrt{hgF \left(1 + \frac{T}{2} F' \right)} \mathrm{d}p}{\int_0^{p_{\max}} g \mathrm{d}p}. \tag{4.16}$$

---

[1]The condition $\left(D - T \ c^2/2 \right) > 0$ follows from $\lambda < 0$ and equation (4.7).

Following the method in reference [30], section 3.3, it is easy to show that there is a function g for which the equality holds. Then

$$\frac{c}{\sqrt{\left(D - \frac{T}{2}c^2\right)}} = \max_g \left(\frac{2\int_0^{p_{\max}} \sqrt{hgF\left(1 + \frac{T}{2}F'\right)}\mathrm{d}p}{\int_0^{p_{\max}} g\mathrm{d}p}\right). \tag{4.17}$$

In order to obtain the upper bound for the front speed we will use Jensen's inequality [55][2]

$$\frac{\int_0^{p_{\max}} \mu\left(p\right)\sqrt{\alpha\left(p\right)}\mathrm{d}p}{\int_0^{p_{\max}} \mu\left(p\right)\mathrm{d}p} \leqslant \sqrt{\frac{\int_0^{p_{\max}} \mu\left(p\right)\alpha\left(p\right)\mathrm{d}p}{\int_0^{p_{\max}} \mu\left(p\right)\mathrm{d}p}}, \tag{4.18}$$

where $\mu(p) > 0$ and $\alpha(p) \geqslant 0$. We define $\mu(p) \equiv g(p)$ and $\alpha(p) \equiv \left\{h(p)F(p)\left[1 + \frac{T}{2}F'(p)\right]\right\}/g(p)$. Using these functions into Jensen's inequality (4.18), and applying the result to equation (4.17), we obtain that

$$\frac{c}{\sqrt{\left(D - \frac{T}{2}c^2\right)}} \leqslant 2\max_g \sqrt{\frac{\int_0^{p_{\max}} hF\left(1 + \frac{T}{2}F'\right)\mathrm{d}p}{\int_0^{p_{\max}} g\mathrm{d}p}}. \tag{4.19}$$

We want an upper bound independent of $g\left(p\right)$, so we will first find an expression in which $h\left(p\right) = -g'\left(p\right)$ no longer appears by integrating by parts the numerator in the right-hand-side of equation (4.19),

$$\int_0^{p_{\max}} hF\left(1 + \frac{T}{2}F'\right)\mathrm{d}p = \int_0^{p_{\max}} g\left[F'\left(1 + \frac{T}{2}F'\right) + \frac{T}{2}FF''\right]\mathrm{d}p, \tag{4.20}$$

where we have assumed that $F\left(0\right) = F\left(p_{\max}\right) = 0$ (this holds for example for the logistic growth, considered in section 4.3).

Moreover, from equation (4.20) we obviously have

$$\int_0^{p_{\max}} hF\left(1 + \frac{T}{2}F'\right)\mathrm{d}p \leqslant \sup_{p\in(0,p_{\max})}\left[F'\left(1 + \frac{T}{2}F'\right) + \frac{T}{2}FF''\right]\int_0^{p_{\max}} g\mathrm{d}p, \tag{4.21}$$

so now the upper bound in (4.19) is independent of $g\left(p\right)$,

$$\frac{c}{\sqrt{\left(D - \frac{T}{2}c^2\right)}} \leqslant 2\sqrt{\sup_{p\in(0,p_{\max})}\left[F'\left(1 + \frac{T}{2}F'\right) + \frac{T}{2}FF''\right]}. \tag{4.22}$$

Let us assume that the population growth function $F\left(p\right)$ is a continuous function with $F''\left(p\right) \leqslant 0$ and $F\left(0\right) = 0$ (again these assumptions are true for the logistic growth, considered in section 4.3). Then $F'\left(p\right)$ is a decreasing function for increasing values of

---

[2]See p. 1133 formula HL151 in this reference. The inequality is given for convex functions ϕ. If ϕ is a convex function, then $-\phi$ is concave and the inequality for $-\phi$ holds with the sign reversed. Take the function $-\phi$ to be the square root.

p. Its maximum value is reached for $p = 0$. Thus, using the value $p = 0$ in equation (4.22) we obtain that the upper bound for the front speed is

$$c \leqslant \frac{2\sqrt{DF'(0)\left[1 + \frac{T}{2}F'(0)\right]}}{1 + TF'(0)}. \tag{4.23}$$

As the lower bound given by equation (4.8) is the same as the upper bound (4.23), we can predict the speed of front solutions to equation (4.10) without any uncertainty,

$$c = \frac{2\sqrt{DF'(0)\left[1 + \frac{T}{2}F'(0)\right]}}{1 + TF'(0)}. \tag{4.24}$$

In contrast, for the HRD equation (4.11), the exact speed was previously shown to be [7]

$$c_{HRD} = \frac{2\sqrt{DF'(0)}}{1 + \frac{T}{2}F'(0)}. \tag{4.25}$$

4.3   Application to the Neolithic transition

In order to compare the predictions from equations (4.24) and (4.25), we will apply them to the spread of the Neolithic transition in Europe, because this is the case to which equation (4.25) was initially applied [7]. The Neolithic transition is the change from hunter-gatherer to farming economics. In Europe, it took place as an invasion of agricultural populations from the Southeast, which spread across Europe from 13000 to 5000 years before present [9].

In order to make quantitative predictions we will use the logistic growth function, which has been widely applied to human populations [7, 21]:

$$F(p) = ap\left(1 - \frac{p}{p_{\max}}\right), \tag{4.26}$$

where a is called the initial growth rate and $p_{\max}$ is the saturation density.

Using the logistic function (4.26), equation (4.24) can be rewritten as

$$c = \frac{2\sqrt{aD\left(1 + \frac{aT}{2}\right)}}{1 + aT}, \tag{4.27}$$

whereas the HRD speed (4.25), used in reference [7], is

$$c_{HRD} = \frac{2\sqrt{aD}}{1 + \frac{aT}{2}}. \tag{4.28}$$

Both equations for the front speed depend on three parameters: the initial growth rate, a, the diffusion coefficient, $D = \frac{\langle \Delta^2 \rangle}{4T}$, and the generation time, T. We will use the
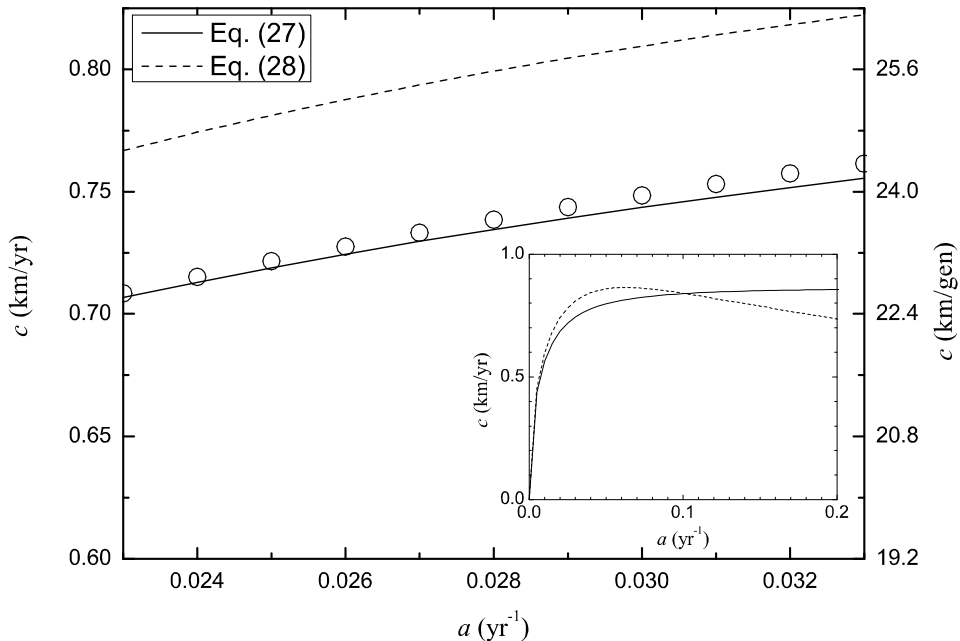
Figure 4.1: Comparative plot between the front speed for equations (4.27) (solid line) and (4.28) (dashed line). The symbols correspond to the speed obtained from numerically integrating equation (4.10), with $F(p)$ given by equation (4.26). All results have been calculated for a characteristic mobility value $\langle \Delta^2 \rangle = 1531$ km^2.

ranges $a = 0.028 \pm 0.005$ yr^{-1} [56], $\langle \Delta^2 \rangle = 900 - 2200$ km^2 [9][3], and the characteristic value $T = 32$ yr [11][4], which have been measured for preindustrial farming populations. For these ranges, the condition (4.15) is fulfilled, so equation (4.27) gives the speed of fronts.

Figure 4.1 shows the front speeds obtained from equations (4.27) and (4.28), for a characteristic mobility value $\langle \Delta^2 \rangle = 1531$ km^2. We can see that, for the range of values for the initial growth rate a appropriate to this application, the new equation (4.27) yields slower speeds than equation (4.28) (about 8% slower). However, this is not the case for all values of a, as can be seen from the inset graph in figure 4.1.

In order to check the validity of equation (4.27), we have also numerically integrated equation (4.10), with $F(p)$ given by equation (4.26), and initially $p = p_{\max}$ in a finite region and $p = 0$ elsewhere. The speed obtained from the numerical integrations corresponds to the circles in figure 4.1. They agree with the new equation (4.27) within less than 0.8%.

The range of speeds for the Neolithic transition front obtained from archaeological data is $0.6 - 1.3$ km/yr [9]. We can see in figure 4.1 that the results from equation (4.27) lie within this range.

To what extent does our new result depend on the uncertainty in the value of the mobility? In Fig 4.2, we consider the front speed values 0.6, 0.95 and 1.3 km/yr,

---

[3]For the estimation of mobility data see Supporting Text 3 for this reference.

[4]For the estimation of the generation time $T = 32$ yr, see note [24] in this reference.
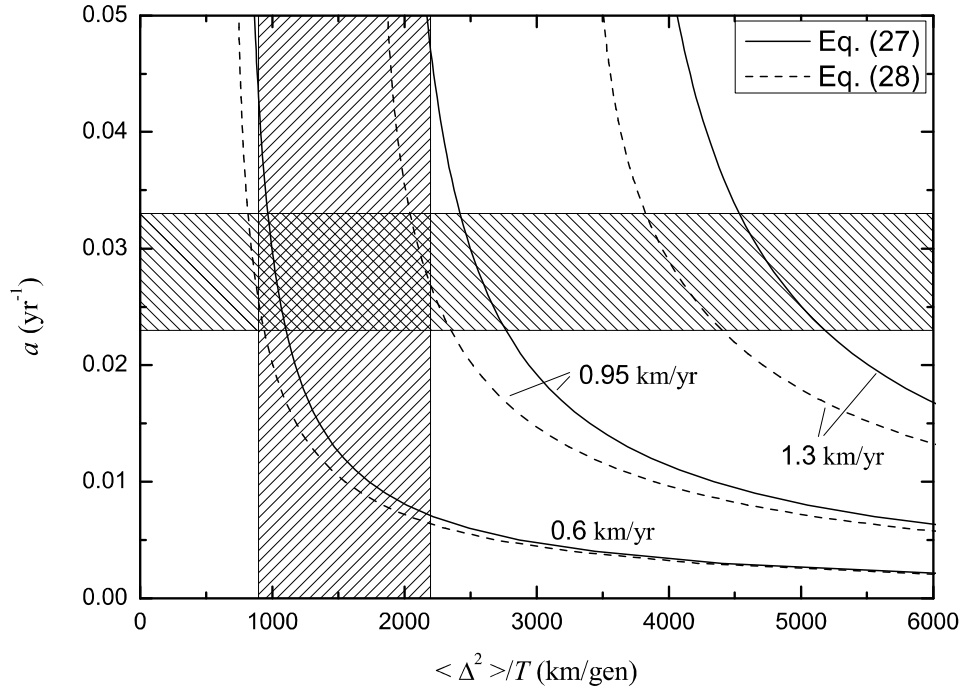
Figure 4.2: Predictions for the speed of the wave of advance in the Neolithic transition. The labeled curves correspond to the maximum, minimum and mean speeds from Neolithic data $(0.6-1.3 \text{ km/yr})$. The hatched regions correspond to realistic ranges of the initial growth rate and mobility for the Neolithic transition.

corresponding to the range obtained from archaeological data, for equations (4.27) (full lines) and (4.28) (dashed lines).[5] It is seen that the predictions of the new model (full lines) are consistent with the observed front speed for most of the values of the mobility appropriate to this system.

4.4   Concluding remarks

In this Brief Report we have improved the derivation of the HRD speed in reference [7]. We have obtained the correct evolution equation (4.10) and the new equation (4.24) for the front speed.

We have applied the new equation (4.24) to the Neolithic transition. Using realistic parameters the front speeds are consistent with the observed range for the Neolithic transition in Europe $(0.6-1.3 \text{ km/yr}$ [9]). Comparing these results with those from the HRD speed, we see that for the Neolithic transition our new equation leads to slower speeds.

In this case, the correction obtained is only about a 10%, but it could be higher in

---

[5]The dashed lines in figure 4.2 are not exactly the same as the lines in figure 3 in reference [7] because some parameter values have been estimated in a more precise way more recently, especially the generation time T [11].

other systems where generalizations of equation (4.24) can be useful. For example, our framework could be applied in order to improve the predicted speeds of viral infection fronts [43].

Acknowledgements

Chapter 5

Anisotropic dispersion, space competition, and the slowdown of the Neolithic transition [*New J Phys 2010; 12: 123002*]

This chapter is an exact transcription of the contents of the following paper (please, find a copy of the published version in appendix A):

> Isern N, Fort J. Anisotropic dispersion, space competition and the slowdown of the Neolithic transition. New J Phys 2010; 12: 123002.

Abstract The front speed of the Neolithic (farmer) spread in Europe decreased as it reached Northern latitudes, where the Mesolithic (hunter-gatherer) population density was higher. Here, we describe a reaction-diffusion model with (i) an anisotropic dispersion kernel depending on the Mesolithic population density gradient and (ii) a modified population growth equation. Both effects are related to the space available for the Neolithic population. The model is able to explain the slowdown of the Neolithic front as observed from archaeological data.

5.1 Introduction

The spread of the Neolithic, one of the most important socioeconomic changes in human history, has been widely studied using physical models in recent years (for a review, see [57]). The Neolithic expansion has been tackled from different approaches such as age-structured population models [39], population spread along rivers [12] and settlement formation [15].
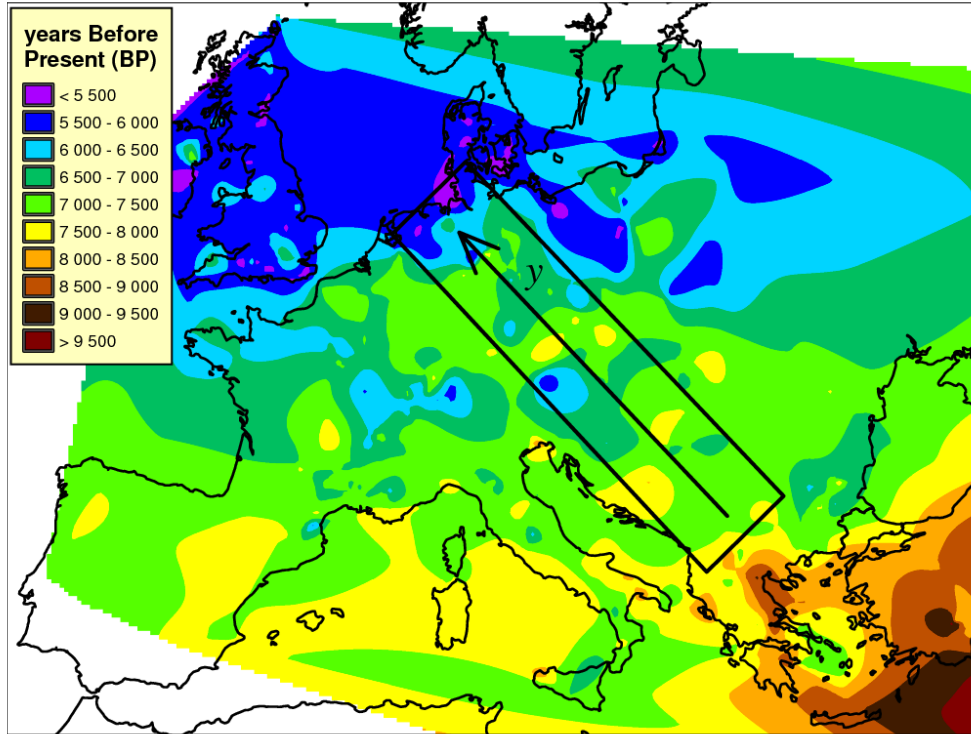
Figure 5.1: Chronology of the Neolithic wave of advance in Europe. Map obtained by interpolation of 765 early Neolithic data published by Pinhasi [9]. The arrow corresponds to the y-direction in our model.

Here we will focus on the fact that the spread of the Neolithic in Europe was not homogeneous from the macroscopic point of view. Archaeological observations show that, as the front propagated from the Near East across Europe, its speed slowed down as higher latitudes were reached [58].

This decrease of the front speed can be intuitively seen from figure 5.1, which shows the arrival time of the Neolithic across Europe. The arrow on the map represents the average direction along which the expansion from the Near East to the Baltic sea took place (within the rectangle). In figure 5.1 it can be seen that the distance advanced during 500 years is lower when reaching northern latitudes (a quantitative analysis will be presented in section 5.5).

Although it would seem that the more intuitive reason for the decrease in speed is the time needed by crops to adapt to temperate climates, evidence exists that this effect was, in fact, minimal [59]. Indeed, when establishing their settlements at colder regions, Neolithic populations just cultivated the more adaptable crops and dropped the rest.

From archaeological studies, one of the most accepted reasons for the presence of a gradient in the front speed when spreading to the North of Europe is the presence of Mesolithic hunter-gatherer populations [60], which had higher densities at Northern latitudes. Thus, motivated by the observational data, in this paper we extend a ho-

mogeneous model [7] to study how the presence of indigenous Mesolithic populations affects the speed of the Neolithic invasion front.

We describe a reaction-diffusion model for Neolithic population density with a direction-dependent dispersion kernel determined by the space dependence of the Mesolithic population density. We also introduce in this model the effect of the presence of Mesolithic populations on the Neolithic population growth process. We compare the results from the model with archaeological data [9].

5.2 Anisotropic dispersion kernel

In case we assumed that the spread of the Neolithic front took place in an homogeneous space, it would be reasonable to consider that the probability ϕ to jump would be the same in all directions; thus, mathematically we would have [7, 56]

$$\phi\left(x, y; \theta, \Delta\right) = \frac{1}{2\pi} \psi\left(\Delta\right), \tag{5.1}$$

that is, the jump probability could be expressed as a function ψ that depends only on the jump distance, Δ, and is independent on the jump direction θ or the position in space (x, y). We have assumed that $\int_0^1 \Delta \psi\left(\Delta\right) \mathrm{d}\Delta = 1$.

However, Neolithic individuals do no move in an homogeneous space, since the density of Mesolithic individuals they encounter depends on the position and direction they move. Then, for a given position (x, y), the Neolithic individuals will preferably move in the direction along which they encounter a lower Mesolithic population density, i.e., along the direction where more free space is available.

Thus, we can assume that, in this situation, the jump distance probability distribution (5.1) will be modulated by the available space, s, at the final jump point $\left(x + \Delta_x, y + \Delta_y\right)$, in each direction $\theta = \tan^{-1}\left(\Delta_y / \Delta_x\right)$ and for every jump distance $\Delta = \sqrt{\Delta_x^2 + \Delta_x^2}$. Thus, the dispersion kernel is now of the form

$$\phi\left(x, y; \theta, \Delta\right) = \alpha \; s\left(x + \Delta_x, y + \Delta_y\right) \; \psi\left(\Delta\right), \tag{5.2}$$

where α is a normalization constant.

We now need a mathematical expression for the available space $s\left(x + \Delta_x, y + \Delta_y\right)$. If M_{max} is the carrying capacity for Mesolithic populations, and $M\left(x, y\right)$ the actual density of Mesolithic individuals at the position (x, y), then the fraction of occupied space at this point can be expressed as

$$m\left(x, y\right) = \frac{M\left(x, y\right)}{M_{\mathrm{max}}}. \tag{5.3}$$

Thus, the fraction of space available for Neolithic settlements is

$$s\left(x + \Delta_x, y + \Delta_y\right) = 1 - m\left(x + \Delta_x, y + \Delta_y\right) \tag{5.4}$$

and the space-dependent jump distance probability (5.2) can be written as

$$\phi\left(x, y; \theta, \Delta\right) = \alpha\left[1 - m\left(x + \Delta_x, y + \Delta_y\right)\right] \psi\left(\Delta\right). \tag{5.5}$$

For simplicity, we assume that the variation in Mesolithic population density takes place mainly in one direction, y, in figure 5.1, whereas it remains approximately constant along the x-direction, i.e.

$$\phi\left(x, y; \theta, \Delta\right) = \alpha\left[1 - m\left(y + \Delta_y\right)\right]\psi\left(\Delta\right). \tag{5.6}$$

Now, Taylor-expanding the term within square brackets in equation (5.6), we obtain that the space-dependent jump distance probability is approximately

$$\phi\left(x, y; \theta, \Delta\right) = \alpha\left[1 - m\left(y\right) - \frac{\partial m}{\partial y}\Delta \sin\theta\right]\psi\left(\Delta\right). \tag{5.7}$$

Normalizing equation (5.7), we obtain that the normalization constant α is,

$$\alpha = \frac{1}{2\pi}\frac{1}{1 - m\left(y\right)}, \tag{5.8}$$

and the jump distance probability becomes

$$\phi\left(x, y; \theta, \Delta\right) = \frac{1}{2\pi}\left[1 - \frac{\partial m/\partial y}{1 - m\left(y\right)}\Delta \sin\theta\right]\psi\left(\Delta\right). \tag{5.9}$$

We can see from equation (5.9) that if the Mesolithic (indigenous) population density M increases along direction y, then the probability of Neolithic invaders to jump forward $(\theta = \pi/2)$ is minimum and the probability to jump backwards $(\theta = 3\pi/2)$ is maximum.

5.3   Population growth

In population dynamics, a commonly used expression to describe the first-order variation in population density due to population growth (reproduction minus deaths), is the logistic growth equation [7, 21, 61],

$$F\left(N\right) = \left.\frac{\partial N}{\partial t}\right|_g = aN\left(1 - \frac{N}{N_{\max}}\right) \tag{5.10}$$

where a is the initial growth rate, $N_{\max}$ the carrying capacity and N the density of the Neolithic population. The subindex g stands for population growth, i.e. for variations in population density N due to births and deaths (but not to dispersal).

The logistic equation (5.10) describes an exponential growth for low values of population density, whereas it is self-limiting for large densities, saturating at $N_{\max}$. Note that the limiting term (within brackets) in equation (5.10) is similar to the expression (5.4) for the available space that we have used in the previous section. Therefore, one can say that population growth, according to equation (5.10), is limited by the fraction of available space [61].

Now, equation (5.10) corresponds to a single population reproducing without external competition. But when we have a second population using the same space and

resources, the presence of this additional population must also contribute to limiting the growth process. Thus, we can modify equation (5.10) so that the growth function of the Neolithic population, N, also includes the effect of the fraction of space occupied by Mesolithic populations, M [61]. A population density M occupies a fraction M/M_{max} of the space available, in addition to that occupied by N. Therefore, N within the parentheses in equation (5.10) should be replaced by $(N + (M/M_{\mathrm{max}}) N_{\mathrm{max}})$. Then,

$$F(N) = aN \left(1 - \frac{N}{N_{\mathrm{max}}} - \frac{M}{M_{\mathrm{max}}} \right). \tag{5.11}$$

Growth functions similar to (5.11) have been applied to competing microorganisms [61].

5.4   Evolution equation

We can describe the variation in the Neolithic population density N, during a generation time T, as the sum of the variation due to the dispersion process and due to population growth (see [7] for details),

$$
\begin{aligned}
N(x, y, t + T) &- N(x, y, t) \\
&= \int \int N(x - \Delta_x, y - \Delta_y, t)\, \phi(x, y; \theta, \Delta)\, \mathrm{d}\Delta_x \mathrm{d}\Delta_y - N(x, y, t) \\
&+ [N(x, y, t + T) - N(x, y, t)]_g,
\end{aligned}
\tag{5.12}
$$

where, as in equation (5.10), the subindex g stands for population growth (as opposed to dispersal, which corresponds to the first two terms on the right-hand side).

Now, if we Taylor-expand equation (5.12) up to first order in time and to second order in space, we find that

$$\frac{\partial N}{\partial t} = -U_x \frac{\partial N}{\partial x} - U_y \frac{\partial N}{\partial y} + U_{xy} \frac{\partial^2 N}{\partial x \partial y} + D_x \frac{\partial^2 N}{\partial x^2} + D_y \frac{\partial^2 N}{\partial y^2} + F(N). \tag{5.13}$$

We could also have Taylor-expanded equation (5.12) up to second order in time [7], finding in this case slightly lower speeds; however, the conclusions we find here would not change.

The direction-dependent diffusion coefficients D_x and D_y, for our kernel (5.9), are

$$D_x = \frac{\langle \Delta_x^2 \rangle}{2T} = \frac{\langle \Delta^2 \rangle}{4T} \equiv D \tag{5.14}$$

$$D_y = \frac{\langle \Delta_y^2 \rangle}{2T} = \frac{\langle \Delta^2 \rangle}{4T} \equiv D \tag{5.15}$$

where T is the generation time, and the mean value of a variable, for example $\langle \Delta_x^2 \rangle$, is defined as

$$\langle \Delta_x^2 \rangle = \int_{-\infty}^{\infty} \int_{-\infty}^{\infty} \Delta_x^2 \phi(\Delta_x, \Delta_y)\, \mathrm{d}\Delta_x \mathrm{d}\Delta_y. \tag{5.16}$$

The advection terms U_x, U_y and U_{xy}, using the kernel (5.9), are

$$U_x = \frac{\langle \Delta_x \rangle}{T} = 0 \qquad (5.17)$$

$$U_y = \frac{\langle \Delta_y \rangle}{T} = -2D\frac{\partial m/\partial y}{1 - m(y)} \qquad (5.18)$$

$$U_{xy} = \frac{\langle \Delta_x \Delta_y \rangle}{T} = 0 \qquad (5.19)$$

As could be expected from the fact that the jump probability distribution (5.9) depends only on $\Delta_y = \Delta \sin\theta$ but not on Δ_x, we have obtained advection only in the y-direction, equation (5.18).

5.5   Front speed

As usual, we apply that for $t \to \infty$ the front can be considered locally planar; thus for $y \to \infty$ we can consider the variation in the x-direction negligible [41], and the evolution equation (5.13) for $y \to \infty$ becomes

$$\frac{\partial N}{\partial t} = 2D\frac{\partial m/\partial y}{1 - m(y)}\frac{\partial N}{\partial y} + D\frac{\partial^2 N}{\partial y^2} + F(N), \qquad (5.20)$$

where we will use equation (5.11) for the growth function $F(N)$.

As usual [41], we look for constant-shaped solutions to equation (5.20) with the form $N = N_0 \exp\left[-\lambda(y - ct)\right]$ for $N \simeq 0$. As the Neolithic population density N at the leading edge of the front is low, $F(N)$ in equation (5.11) can be linearized, and we obtain from equation (5.20),

$$\lambda = \frac{(c - U_y) \pm \sqrt{(c - U_y)^2 - 4aD(1 - m)}}{2D}. \qquad (5.21)$$

In order for λ to be real, the term within the squared-root must be non-negative, so the front speed c is

$$c = 2\sqrt{aD}\sqrt{1 - m(y)} - 2D\frac{\partial m/\partial y}{1 - m(y)}. \qquad (5.22)$$

Equation (5.22) can be also obtained, without need of equation (5.21), by noting that equation (5.20) is simply Fisher's equation with (i) a modified growth term (5.11), which after linearization leads to a modified initial growth rate $\tilde{a} = a(1 - m(y))$, and (ii) an advection velocity $v = 2D\frac{\partial m/\partial y}{1-m(y)}$. Thus, the speed of front solutions to equation (5.20) must de Fisher's, namely $2\sqrt{\tilde{a}D}$, minus the advection velocity, in agreement with equation (5.22). Moreover, the front speed obtained from the linear analysis described above is a lower bound to the front speed c. However, it is easy to apply variational
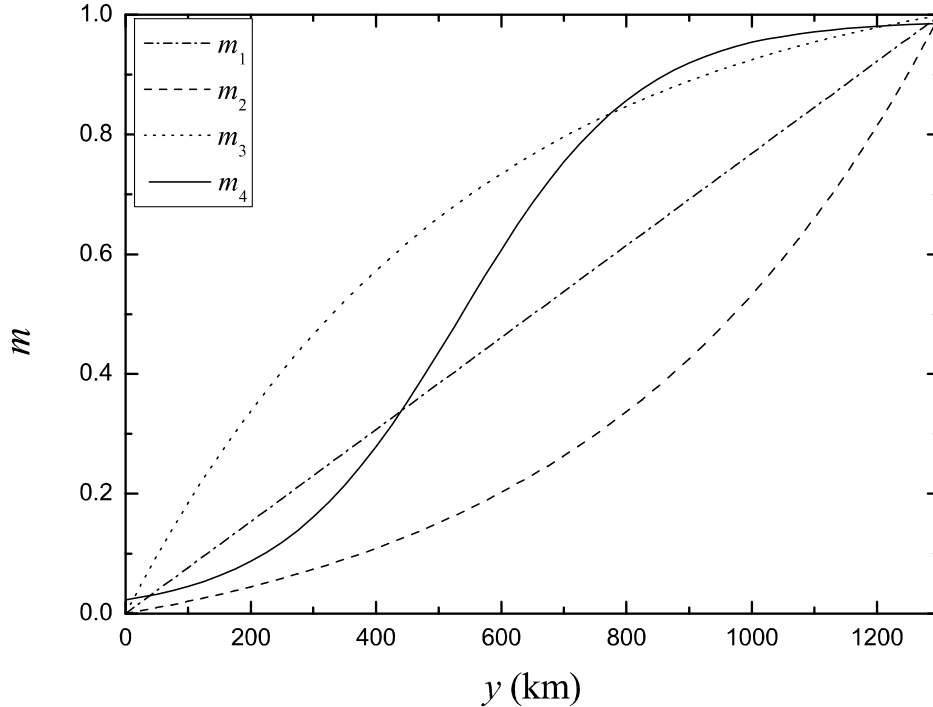
Figure 5.2: Test functions used for the increase of the reduced Mesolithic population density ($m = M/M_{\mathrm{max}}$) along the y-direction. $A_1 = 0.999/1300$, $B_1 = 0$; $A_2 = -0.1 = -B_2 = A_3 = B_3$, $\tau_2 = -\ln(10.99)/1300 = -\tau_3$; $A_4 = 0.99$, $B_4 = 42$, $\tau_4 = 1/0.007$.[*]

analysis [32] and derive an upper bound with the same result, so equation (5.22) is the exact front speed for equation (5.20).

From equation (5.22), we see that if the Mesolithic population density increases with y, then the front speed decreases due to two effects: (i) the higher the gradient of the reduced Mesolithic density m, the higher the correction on the front speed; (ii) the speed also changes if there is less available space for the Neolithic population, i.e. for lower values of $s = (1 - m(y))$ (if $s = 1$, this second effect disappears).

To see the actual behavior of the front speed, equation (5.22), we need an expression for the variation of the Mesolithic population density M with y. However, the precise function $M(y)$ is unknown because published data on Mesolithic settlements are scarce and restricted to very specific local areas, and also because the estimation of population densities from archaeological data relies on assumptions which are difficult to test and cause important methodological problems [62]. However, as explained in the introduction, we do know that the Mesolithic density increased at northern latitudes [60]. Thus, we apply equation (5.22) to four different test functions for the reduced

---

[*]In the published version of this work (Appendix A) some errors appeared in the caption to this figure. The right values are $A_3 = B_3 = 1.1$, $\tau_2 = 1300/\ln(10.99)$ and $\tau_3 = 1300/\ln(11/1.01)$.
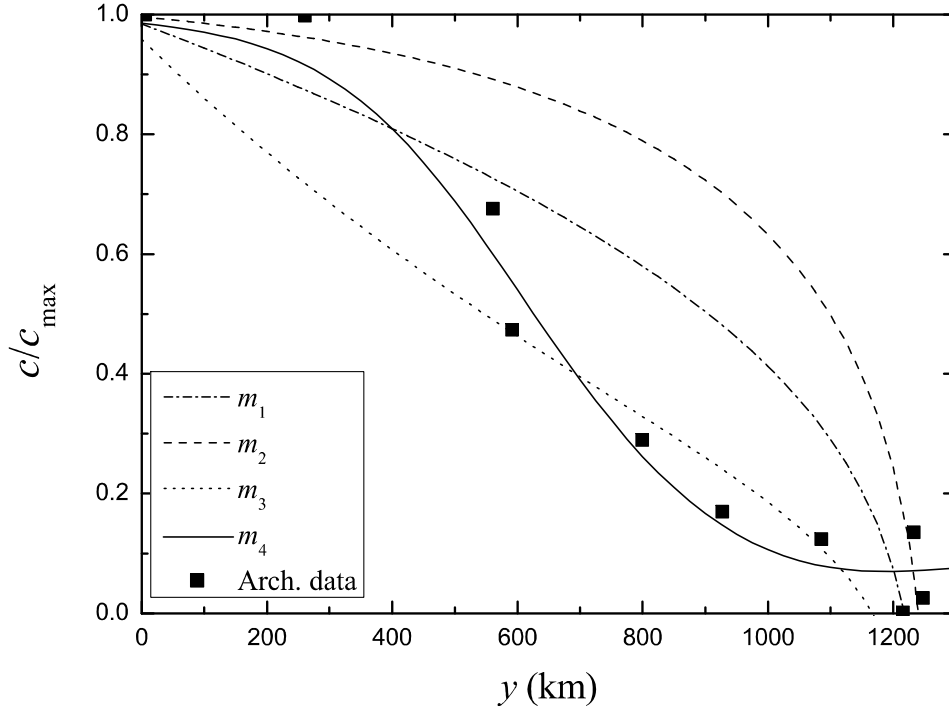
Figure 5.3: Curves: relative Neolithic front speed predicted by a model with the dispersion and growth processes dependent on the presence of Mesolithic populations, equation (5.25). Symbols: observed front speeds calculated from archaeological data [9].

Mesolithic density $m(y) = M(y)/M_{\max}$ (see figure 5.2),

$$
\begin{aligned}
m_1 &= A_1 y + B_1, \\
m_2 &= A_2 + B_2 \exp\left(y/\tau_2\right), \\
m_3 &= A_3 - B_3 \exp\left(-y/\tau_3\right), \\
m_4 &= \frac{A_4}{1 + B_4 \exp(-y/\tau_4)}.
\end{aligned}
\tag{5.23}
$$

To estimate the anthropological parameters a and D appearing in equation (5.22), we apply that the initial growth rate for preindustrial populations has a mean value of $a = 0.028$ year^{-1} [56], the mean-squared jump distance is $\langle \Delta^2 \rangle = 1531$ km^2 [7] and the mean generation time is $T = 32$ years [11][1].

As we expected from equation (5.22), we see in figure 5.3 that each of the four test functions leads to a decrease in the front speed along the y-direction. To better compare the results with archaeological data, in figure 5.3 we have plotted $c/c_{\max}$, where the maximum speed from equation (5.22) is given by Fisher's value [21],

$$
c_{\max} = 2\sqrt{aD}.
\tag{5.24}
$$

---

[1]For the estimation of the generation time $T = 32$ years, see note [24] in this reference.

In fact, this should be corrected due to a time-delay effect [7]. This would further complicate our equations, so we will not include this effect because, rather than comparing to the absolute value of the maximum front speed (which we already analyzed in [7]), here we are interested in focusing our attention on the slowdown effect. This is simpler by considering the relative speed from equation (5.22),

$$\frac{c}{c_{\max}} = \sqrt{1 - m\left(y\right)} - \sqrt{\frac{D}{a}}\frac{\partial m/\partial y}{1 - m\left(y\right)}. \tag{5.25}$$

In figure 5.3 we compare the results obtained from equation (5.25) (curves) with Neolithic front speed data (symbols). The latter was obtained by computing the areas within isochrones separated 250 years inside the rectangle in figure 5.1 (such isochrones are shown in figure 5.1 every 500 years for clarity).[2]

Comparing the results from equation (5.25) to those from archaeological data in figure 5.3 we see that, even though none of the four test functions reproduce exactly the behavior of the archaeological data (which is not surprising for such a complex phenomenon), they do give a good approximation to the general behavior (specially m_4). Thus, a simple physical model can explain qualitatively the decrease in the front speed during the Neolithic expansion range in Europe. Therefore, physical models are useful no only to explain the average Neolithic front speed [7], but also its gradual slowdown in space.

The reaction-diffusion model presented in this work could be applied to many examples of invasion fronts in which the indigenous population and the invasive one compete for space in a single biological niche, both in natural habitats [63, 64] and in microbiological essays [61, 65].

Acknowledgements

---

[2]In figure 5.3 we compare only the speed data calculated for latitudes above 45°, since for lower latitudes there is an important effect due to sea travel. The sites and dates used in our interpolations are those in [9].

Chapter 6

Cohabitation effect on the slowdown of the Neolithic expansion
[*Europhys Lett, submitted*]

This chapter is an exact transcription of the contents of the following manuscript summited for publication at EPL: Europhysics Letters and that is being revised at the moment of writing this Ph. D. thesis:

Abstract We introduce the effect of cohabitation between generations to a previous model on the slowdown of the Neolithic in Europe. This effect consists on the fact that human beings do not leave their children alone when they migrate, but on the contrary they cohabit until their children reach adulthood. The new equation leads to a substantial correction, up to 35%, relative to previous results. The new model is able to explain not only the relative speed but also the absolute speed of the Neolithic front.

6.1 Introduction

Reaction-diffusion models have been applied to model many biological and cross-disciplinary complex systems such as the Neolithic transition, viral infections or tumor growth (for recent reviews see [41, 57]).

The change from hunter-gathering economics to farming, known as Neolithic transition, has been analyzed in several studies using physical and mathematical models

Chapter 7

Results and discussion

This Ph.D. thesis has been prepared as a collection of papers, and as such, chapters 3 to 6 all discuss their own results and conclusions. Thus this chapter aims to give a more global view discussing some important points studied in this thesis and comparing, when possible, the results and conclusions from more than one of the papers. The first section bellow focuses basically on the methods applied to solve the different models described in this thesis, while the rest of the sections deal with the results and comparison of the different approximations applied.

7.1 Front speeds from analytical and numerical methods

The main aim of this thesis is to construct population dynamics models that can be applied to the Neolithic transition in Europe to predict the observed speed of the range expansion of this sociocultural change. To find the front speed for reaction-diffusion models, one can apply both analytical and numerical methods, which will yield, in principle, the same results. Indeed, as shown in chapters 3 (figure 3.2) and 4 (figure 4.1), the differences between the results from numerical simulations and analytical expressions are minimal. Thus, the discussion here will focus on comparing the advantages and drawbacks of using analytical and numerical methods.[1]

Analytical approximations to the speed of spreading fronts for a reaction-diffusion model constitute a practical tool that allows, for example, the study of the sensitivity of the front speed to parameters in a simpler and faster way than using simulations. In addition, analytical expressions provide a general result that can be easily applied to similar systems (for example, when studying populations with different dispersal behaviors in chapter 3). On the other hand, a potential drawback of analytical solutions is the fact they are obtained by making assumptions for the conditions at the front (e.g., the validity of the linear approximation for the reactive process); these approximations

---

[1]The techniques required to calculate the front speed depend on if one is dealing with integrodifference or differential equations, as explained in chapter 2, but as this is not an important point for the purpose in this section, it will not be further discussed.

are corroborated by the consistency between analytical and numerical results, as seen in chapters 3 and 4.

Numerical simulations, on the other hand, might in principle provide more exact results as no approximations to the front conditions are necessary. Yet, what is necessary in this case is the discretization of the space domain, which can also modify the results. For example, in chapter 3, when studying the effect of using dispersion kernels, the discretization changes the shape of the kernel and modifies the front speed calculated along the x-direction;[2] however this could be partially solved by defining grids with finer spatial resolution. The main disadvantage of numerical simulations, when compared with analytical solutions, is the computing time required to obtain results. Even with a coarse grid as the one used in chapter 3, when simulating the Dirac deltas kernels, the computing time spent was of around 15 hours per simulation.[3] For this reason, repeating the calculation for multiple values of the parameters is tedious and usually impractical.

A distinctive feature of numerical simulations is that they make it possible to follow the evolution of the population in time and space. This is important in chapter 3 when studying the effect of applying a stochastic dispersion routine. The results show that for the estimated values of the Neolithic population densities, the stochastic effect is not strong. What does have an effect on the front speed is the fact of considering the population as discrete individuals instead of a continuous populations density, i.e., without allowing fractional values for the population number. But is this effect really important enough so that it should be included in future models? According to the results in section 3.6, when forcing the population per cell to be an integer, the speeds are about $3-5\%$ slower. Probably a more extensive study should be necessary because in that section the focus was on the stochastic effect, but it is possible to draw some conclusions from the information available. On the one hand, clearly having half an individual makes no sense; however, a population density of 0.5 individuals per cell does simply mean that there is on average only one individual every two cells, and if the stochastic dispersion routine is well constructed, this should not have in average an important effect. What must have the strongest effect on the results is that, at each time step, after the population growth process, the population number was made integer by just taking the integer part of the number of individuals in each cell. Thus, a cell with 11.01 individuals in it and another with 11.99 individuals are both approximated to having 11 individuals. Obviously 0.99 individuals is no individual, but the population growth equation is a statistical function which is continuous in time, thus maybe taking only the integer part amounts to introducing an error by underestimating the population growth, and a better approximation might have been, for example, rounding to the nearest integer. Even though results for this rounding scheme are not presented in the

---

[2]Although not shown (nor discussed) in chapter 3, the discretization of the kernel does also modify the diagonal speed making this result faster than the CSRW results, as opposed to the slower speeds obtained for the horizontal direction. This is due to using a non-isotropic square-shaped kernel instead of the isotropic kernel considered for the CSRW results.

[3]These simulations were performed with a personal computer with an AMD Athlon64 3200+ CPU and 1024Mb RAM.

previous chapters, it is reasonable to infer that in this case the correction will be lower than the range $3-5\%$ obtained in section 3.6.

In conclusion, even though the use of numerical simulations does offer more information on the step-by-step process, as the purpose in this thesis is to study the speed of propagating fronts, analytical results offer in this case a tool as accurate as numerical simulations, while being more practical and specially less time consuming. Consequently, the studies in this thesis have favoured obtaining analytical results in order to apply them to the Neolithic transition, while numerical simulations have been considered mainly as a means to verify the analytical results.

7.2   Cohabitation and non-cohabitation models

From a conceptual point of view, the difference between cohabitation and non-cohabitation models lies on the fact that cohabitation models (such as equation (1.6)) take into account that children cohabit with their parents until adulthood, while in non-cohabitation models (such as equation (1.7)) parents leave their children behind (figures 3.1 and 7.1 show diagrams comparing both kinds of models). As the models in this thesis are intended to be applied to the Neolithic transition, cohabitation models do agree better with the expected behavior for human farming societies so they provide a more realistic framework.

When translated into a mathematical model this difference lies on how the function $R\,[p]$ (giving the increase due to population growth) is applied in the evolution equation describing the model. With a non-cohabitation model, when describing the final population density $p\,(x,y,t+T)$ at position (x,y), the population growth is applied to the individuals who were initially at position (x,y), i.e. $R\,[p\,(x,y,t)]\,,$ so

$$p\,(x,y,t+T) = \iint p\,(x-\Delta_x,y-\Delta_y,t)\,\phi\,(x,y;\Delta,\theta)\,\mathrm{d}\Delta_x\mathrm{d}\Delta_y$$
$$+\,R\,[p\,(x,y,t)] \tag{7.1}$$

with, as usual, $\phi\,(x,y;\Delta,\theta)$ the probability that the population will move from $(x-\Delta_x,y-\Delta_y)$ to (x,y), $\Delta = \sqrt{\Delta_x^2+\Delta_y^2}$ and $\theta = \tan^{-1}(\Delta_y/\Delta_x)$. Clearly, for any space point, new individuals (children) will appear at $(x-\Delta_x,y-\Delta_y)$ due to the initial population at the very same point (last term in (7.1), empty circles in figure 7.1.a), whereas due to the dispersion (first term in (7.1)), the parent population will migrate away (full circles in figure 7.1.a). On the other hand, to describe a cohabitation model, where parents do not leave their children behind, there are different options. In this thesis the equation applied is

$$p\,(x,y,t+T) = \iint p\,(x-\Delta_x,y-\Delta_y,t)\,\phi\,(x,y;\Delta,\theta)\,\mathrm{d}\Delta_x\mathrm{d}\Delta_y$$
$$+\,R\left[\iint p\,(x-\Delta_x,y-\Delta_y,t)\,\phi\,(x,y;\Delta,\theta)\,\mathrm{d}\Delta_x\mathrm{d}\Delta_y\right]. \tag{7.2}$$

(a) Non-cohabitation

$(x\text{-}\Delta_x, y\text{-}\Delta_y)$ $(x\text{-}\Delta_x, y\text{-}\Delta_y)$ (x, y)

(b) Cohabitation model

$(x\text{-}\Delta_x, y\text{-}\Delta_y)$ $(x\text{-}\Delta_x, y\text{-}\Delta_y)$ (x, y)
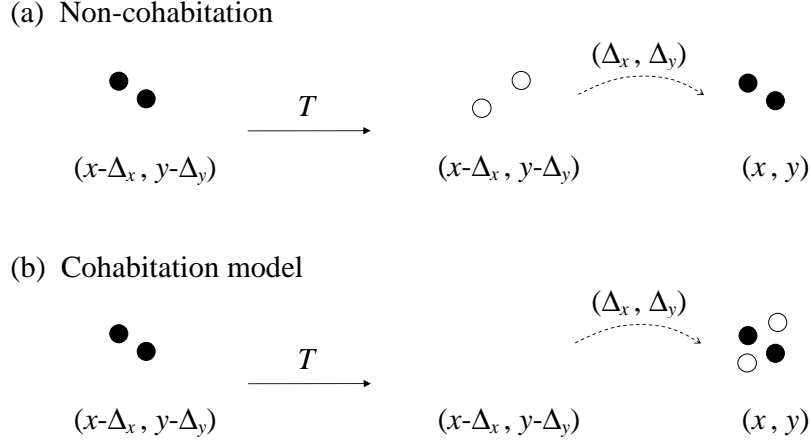
Figure 7.1: Diagram comparing non-cohabitation (a) and cohabitation (b) reaction-diffusion models for a simple kernel with all individuals migrating. Full circles represent the parent population and empty circles represent children (population growth).[4]

In this case the increase in population due to net reproduction (last term) is calculated on the population density after dispersion, that is, the new individuals at position (x, y) due to reproduction will be the children from the population that has settled at (x, y) after migration and who will stay there for a generation time (see figure 7.1.b). Another possible approach is to calculate the population growth on the population before migration, and then apply the migration term on the whole population (initial plus children)

$$p\left(x, y, t+T\right) = \iint \left(p\left(x - \Delta_x, y - \Delta_y, t\right) + R\left[p\left(x - \Delta_x, y - \Delta_y, t\right)\right]\right)$$
$$\times \phi\left(x, y; \Delta, \theta\right) \mathrm{d}\Delta_x \mathrm{d}\Delta_y. \tag{7.3}$$

Other more general cases could also be defined [41], but even though it may not be initially obvious, they will yield the same front speed. Indeed, if we assume as usual that at the leading edge of the front population growth is exponential (see figure 2.1), R can be expressed as $R\left[p\right] \simeq p\left(e^{aT} - 1\right)$ (see equation 2.2), and then it is easy to see that both equations (7.2) and (7.3) become

$$p\left(x, y, t+T\right) = e^{aT} \iint p\left(x - \Delta_x, y - \Delta_y, t\right) \phi\left(x, y; \Delta, \theta\right) \mathrm{d}\Delta_x \mathrm{d}\Delta_y. \tag{7.4}$$

This means that, even though there are different options to mathematically describe a cohabitation model, they will all lead to the same results when searching for the speed

---

[4]More precisely, in figure 7.1 the empty circles correspond to the net population growth (i.e., the function $R\left[...\right]$ in equations (7.1) and (7.2)) and the full circles represent both the individuals at time t (i.e., $p\left(x - \Delta_x, y - \Delta_y, t\right)$) and the same number of individuals a generation T later (first term on the right-hand side in equations (7.1) and (7.2)).

of spreading fronts. Thus the fact that in this thesis cohabitation models have been described using equation (7.2) rather than other possible cohabitation equations has no effect on the results.

Note, however, that even though up to now we have assumed that the contributions $p(x - \Delta_x, y - \Delta_y, t)$ and $R[...]$ to the final population (i.e., $p(x, y, t + T)$) can be described as the parent population and the children respectively, this is not completely accurate. In fact, both the initial and the final populations $[p(x - \Delta_x, y - \Delta_y, t)$ and $p(x, y, t + T)]$ are age-structured, i.e., both are formed by individuals of all ages.[5] Thus, this implies that after a generation time T, part of the individuals belonging to the initial population $p(x - \Delta_x, y - \Delta_y, t)$ will indeed become the parents of the new children, but also part of the initial population will have died at time $t + T$. Therefore, the number of new individuals that appear due to reproduction (children) during a time generation T is $R[...]$ plus the number of individuals necessary to compensate the mortality of the initial population $p(x - \Delta_x, y - \Delta_y, t)$. Thus, in equations (7.1) and (7.2), $R[...]$ are indeed children born during a generation time T (empty circles in figure 7.1), and $p(x - \Delta_x, y - \Delta_y, t)$ is equal in number to the initial population (full circles on the left in figure 7.1) but correspond to the individuals from that initial population who are still alive, as well as part of the new children born during T (full circles on the right in figure 7.1). So, this means that in equation (7.1) not all members of the new population are left behind, but some of them, namely $R[...]$ (empty circles in figure 7.1.a). In any case, even though a very precise description is somewhat complex, it is right to say that equation (7.2) describes the cohabitation between parents and children while equation (7.1) does not.

Now, focusing on the results, in all studies cohabitation equations lead to faster front speeds than non-cohabitation ones, with corrections up to 38% in the models studied in this thesis. The reason is that in cohabitation models the whole population is allowed to disperse while in non-cohabitation models, such as equation (7.1), a fraction of the final population ($R[...]$ individuals) have their capability to disperse suppressed (figure 7.1.a). Apart from the fact that the number of individuals that cannot migrate can be interpreted as children left behind, preventing the dispersive behavior is conceptually similar to introducing a persistency effect, in addition to the dispersion pattern defined by $\phi(x, y; \Delta, \theta)$. This additional persistency effect can be clearly observed in figure 7.1 which describes an extreme case with the kernel forcing all individuals to leave the original site. See that for the cohabitation model, figure 7.1.b, after a generation time the original site is in fact abandoned. On the contrary, at figure 7.1.a after a generation time T new individuals appear at the original site regardless of how the dispersion kernel has been defined.

But, even though from a conceptual point of view cohabitation models are more realistic, do they lead to more consistent results? Actually, in most cases, when comparing to the archaeological results, this comparison does not give a clear indication that cohabitation models perform better, because the range of estimated speeds for the

---

[5]Both the non-cohabitation equation (7.1) and the cohabitation equation (7.2) are consistent with a distribution of ages in the population, as well as with age-dependant natality and mortality. For age-structured derivations of these equations, see the appendixes in [13].

Neolithic expansion in Europe at the continental scale ($0.6 - 1.3$ km/yr) is wide enough so that results from both frameworks lie within this interval. A clear example are the results in chapter 3, where the speeds obtained from models using data from six populations with different dispersive behaviors are, for the most part, consistent with this measured range. On the other hand, a case which does yield markedly better results when using cohabitation models is the regional study of the slowdown of the Neolithic transition when reaching the North of Europe, as shown in chapter 6.

In conclusion, when constructing a population dynamics model for human societies, cohabitation models provide a better framework as they give a more realistic description of human behavior. Besides, cohabitation models lead to faster speeds (up to 38% faster) than non-cohabitation models, the former are in general consistent with the observations, and even noticeably more accurate than the latter in some cases. Thus, cohabitation models should be the preferred framework to model human population dynamics.

7.3 Explicit dispersion kernels and diffusive approximation

Integrodifference equations, as opposed to differential equations, allow the inclusion of explicit dispersal patterns when modeling reaction-dispersion systems, because the dispersal kernel $\phi\left(x, y ; \Delta, \theta\right)$ appears in the former but not in the latter type of equations (compare, e.g., equation (1.6) to (1.2)). This is why in chapter 3, where the focus was on the effect on the spreading front of dispersion kernels, the studied models are described using integrodifference equations. Chapter 3 includes the analysis of four kernels giving different approximations to human dispersion behavior: jumping to a single distance, jumping to several discrete distances (chosen according to the recorded intervals of human dispersal data), jumping according to a Gauss distribution and to a Laplace distribution. The results from these kernels when applied to dispersion data for six human populations are tabulated in chapter 3, and figure 7.2 also shows a graphical comparison, when using $T = 32$ yr and $a = 0.033$ yr^{-1}.[6] This figure also includes results from the HRD equation (1.4) as well as from the new time-delayed speed derived in chapter 4 (labeled as time-delayed) and Fisher's equation (1.2). Note that, even though chapter 3 studies the results from cohabitation models and that this framework is more realistic, the results in figure 7.2 correspond to a non-cohabitation model scenario so that Fisher's, HRD and time-delayed equations can be included.[7]

We now turn to the kernels studied to describe realistic dispersion patterns. A very simple approximation is to assume an isotropic kernel where individuals can either stay or jump a single distance. When using dispersion data of real populations one obtains

---

[6]Using the minimum value of the initial growth rate $a = 0.023$ yr^{-1} would lead to similar results, but in that case Fisher's model and Laplace distribution nearly overlap and this could lead to incorrect conclusions.

[7]As explained in section 1.2.3 and in chapter 4, Fisher's, HRD and the corrected time-delayed equation can be obtained from non-cohabitation evolution equations, but not from cohabitation equations.
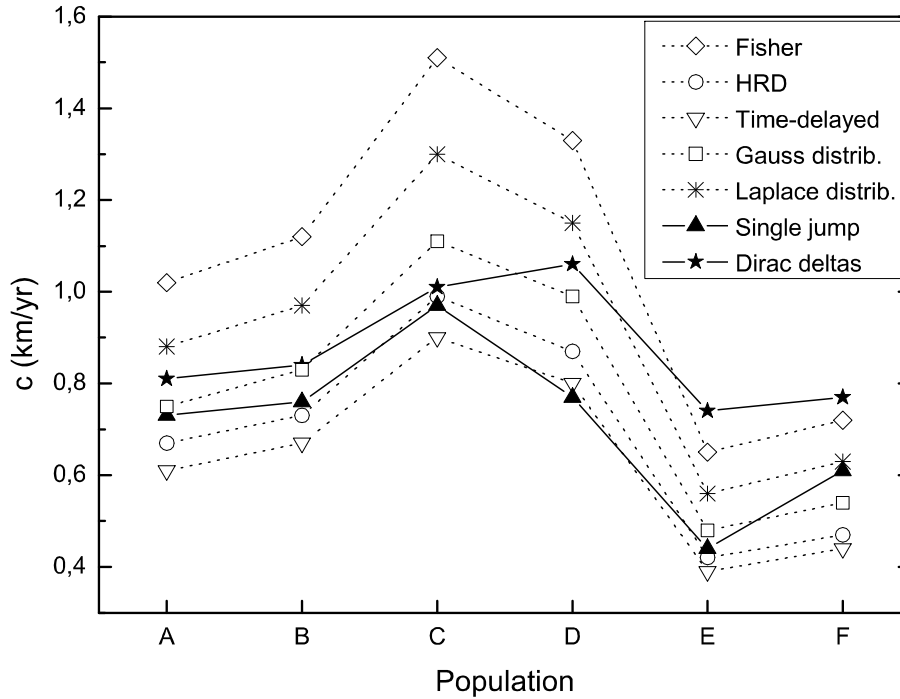
Figure 7.2: Comparison of the front speeds calculated using different analytic models for six farming populations. Lines joining symbols are plotted to facilitate comprehension, not as trends. ($T = 32$yr, $a = 0.033$yr^{-1})

two easily foreseeable results: (i) given two populations with the same persistency (probability to stay), the front speed will be faster for the population with higher mobility $\langle \Delta^2 \rangle / T$, and (ii) for two populations with the same mobility, if one has a higher value of the persistency, the speed of the spreading front will also be faster (because jumping individuals move a longer distance). Thus, even being a very simple approximation, these predictions do already include certain variability related to real dispersive patterns that differential-equation models cannot provide, because the latter depend only on the mobility ("diffusive" approximation).[8]

A better approximation to the real behavior might obviously be obtained by using more detailed information on the kernel shape. So, even though still being an approximation, the results from the Dirac deltas model, which gives a discrete approximation to the recorded data, can be assumed as leading to more realistic results, because it contains more detailed information on the dispersive patterns for each population. The results from this approximation to the real kernel are given in table 3.2, and it is important to notice that they are always consistent (at least marginally) with the observed speeds, which is a desirable result but not obvious beforehand. Comparing these two discrete models (emphasized results in figure 7.2), for the Dirac deltas approximation the speeds are faster as they always include a certain probability to move to further

---

[8]Similar aproximations with each individual being either a non-disperser or a disperser have previously been applied to the Neolithic transition [13, 40, 53].

distances than with the single-distance case. Moreover, the difference is larger for populations with a slight probability to disperse large distances (110 km and 100 km for populations D and E respectively) than those with shorter dispersive ranges. On the other hand, population C, with more than 50% probability to move to large distances, behaves in a similar way as the single-distance model, so in this case, the single-distance and Dirac deltas models yield nearly the same results.

Contrarily to these discrete approximations to the real kernel, when using Gauss and Laplace distributions, the real kernel shape is not really taken into account, except for the mobility value (see section 3.5.3). Gauss and Laplace distributions have been widely applied to population dispersal because they provide a reasonable scenario where most individuals move relatively short distances, whereas long-distance dispersal is restricted to very few individuals. Examining the dispersion data in chapter 3 (equations (3.25)–(3.28)) this is roughly the behavior of the studied dispersion patterns, and for populations A, B and D the Gauss distribution yields a fairly good approximation. The differences between these kernels and the discrete approximations increase specially when the population has a large probability to move either to large distances (e.g., population C) or to very close destinations (e.g., population F). Moreover, according to the explicit equations for Gauss and Laplace distributions (section 3.4), the dispersive behavior is only included in terms of the mean-squared displacement $\langle \Delta^2 \rangle$ (see section 3.5.3). So, they provide in fact another possible "diffusive" approximation to the dispersion depending on the diffusion coefficient $D = \langle \Delta^2 \rangle /4T$, as with Fisher's speed (1.3)

$$c_{Fisher} = 2\sqrt{aD}, \tag{7.5}$$

the HRD speed (1.5)

$$c_{HRD} = \frac{2\sqrt{aD}}{1 + aT/2}, \tag{7.6}$$

and the new time-delayed speed (4.27)

$$c_{time\text{-}delayed} = \frac{2\sqrt{aD\left(1 + aT/2\right)}}{1 + aT}. \tag{7.7}$$

One can see from figure 7.2 how all these five "diffusive" approximations lead in fact to equivalent solutions, only with different scaling (in contrast to the single-jump and Dirac deltas kernels). This is due to the fact that the speeds given by equations (7.5), (7.6), (7.7), (3.21) and (3.24) are proportional to $\sqrt{D}$.[9]

According to these results, expressions for the front speed depending only on the diffusion coefficient D cannot predict the effects of real dispersion patterns. Besides, from the dispersive patterns used in chapter 3 one cannot infer a standard pattern to describe the dispersive behavior for pre-industrial farming societies. Yet, the results in chapter 3 and figure 7.2 show that the use of realistic dispersion kernels leads to

---

[9]According to section 3.5.3 and the definition $D \equiv \langle \Delta^2 \rangle /4T$, for the Gauss distribution, $\varphi\left(\Delta\right) = \left(2\Delta/\alpha^2\right) \exp\left[-\left(\Delta/\alpha\right)^2\right]$ (see section 3.4.1), the parameter α is $\alpha = \sqrt{4T}\sqrt{D}$ and for the Laplace distribution, $\varphi\left(\Delta\right) = \left(\Delta/\alpha^2\right) \exp\left[-\Delta/\alpha\right]$ (see section 3.4.2), $\alpha = \sqrt{T/3}\sqrt{D}$.

front speeds consistent with the estimated speeds for the Neolithic transition ($0.6 -$ 1.3 km/yr) and that, for non-cohabitation equations, in most cases the time-delayed equation (7.7) gives a lower bound and Fisher's equation (7.5) an upper bound to these results. Therefore it is reasonable to expect that, in general, front speeds from realistic dispersion kernels will lie within the range between the speed predicted by reaction-diffusion equations with second-order terms in time (slower speeds) and the predictions when using only first-order terms in time (faster speeds). Moreover, among the models describing the dispersion in terms of D, the Gauss distribution seems to provide the best approximation to the speeds predicted by the kernels based on discrete data (Dirac deltas in figure 7.2).

7.4 Time delay

In general, in farming societies one assumes that children stay with their parents at their birthplace until they reach adulthood and migrate to form their own families. The effect of this time delay between birth and migration was first applied to the Neolithic transition in Europe in reference [7]. However, that derivation did not take proper care of the reaction term, so chapter 4 includes the correct derivation of the front speed for a non-cohabitation reaction-diffusion equation including the effect of the time delay up to second order and assuming isotropic kernels. The new time-delayed result leads to slower speeds, up to 10% slower, than the previous HRD equation for the ranges of anthropological parameters estimated for pre-industrial farming populations.

When working with integrodifference equations, as in chapter 3, the time delay T is also taken into account because the generation time T is used as the time step of the recurrence process. In fact, in this case the time delay is taken into account up to infinite order and not just in a second-order approximation as with reaction-diffusion equations (chapter 4). However, according to the results in reference [67] the second-order approximation leads to approximately the same results as when using a differential equation with infinite terms. Even though this conclusion was drawn by treating the reaction term in the same way as in reference [7] for the HRD equation, if assuming that this conclusion still stands for the correct derivation, then the differences with the results using integrodifference equations should be only due to the use of dispersion kernels and not the second order approximation in time. In any case, it would also be interesting to check if with the correct time-delayed result, the second order approximation in time does still yield nearly the same result as with infinite terms.

Note that these equations are obtained from non-cohabitation models, while it has been discussed before that a cohabitation model is a better representation when modeling human population dynamics. A second-order time-delayed equation for cohabitation models was derived in reference [13][10], even though the reaction term was only a first-

---

[10]In this reference cohabitation models were called sequential models to stress the fact that reaction and dispersion should not be applied simultaneously in the models (leading to parents abandoning their children), but that the time order is important when constructing mathematical models for human populations.

order approximation that could also be interesting to generalize to higher orders using equations (3.2) and (3.3).

7.5 Environmental effects: presence of Mesolithic populations

According to archaeological observations, the rate of spread of the Neolithic transition slowed down when reaching northern regions in Europe. This evolution of the front speed has been estimated in chapters 5 (relative speed) and 6 (absolute speed) for a region of study located between the Balkans and the North Sea (see the map in figure 5.1). A possible cause for this slowdown has been inferred to be the higher presence of Mesolithic populations at northern regions; chapters 5 and 6 present models that can indeed explain the observed slowdown in terms of this premise.

The effect of encountering pre-Neolithic populations is taken into account in the models in terms of the available space for the Neolithic invaders, and by making the reasonable assumption that Neolithic individuals will preferably move to locations where more unoccupied space is available. This competition for space between Neolithic and Mesolithic populations is also taken into account in the reaction term in chapters 5 and 6, because the presence of another population using the same space and resources limits the increase in population number as the carrying capacity is modified. These limitations introduced by the presence of Mesolithic populations have been neglected in chapters 1 - 4, as well as in other previous models such as Fisher's [17] or the HRD model [7], even though Mesolithic populations were present in most of the continent. This is reasonable because Mesolithic population densities are estimated to be very low, about 0.03 inhabitant per km^2 [68], and as the Neolithic population density at the leading edge of the front is also considered very low, at first approximation the interaction at the front can be considered negligible. However, when studying the slowdown of the Neolithic front, the densities of Mesolithic populations at Northern Europe are considered to be large enough to have an effect on the front speed, so in this case taking into account Mesolithic populations in the models is more reasonable. In any case, from the results in chapter 5 one can also see that indeed, when Mesolithic population densities are low and approximately constant (for example with test function m_4 in figure 5.2), the effect introduced by considering the presence of Mesolithic populations is not very significant (figure 5.3), whereas for higher population densities the correction increases.

As explained in chapters 5 and 6, the fact that the density of Mesolithic populations varies in space (and so does the free space) implies that, in this case, the dispersion will take place in a non-isotropic way, as opposed to the isotropic dispersion kernels considered in chapters 3 and 4. When searching for general results to be compared with average values of the spreading speed in Europe, it is reasonable to use isotropic kernels because, as explained in the Introduction (section 1.1), the analysis of early Neolithic archaeological data suggests a fairly constant rate of spread of this cultural change all across the continent. On the other hand, as chapters 5 and 6 make reference to a regional variability, in this case the use of an anisotropic kernel is more adequate.

Thus, from the results in chapters 5 and 6 one can see that, just by introducing a limitation on the available space due to Mesolithic populations in a simple reaction-diffusion model, it is possible to predict a decrease of the front speed similar to estimated results from archaeological data. Chapter 5 compares with archaeological estimations the prediction obtained when using four possible functions to describe the variation of the Mesolithic population density in space, finding that the best fit is achieved when using a S-shaped function (function m_4 in figure 5.3). Even without having Mesolithic data to compare this result with, in the literature the effect of Mesolithic population to the Neolithic expansion is usually only described in studies concerning the North of Europe [60], thus in principle it seems to make sense to consider that Mesolithic densities are only significant enough at northern regions. Moreover, if comparing not only the trend but also the absolute values for the front speed, the cohabitation model in chapter 6 provides a much better approximation to the archaeological results, with corrections up to 35%.

All in all, both models presented in chapters 5 and 6 are very simple and could be improved by including the effect of the time delay (by using terms up to second order in time), which would yield slower speeds, as seen in previous sections. Also the function $\psi(\Delta)$ in the dispersion kernel could be described using an explicit distribution (for example, a Gauss distribution, as it is more practical than the Dirac deltas models while leading to reasonable results). This would lead to faster speeds than the time-delayed approximation. Such modifications will probably be included in future work, together with the analysis of a new database for the Mesolithic in Europe that was not available at the moment of preparing chapters 5 and 6. But in any case, the main conclusion will presumably still stand, that a simple physical model can predict a decrease in the front speed similar to the observed one, and that the cohabitation model yields a better approximation to the archaeological data.

Chapter 8

Conclusions

We have developed population dynamics models that can be applied to the Neolithic transition (or other similar processes involving human dynamics) and analyzed several effects such as the use of explicit dispersive patterns, the time delay between migrations, the cohabitation or not between generations, and the influence on the front speed of encountering indigenous (Mesolithic) populations. We have applied our models to predict both average results and regional variabilities, obtaining consistent results when compared to archaeological data. In addition to archaeological dates for the arrival time of the Neolithic front at 765 sites, we have also used ethnographic data to estimate the dispersion kernels and reproductive parameter values (chapter 2). We have applied both analytical and numerical approaches to solve our new mathematical models.

We have considered both cohabitation and non-cohabitation frameworks in our study. A cohabitation framework is more realistic for human populations as it assumes that parents and children cohabit until adulthood of the latter, as opposed to parents migrating away from their children as considered in non-cohabitation models. However, even though cohabitation models lead to speeds up to 38% faster, in most cases the results from cohabitation and non-cohabitation models are both consistent with the estimated average speed for the Neolithic expansion (as seen in chapter 3). The regional study of the slowdown of the Neolithic in norther Europe (studied in chapters 5 and 6) does, on the other hand, provide a clear example where a cohabitation framework leads to substantially better results.

When studying the Neolithic transition, the dispersion process is usually taken into account only in terms of the diffusion coefficient D, and in fewer cases [13, 40, 53] the dispersion has been studied considering the individuals as being either non-dispersers or dispersers, with all disperses moving the same distance. We have generalized these models by applying fully explicit dispersion kernels. We have derived a discrete approximation to recorded dispersion data and applied this model to the dispersive patterns from six farming populations (chapter 3). For all six populations the predicted speeds are consistent with the average range for the Neolithic expansion in Europe $(0.6 - 1.3$ km/yr$)$, at least marginally, thus the use of realistic dispersion patterns in a simple integrodifference model leads to reasonable results.

In chapter 3, we have also derived explicit equations for the front cohabitation

speed when assuming Gauss or Laplace kernels. When compared with the discrete approximation, even though the Gauss and Laplace kernels do not include the real shape of the kernels, the Gauss distribution does lead to a fairly good approximation to speeds predicted with the discrete kernels, while the Laplace distribution overestimates them.

In chapter 4, we have derived a new time-delayed reaction-diffusion equation, including second-order terms in time and space, and taking proper care of the growth process as opposed to the derivation of the HRD equation in reference [7]. When applied to the Neolithic transition, the new results yield speeds 10% slower than the HRD equation, and when compared to results from other non-cohabitation models, the new time-delayed equation constitutes in general a lower bound for the predicted front speeds (chapter 7).

On a regional level, we have studied the observed decrease in the rate of expansion of the Neolithic transition in northern Europe. The study is centered in a region located between the Balkans and the North Sea, leaving out latitudes below 45° in order as to exclude the sea-travel effects in the Mediterranean coast. We have obtained an estimation of the average front speed at different positions within the studied area, by analyzing an interpolation map of Early Neolithic dates, which clearly show a decrease in the front speed (chapters 5 and 6).

A theorized cause for this slowdown in the front speed is the higher presence of Mesolithic settlements at higher latitudes. This had been proposed by archaeologists but no mathematical models of this effect had been proposed previously. We have derived a model in which the influence of these pre-Neolithic populations has been taken into account by means of a reduction of the free space available for the Neolithic invaders, which affects the dispersal capability of individuals and reduces their reproductive dynamics. The results from this model show a decrease in the front speed consistent with the relative speed values estimated from archaeological data (chapter 5). Taking into account the cohabitation effect, the agreement is better and consistent also with the observed trend for the absolute speed (chapter 6). Hence, we have proved with simple mathematical models that the higher density of Mesolithic settlements at northern Europe is indeed a plausible cause for the observed decrease in the speed of the Neolithic expanding front.

Appendix A

Copy of published papers

In agreement with the regulations of the University of Girona, chapters 3-5 are an exact transcription of the papers reproduced in this appendix.

Realistic dispersion kernels applied to cohabitation reaction–dispersion equations

Neus Isern, Joaquim Fort and Joaquim Pérez-Losada

Departament de Física, Universitat de Girona, 17071 Girona, Catalonia, Spain
E-mail: neus.isern@udg.edu, joaquim.fort@udg.edu and joaquim.perez@udg.edu

Abstract. We develop front spreading models for several jump distance probability distributions (dispersion kernels). We derive expressions for a cohabitation model (cohabitation of parents and children) and a non-cohabitation model, and apply them to the Neolithic using data from real human populations. The speeds that we obtain are consistent with observations of the Neolithic transition. The correction due to the cohabitation effect is up to 38%.

Keywords: dynamics (theory), population dynamics (theory)

J. Stat. Mech. (2008) P10012

Abstract

We develop front spreading models for several jump distance probability distributions (dispersion kernels). We derive expressions for a cohabitation model (cohabitation of parents and children) and a non-cohabitation model, and apply them to the Neolithic using data from real human populations. The speeds that we obtain are consistent with observations of the Neolithic transition. The correction due to the cohabitation effect is up to 38%.

Time-delayed reaction-diffusion fronts

Neus Isern and Joaquim Fort

Departament de Física, Universitat de Girona, 17071 Girona, Catalonia, Spain

A time-delayed second-order approximation for the front speed in reaction-dispersion systems was obtained by Fort and Méndez [Phys. Rev. Lett. **82**, 867 (1999)]. Here we show that taking proper care of the effect of the time delay on the reactive process yields a different evolution equation and, therefore, an alternate equation for the front speed. We apply the new equation to the Neolithic transition. For this application the new equation yields speeds about 10% slower than the previous one.

PACS number(s): 89.65.Ef, 87.23.Cc, 89.20.−a

I. INTRODUCTION

Reaction-diffusion systems have been applied to many complex biological and physical systems such as population dispersals [1], viral infections [2], chemical reaction processes [3], combustion flames [4], etc. In Ref. [5] a time-delayed model for the front speed was presented including terms up to second order. However, here we will show that there was an error in the mathematical derivation, and we will derive and analyze the behavior of the correct time-delayed equation for the front speed.

In biological systems, variations in the population number density, p, are due to two processes: population growth (reproduction minus deaths) and migration (dispersion). The variation due to population growth can be expressed as a Taylor series,

$$[p(x,y,t+T) - p(x,y,t)]_g = T\left.\frac{\partial p}{\partial t}\right|_g + \left.\frac{T^2}{2}\frac{\partial^2 p}{\partial t^2}\right|_g + \cdots$$
$$= TF + \left.\frac{T^2}{2}\frac{\partial F}{\partial t}\right|_g + \cdots, \quad (1)$$

where the subindex g denotes growth, we have introduced the growth function as $F(p) = \frac{\partial p}{\partial t}|_g$, and T is the time delay (one generation in most applications [5]). As usual, we assume that $F(p) > 0$.

On the other hand, for the migration (dispersion) we will define the dispersion kernel $\phi(\Delta_x, \Delta_y)$ which gives the probability per unit area that an individual initially placed at $(x+\Delta_x, y+\Delta_y)$ has moved to (x,y) after a time interval T. Thus, the variation in population number density due to migration can be expressed as [5]

$$[p(x,y,t+T) - p(x,y,t)]_m = \int\int p(x+\Delta_x,y$$
$$+\Delta_y,t)\phi(\Delta_x,\Delta_y)d\Delta_x d\Delta_y$$
$$- p(x,y,t). \quad (2)$$

In a system involving the two processes (population growth and migration), the total variation in population density during a time interval T can be expressed as the sum of both contributions,

$$p(x,y,t+T) - p(x,y,t) = \int\int p(x+\Delta_x,y$$
$$+\Delta_y,t)\phi(\Delta_x,\Delta_y)d\Delta_x d\Delta_y - p(x,y,t)$$
$$+ TF + \left.\frac{T^2}{2}\frac{\partial F}{\partial t}\right|_g + \cdots. \quad (3)$$

We assume that the kernel is isotropic, i.e., $\phi(\Delta_x, \Delta_y) = \phi(\Delta)$, with $\Delta = \sqrt{\Delta_x^2 + \Delta_y^2}$, and we Taylor expand Eq. (3) up to second order in time and space, thus, obtaining the following reaction-diffusion equation:

$$\frac{\partial p}{\partial t} + \frac{T}{2}\frac{\partial^2 p}{\partial t^2} = D\left(\frac{\partial^2 p}{\partial x^2} + \frac{\partial^2 p}{\partial y^2}\right) + F + \left.\frac{T}{2}\frac{\partial F}{\partial t}\right|_g, \quad (4)$$

where D is the diffusion coefficient $D = \frac{\langle\Delta^2\rangle}{4T} = \frac{\langle\Delta_x^2\rangle}{2T} = \frac{\langle\Delta_y^2\rangle}{2T}$.

Since $F(p)$ depends only on the population density p, then the last term in Eq. (4) can be written as

$$\left.\frac{T}{2}\frac{\partial F}{\partial t}\right|_g = \frac{T}{2}\frac{dF}{dp}\left.\frac{\partial p}{\partial t}\right|_g = \frac{T}{2}F'F. \quad (5)$$

In addition, as the density at the leading edge of the front is low, $p \approx 0$, we have that $F(p) \approx pF'(0)$ and $F'(p) \approx F'(0)$. Therefore, for $p \approx 0$ Eq. (4) may be rewritten as

$$\frac{\partial p}{\partial t} + \frac{T}{2}\frac{\partial^2 p}{\partial t^2} = D\left(\frac{\partial^2 p}{\partial x^2} + \frac{\partial^2 p}{\partial y^2}\right) + pF'(0) + \frac{T}{2}pF'(0)F(0).$$
$$(6)$$

We now assume that for $t \to \infty$ and $r \to \infty$ the front can be considered locally planar. Thus, choosing the x axis parallel to the local speed of the front, $c \equiv |c_x|$, we can look for constant-shape solutions with the form $p = \bar{p}\exp[\lambda(x-ct)]$. Applying this *ansatz* to Eq. (6) we see that the value of λ can be obtained from

$$\lambda = \frac{-c \pm \sqrt{c^2 - 4\left(D - \frac{T}{2}c^2\right)F'(0)\left[1 + \frac{T}{2}F'(0)\right]}}{2\left(D - \frac{T}{2}c^2\right)}. \quad (7)$$

As λ has to be real, we obtain a lower bound for the front speed

$$c \geq \frac{2\sqrt{DF'(0)\left[1+\frac{T}{2}F'(0)\right]}}{1+TF'(0)}. \tag{8}$$

However, the result obtained in Ref. [5] was the so-called HRD speed, namely,

$$c_{HRD} \geq \frac{2\sqrt{DF'(0)}}{1+\frac{T}{2}F'(0)}, \tag{9}$$

which is different from Eq. (8).

The reason for this difference is the following. Here we have used Eq. (5), which allows us to rewrite Eq. (4) as

$$\frac{\partial p}{\partial t} + \frac{T}{2}\frac{\partial^2 p}{\partial t^2} = D\left(\frac{\partial^2 p}{\partial x^2} + \frac{\partial^2 p}{\partial y^2}\right) + F(p) + \frac{T}{2}\frac{dF}{dp}F. \tag{10}$$

In contrast, in Ref. [5] the following equation was used:

$$\frac{\partial p}{\partial t} + \frac{T}{2}\frac{\partial^2 p}{\partial t^2} = D\left(\frac{\partial^2 p}{\partial x^2} + \frac{\partial^2 p}{\partial y^2}\right) + F(p) + \frac{T}{2}\frac{dF}{dp}\frac{\partial p}{\partial t}. \tag{11}$$

We can see that the last term is different. The reason is that in Ref. [5] the subindex g was omitted in the last term in Eq. (4). Therefore, in Ref. [5], the last term in Eq. (4) was not written as in Eq. (5) but as follows:

$$\frac{T}{2}\frac{\partial F}{\partial t} = \frac{T}{2}\frac{dF}{dp}\frac{\partial p}{\partial t} = \frac{T}{2}F'\frac{\partial p}{\partial t}, \tag{12}$$

and thus leading to Eq. (11) instead of Eq. (10). This is why in Ref. [5], speed (9) was obtained instead of Eq. (8). However, the derivation above clearly shows that Eq. (8) is the right result. In this Brief Report, we will apply variational analysis and show that Eq. (8) is not only a lower bound but the exact speed (Sec. II). We will also analyze the difference between the new Eq. (8) and the HRD speed (9) by applying both equations to the Neolithic transition (Sec. III). In Sec. IV we present our conclusions.

II. VARIATIONAL ANALYSIS: UPPER BOUND

Equation (8) is just a lower bound for the speed of front solutions to the new differential equation (4) [or Eq. (10)]. In order to find an upper bound, we apply variational analysis [6] to Eq. (10). As mentioned above, we assume that the fronts have a profile $p(z)=p(x-ct)$ traveling with a speed $c>0$, so all of the derivatives in Eq. (10) can be expressed in terms of z. We also assume that the population number density $p>0$ cannot attain values above some value p_{max}, the so-called saturation density. Then, defining $n(p)=-p_z$ and assuming that $n(0)=n(p_{max})=0$ and $n>0$ in $(0,p_{max})$, differential equation (10) can be rewritten as

$$\left(D-c^2\frac{T}{2}\right)n\frac{\partial n}{\partial p} - cn + F\left(1+\frac{T}{2}F'\right) = 0. \tag{13}$$

Now, introducing an arbitrary function $g(p)$ such that $g(p)>0$ and $h(p)=-g'(p)>0$, we multiply Eq. (13) by $g(p)/n(p)$. Integrating the resulting expression by parts, we obtain

$$c\int_0^{p_{max}} g\,dp = \int_0^{p_{max}}\left[\left(D-\frac{T}{2}c^2\right)hn + \frac{g}{n}F\left(1+\frac{T}{2}F'\right)\right]dp. \tag{14}$$

Now, we can eliminate $n(p)$ from Eq. (14) applying that for any positive numbers r and s, it follows from $(r-s)^2 \geq 0$ that $(r+s)\geq 2\sqrt{rs}$. Let us assume that the condition

$$1+\frac{T}{2}F'(p)>0 \tag{15}$$

holds for all $p\in(0,p_{max})$. As $g(p)$, $h(p)$, $n(p)$, $F(p)$, and $(D-\frac{T}{2}c^2)$ are positive [7], we may choose $r\equiv(D-\frac{T}{2}c^2)hn$ and $s\equiv\frac{g}{n}F(1+\frac{T}{2}F')$ into $(r+s)\geq 2\sqrt{rs}$ and use Eq. (14) to get the following restriction:

$$\frac{c}{\sqrt{\left(D-\frac{T}{2}c^2\right)}} \geq \frac{2\int_0^{p_{max}}\sqrt{hgF\left(1+\frac{T}{2}F'\right)}\,dp}{\int_0^{p_{max}}g\,dp}. \tag{16}$$

Following the method in Ref. [8], Sec. 3.3, it is easy to show that there is a function g for which the equality holds. Then,

$$\frac{c}{\sqrt{\left(D-\frac{T}{2}c^2\right)}} = \max_g\left(\frac{2\int_0^{p_{max}}\sqrt{hgF\left(1+\frac{T}{2}F'\right)}\,dp}{\int_0^{p_{max}}g\,dp}\right). \tag{17}$$

In order to obtain the upper bound for the front speed we will use Jensen's inequality [9]

$$\frac{\int_0^{p_{max}}\mu(p)\sqrt{\alpha(p)}\,dp}{\int_0^{p_{max}}\mu(p)\,dp} \leq \sqrt{\frac{\int_0^{p_{max}}\mu(p)\alpha(p)\,dp}{\int_0^{p_{max}}\mu(p)\,dp}}, \tag{18}$$

where $\mu(p)>0$ and $\alpha(p)\geq 0$. We define $\mu(p)\equiv g(p)$ and $\alpha(p)\equiv\{h(p)F(p)[1+\frac{T}{2}F'(p)]\}/g(p)$. Using these functions into Jensen's inequality (18), and applying the result to Eq. (17), we obtain that

$$\frac{c}{\sqrt{\left(D-\frac{T}{2}c^2\right)}} \leq 2\max_g\sqrt{\frac{\int_0^{p_{max}}hF\left(1+\frac{T}{2}F'\right)dp}{\int_0^{p_{max}}g\,dp}}. \tag{19}$$

We want an upper bound independent of $g(p)$, so we will first find an expression in which $h(p)=-g'(p)$ no longer appears by integrating by parts the numerator in the right-hand side of Eq. (19),

$$\int_0^{p_{max}} hF\left(1 + \frac{T}{2}F'\right)dp = \int_0^{p_{max}} g\left[F'\left(1 + \frac{T}{2}F'\right) + \frac{T}{2}FF''\right]dp, \tag{20}$$

where we have assumed that $F(0)=F(p_{max})=0$ (this holds, for example, for the logistic growth considered in Sec. III).

Moreover, from Eq. (20) we obviously have

$$\int_0^{p_{max}} hF\left(1 + \frac{T}{2}F'\right)dp \leq \sup_{p \in (0,p_{max})}\left[F'\left(1 + \frac{T}{2}F'\right) + \frac{T}{2}FF''\right]\int_0^{p_{max}} g\,dp, \tag{21}$$

so now the upper bound in Eq. (19) is independent of $g(p)$,

$$\frac{c}{\sqrt{\left(D - \frac{T}{2}c^2\right)}} \leq 2\sqrt{\sup_{p \in (0,p_{max})}\left[F'\left(1 + \frac{T}{2}F'\right) + \frac{T}{2}FF''\right]}. \tag{22}$$

Let us assume that the population growth function $F(p)$ is a continuous function with $F''(p) \leq 0$ and $F(0)=0$ (again these assumptions are true for the logistic growth considered in Sec. III). Then $F'(p)$ is a decreasing function for increasing value of p. Its maximum value is reached for $p=0$. Thus, using the value $p=0$ in Eq. (22) we obtain that the upper bound for the front speed is

$$c \leq \frac{2\sqrt{DF'(0)\left[1 + \frac{T}{2}F'(0)\right]}}{1 + TF'(0)}. \tag{23}$$

As the lower bound given by Eq. (8) is the same as upper bound (23), we can predict the speed of front solutions to Eq. (10) without any uncertainty,

$$c = \frac{2\sqrt{DF'(0)\left[1 + \frac{T}{2}F'(0)\right]}}{1 + TF'(0)}. \tag{24}$$

In contrast, for the HRD Eq. (11), the exact speed was previously shown to be [5]

$$c_{HRD} = \frac{2\sqrt{DF'(0)}}{1 + \frac{T}{2}F'(0)}. \tag{25}$$

III. APPLICATION TO THE NEOLITHIC TRANSITION

In order to compare the predictions from Eqs. (24) and (25), we will apply them to the spread of the Neolithic transition in Europe, because this is the case to which Eq. (25) was initially applied [5]. The Neolithic transition is the change from hunter-gatherer to farming economics. In Europe, it took place as an invasion of agricultural populations from the Southeast, which spread across Europe from 13 000 to 5000 years before present [10].
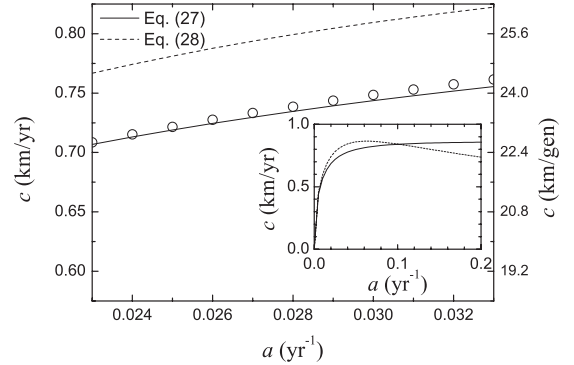

FIG. 1. Comparative plot between the front speed for Eq. (27) (solid line) and Eq. (28) (dashed line). The symbols correspond to the speed obtained from numerically integrating Eq. (10), with $F(p)$ given by Eq. (26). All results have been calculated for a characteristic mobility value $\langle\Delta^2\rangle = 1531$ km^2.

In order to make quantitative predictions we will use the logistic growth function, which has been widely applied to human populations [5,11]:

$$F(p) = ap\left(1 - \frac{p}{p_{max}}\right), \tag{26}$$

where a is called the initial growth rate and p_{max} is the saturation density.

Using logistic function (26), Eq. (24) can be rewritten as

$$c = \frac{2\sqrt{aD\left(1 + \frac{aT}{2}\right)}}{1 + aT}, \tag{27}$$

whereas the HRD speed (25), used in Ref. [5], is

$$c_{HRD} = \frac{2\sqrt{aD}}{1 + \frac{aT}{2}}. \tag{28}$$

Both equations for the front speed depend on three parameters: the initial growth rate, a, the diffusion coefficient, $D = \frac{\langle\Delta^2\rangle}{4T}$, and the generation time, T. We will use the ranges $a = 0.028 \pm 0.005$ yr^{-1} [12], $\langle\Delta^2\rangle = 900$–2200 km^2 [10], and the characteristic value $T=32$ yr [13], which have been measured for preindustrial farming populations. For these ranges, condition (15) is fulfilled, so Eq. (27) gives the speed of fronts.

Figure 1 shows the front speeds obtained from Eqs. (27) and (28) for a characteristic mobility value $\langle\Delta^2\rangle = 1531$ km^2. We can see that, for the range of values for the initial growth rate a appropriate to this application, the new Eq. (27) yields slower speeds than Eq. (28) (about 8% slower). However, this is not the case for all values of a, as can be seen from the inset graph in Fig. 1.

In order to check the validity of Eq. (27), we have also numerically integrated Eq. (10), with $F(p)$ given by Eq. (26), and initially $p=p_{max}$ in a finite region and $p=0$ elsewhere.
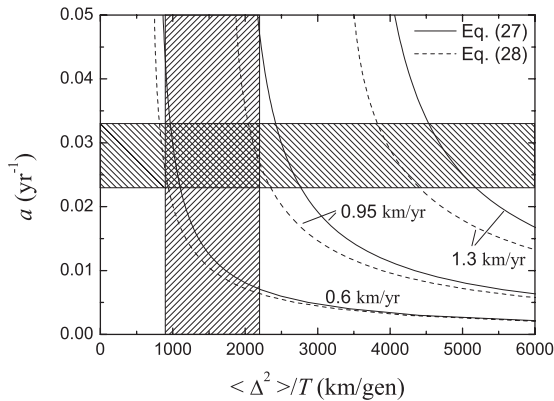
FIG. 2. Predictions for the speed of the wave of advance in the Neolithic transition. The labeled curves correspond to the maximum, minimum, and mean speeds from Neolithic data (0.6–1.3 km/yr). The hatched regions correspond to realistic ranges of the initial growth rate and mobility for the Neolithic transition.

The speed obtained from the numerical integrations corresponds to the circles in Fig. 1. They agree with the new Eq. (27) within less than 0.8%.

The range of speeds for the Neolithic transition front obtained from archeological data is 0.6–1.3 km/yr [10]. We can see in Fig. 1 that the results from Eq. (27) lie within this range.

To what extent does our result depend on the uncertainty in the value of the mobility? In Fig. 2, we consider the front speed values 0.6, 0.95, and 1.3 km/yr, corresponding to the range obtained from archeological data, for Eq. (27) (full lines) and Eq. (28) (dashed lines) [14]. It is seen that the predictions of the new model (full lines) are consistent with the observed front speed for most of the values of the mobility appropriate to this system.

IV. CONCLUDING REMARKS

In this Brief Report we have improved the derivation of the HRD speed in Ref. [5]. We have obtained the correct evolution Eq. (10) and the new Eq. (24) for the front speed.

We have applied the new Eq. (24) to the Neolithic transition. Using realistic parameters the front speeds are consistent with the observed range for the Neolithic transition in Europe (0.6–1.3 km/yr [10]). Comparing these results with those from the HRD speed, we see that for the Neolithic transition our new equation leads to slower speeds.

In this case, the correction obtained is only about 10%, but it could be higher in other systems where generalizations of Eq. (24) can be useful. For example, our framework could be applied in order to improve the predicted speeds of viral infection fronts [2].

[1] K. Davison, P. Dolukhanov, G. R. Sarson, and A. Shukurov, J. Archaeol. Sci. **33**, 641 (2006).

[2] J. Fort and V. Méndez, Phys. Rev. Lett. **89**, 178101 (2002).

[3] L. Gálfi and Z. Rácz, Phys. Rev. A **38**, 3151 (1988).

[4] J. Merikoski, J. Maunuksela, M. Myllys, J. Timonen, and M. J. Alava, Phys. Rev. Lett. **90**, 024501 (2003).

[5] J. Fort and V. Méndez, Phys. Rev. Lett. **82**, 867 (1999).

[6] R. D. Benguria and M. C. Depassier, Phys. Rev. E **57**, 6493 (1998).

[7] The condition $(D - Tc^2/2) > 0$ follows from $\lambda < 0$ and Eq. (7).

[8] J. Fort and V. Méndez, Rep. Prog. Phys. **65**, 895 (2002).

[9] S. Gradshteyn and I. M. Ryzhik, *Table of Integrals, Series and Products* (Academic, San Diego, 1994); see p. 1133 formula HL151. The inequality is given for convex functions ϕ. If ϕ is a convex function, then $-\phi$ is concave and the inequality for $-\phi$ holds with the sign reversed. Take the function $-\phi$ to be the square root.

[10] R. Pinhasi, J. Fort, and A. J. Ammerman, PLoS Biol. **3**, e410 (2005); for the estimation of mobility data see supporting text 3.

[11] J. D. Murray, *Mathematical Biology*, 3rd ed. (Springer-Verlag, Berlin, 2002), Vol. 1.

[12] N. Isern, J. Fort, and J. Pérez-Losada, J. Stat. Mech.: Theory Exp. (2008) P10012.

[13] J. Fort, D. Jana, and J. Humet, Phys. Rev. E **70**, 031913 (2004); for the estimation of the generation time $T = 32$ yr, see note [24] in this reference.

[14] The dashed lines in Fig. 2 are not exactly the same as the lines in Fig. 3 in Ref. [5] because some parameter values have been estimated in a more precise way more recently especially the generation time T [13].

Anisotropic dispersion, space competition and the slowdown of the Neolithic transition

Neus Isern[1] and Joaquim Fort[1]

Complex Systems Lab, Departament de Física, Universitat de Girona,
17071 Girona, Catalonia, Spain
E-mail: neus.isern@udg.edu and joaquim.fort@udg.edu

Abstract. The front speed of the Neolithic (farmer) spread in Europe decreased as it reached Northern latitudes, where the Mesolithic (hunter-gatherer) population density was higher. Here, we describe a reaction–diffusion model with (i) an anisotropic dispersion kernel depending on the Mesolithic population density gradient and (ii) a modified population growth equation. Both effects are related to the space available for the Neolithic population. The model is able to explain the slowdown of the Neolithic front as observed from archaeological data.

Contents

[1] Authors to whom any correspondence should be addressed.

1. Introduction

The spread of the Neolithic, one of the most important socioeconomic changes in human history, has been widely studied using physical models in recent years (for a review, see [1]). The Neolithic expansion has been tackled from different approaches such as age-structured population models [2], population spread along rivers [3] and settlement formation [4].

Here, we will focus on the fact that the spread of the Neolithic in Europe was not homogeneous from the macroscopic point of view. Archaeological observations show that, as the front propagated from the Near East across Europe, its speed slowed down as higher latitudes were reached [5].

This decrease of the front speed can be intuitively seen from figure 1, which shows the arrival time of the Neolithic across Europe. The arrow on the map represents the average direction along which the expansion from the Near East to the Baltic Sea took place (within the rectangle). In figure 1, it can be seen that the distance advanced during 500 years is lower on reaching northern latitudes (a quantitative analysis will be presented in section 5).

Although it would seem that the more intuitive reason for the decrease in speed is the time needed by crops to adapt to temperate climates, evidence exists that this effect was, in fact, minimal [6]. Indeed, when establishing their settlements in colder regions, Neolithic populations just cultivated the more adaptable crops and dropped the rest.

From archaeological studies, one of the most accepted reasons for the presence of a gradient in the front speed when spreading to the North of Europe is the presence of Mesolithic hunter-gatherer populations [7], which had higher densities at Northern latitudes. Thus, motivated by the observational data, in this paper we extend a homogeneous model [8] to study how the presence of indigenous Mesolithic populations affects the speed of the Neolithic invasion front.

We describe a reaction–diffusion model for Neolithic population density with a direction-dependent dispersion kernel determined by the space dependence of the Mesolithic population density. We also introduce in this model the effect of the presence of Mesolithic populations on the Neolithic population growth process. We compare the results from the model with archaeological data [9].

2. Anisotropic dispersion kernel

In the case we assumed that the spread of the Neolithic front took place in a homogeneous space, it would be reasonable to consider that the probability ϕ to jump would be the same in all directions; thus, mathematically we would have [8, 10]

$$\phi(x, y; \theta, \Delta) = \frac{1}{2\pi}\psi(\Delta), \tag{1}$$

that is, the jump probability could be expressed as a function ψ that depends only on the jump distance, Δ, and is independent of the jump direction θ or the position in space (x, y). We have assumed that $\int_0^\infty \Delta\psi(\Delta)\mathrm{d}\Delta = 1$.

However, Neolithic individuals do not move in a homogeneous space, since the density of Mesolithic individuals they encounter depends on the position and direction they move. Then, for a given position (x, y), the Neolithic individuals will preferably move in the direction along which they encounter a lower Mesolithic population density, i.e. along the direction where more free space is available.
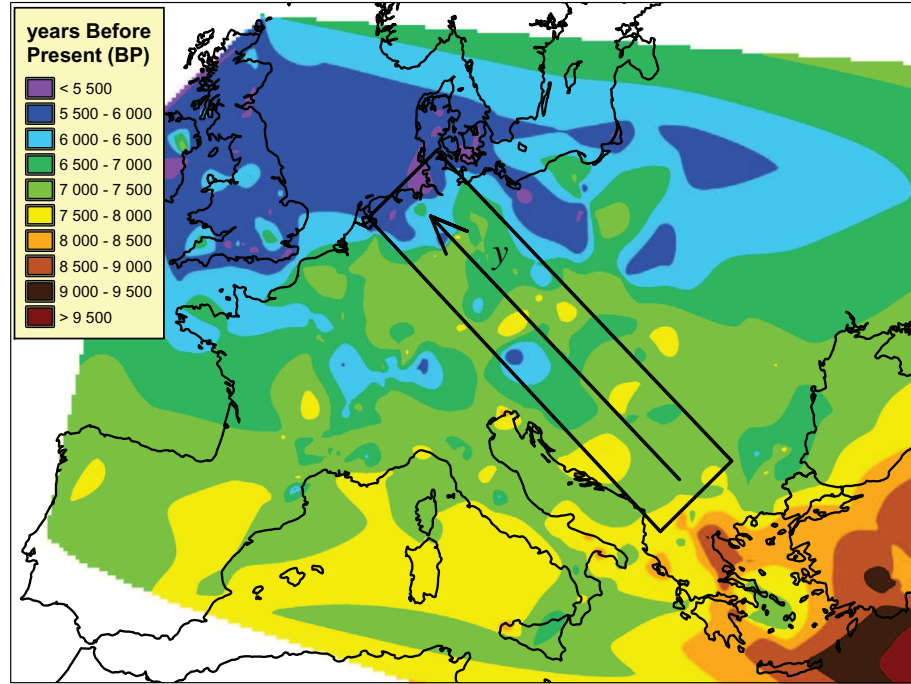
Figure 1. Chronology of the Neolithic wave of advance in Europe. Map obtained by interpolation of 765 early Neolithic data published by Pinhasi [9]. The arrow corresponds to the y-direction in our model.

Thus, we can assume that, in this situation, the jump distance probability distribution (1) will be modulated by the available space, s, at the final jump point $(x + \Delta_x, y + \Delta_y)$, in each direction $\theta = \tan^{-1}(\Delta_y / \Delta_x)$ and for every jump distance $\Delta = \sqrt{\Delta_x^2 + \Delta_x^2}$. Thus, the dispersion kernel is now of the form

$$\phi(x, y; \theta, \Delta) = \alpha s(x + \Delta_x, y + \Delta_y)\psi(\Delta), \tag{2}$$

where α is a normalization constant.

We now need a mathematical expression for the available space $s(x + \Delta_x, y + \Delta_y)$. If $M_{\max}$ is the carrying capacity for Mesolithic populations and $M(x, y)$ the actual density of Mesolithic individuals at the position (x, y), then the fraction of occupied space at this point can be expressed as

$$m(x, y) = \frac{M(x, y)}{M_{\max}}. \tag{3}$$

Thus, the fraction of space available for Neolithic settlements is

$$s(x + \Delta_x, y + \Delta_y) = 1 - m(x + \Delta_x, y + \Delta_y) \tag{4}$$

and the space-dependent jump distance probability (2) can be written as

$$\phi(x, y; \theta, \Delta) = \alpha[1 - m(x + \Delta_x, y + \Delta_y)]\psi(\Delta). \tag{5}$$

For simplicity, we assume that the variation in Mesolithic population density takes place mainly in one direction, y, in figure 1, whereas it remains approximately constant along the x-direction, i.e.

$$\phi(x, y; \theta, \Delta) = \alpha[1 - m(y + \Delta_y)]\psi(\Delta). \tag{6}$$

Now, Taylor-expanding the term within square brackets in equation (6), we obtain that the space-dependent jump distance probability is approximately

$$\phi(x, y; \theta, \Delta) = \alpha \left[1 - m(y) - \frac{\partial m}{\partial y} \Delta \sin \theta \right] \psi(\Delta). \tag{7}$$

Normalizing equation (7), we obtain that the normalization constant α is

$$\alpha = \frac{1}{2\pi} \frac{1}{1 - m(y)}, \tag{8}$$

and the jump distance probability becomes

$$\phi(x, y; \theta, \Delta) = \frac{1}{2\pi} \left[1 - \frac{\partial m/\partial y}{1 - m(y)} \Delta \sin \theta \right] \psi(\Delta). \tag{9}$$

We can see from equation (9) that if the Mesolithic (indigenous) population density M increases along the direction y, then the probability of Neolithic invaders to jump forward ($\theta = \pi/2$) is minimum and the probability to jump backwards ($\theta = 3\pi/2$) is maximum.

3. Population growth

In population dynamics, a commonly used expression to describe the first-order variation in population density due to population growth (reproduction minus deaths) is the logistic growth equation [8, 11, 12],

$$F(N) = \left. \frac{\partial N}{\partial t} \right|_g = aN \left(1 - \frac{N}{N_{\text{max}}} \right), \tag{10}$$

where a is the initial growth rate, N_{max} the carrying capacity and N the density of the Neolithic population. The subindex g stands for population growth, i.e. for variations in population density N due to births and deaths (but not to dispersal).

The logistic equation (10) describes an exponential growth for low values of population density, whereas it is self-limiting for large densities, saturating at N_{max}. Note that the limiting term (within brackets) in equation (10) is similar to expression (4) for the available space that we have used in the previous section. Therefore, one can say that population growth, according to equation (10), is limited by the fraction of available space [12].

Now, equation (10) corresponds to a single population reproducing without external competition. But when we have a second population using the same space and resources, the presence of this additional population must also contribute to limiting the growth process. Thus, we can modify equation (10) so that the growth function of the Neolithic population, N, also includes the effect of the fraction of space occupied by Mesolithic populations, M [12]. A population density M occupies a fraction M/M_{max} of the space available, in addition to

that occupied by N. Therefore, N within parentheses in equation (10) should be replaced by $(N + (M/M_{max})N_{max})$. Then,

$$F(N) = aN \left(1 - \frac{N}{N_{max}} - \frac{M}{M_{max}} \right). \tag{11}$$

Growth functions similar to (11) have been applied to competing micro-organisms [12].

4. Evolution equation

We can describe the variation in the Neolithic population density N, during a generation time T, as the sum of the variations due to the dispersion process and due to population growth (see [8] for details),

$$N(x, y, t+T) - N(x, y, t)$$
$$= \iint N(x - \Delta_x, y - \Delta_y, t)\phi(x, y; \theta, \Delta) \mathrm{d}\Delta_x \, \mathrm{d}\Delta_y - N(x, y, t)$$
$$+ [N(x, y, t+T) - N(x, y, t)]_g, \tag{12}$$

where, as in equation (10), the subindex g stands for population growth (as opposed to dispersal, which corresponds to the first two terms on the right-hand side).

Now, if we Taylor-expand equation (12) up to first order in time and to second order in space, we find that

$$\frac{\partial N}{\partial t} = -U_x \frac{\partial N}{\partial x} - U_y \frac{\partial N}{\partial y} + U_{xy} \frac{\partial^2 N}{\partial x \partial y} + D_x \frac{\partial^2 N}{\partial x^2} + D_y \frac{\partial^2 N}{\partial y^2} + F(N). \tag{13}$$

We could also have Taylor-expanded equation (12) up to second order in time [8], finding in this case slightly lower speeds; however, the conclusions we find here would not change.

The direction-dependent diffusion coefficients D_x and D_y, for our kernel (9), are

$$D_x = \frac{\langle \Delta_x^2 \rangle}{2T} = \frac{\langle \Delta^2 \rangle}{4T} \equiv D, \tag{14}$$

$$D_y = \frac{\langle \Delta_y^2 \rangle}{2T} = \frac{\langle \Delta^2 \rangle}{4T} \equiv D, \tag{15}$$

where T is the generation time, and the mean value of a variable, for example $\langle \Delta_x^2 \rangle$, is defined as

$$\langle \Delta_x^2 \rangle = \int_{-\infty}^{\infty} \int_{-\infty}^{\infty} \Delta_x^2 \phi(\Delta_x, \Delta_y) \mathrm{d}\Delta_x \, \mathrm{d}\Delta_y. \tag{16}$$

The advection terms U_x, U_y and U_{xy}, using the kernel (9), are

$$U_x = \frac{\langle \Delta_x \rangle}{T} = 0, \tag{17}$$

$$U_y = \frac{\langle \Delta_y \rangle}{T} = -2D \frac{\partial m/\partial y}{1 - m(y)}, \tag{18}$$

$$U_{xy} = \frac{\langle \Delta_x \Delta_y \rangle}{T} = 0. \tag{19}$$

As could be expected from the fact that the jump probability distribution (9) depends only on $\Delta_y = \Delta \sin \theta$ but not on Δ_x, we have obtained advection only in the y-direction, equation (18).

5. Front speed

As usual, we apply that for $t \to \infty$ the front can be considered locally planar; thus for $y \to \infty$ we can consider the variation in the x-direction negligible [13], and the evolution equation (13) for $y \to \infty$ becomes

$$\frac{\partial N}{\partial t} = 2D \frac{\partial m / \partial y}{1 - m(y)} \frac{\partial N}{\partial y} + D \frac{\partial^2 N}{\partial y^2} + F(N), \tag{20}$$

where we will use equation (11) for the growth function $F(N)$.

As usual [13], we look for constant-shaped solutions to equation (20) with the form $N = N_0 \exp[-\lambda(y - ct)]$ for $N \simeq 0$. As the Neolithic population density N at the leading edge of the front is low, $F(N)$ in equation (11) can be linearized, and we obtain from equation (20)

$$\lambda = \frac{(c - U_y) \pm \sqrt{(c - U_y)^2 - 4aD(1 - m)}}{2D}. \tag{21}$$

In order for λ to be real, the term within the square-root must be non-negative, so the front speed c is

$$c = 2\sqrt{aD}\sqrt{1 - m(y)} - 2D \frac{\partial m / \partial y}{1 - m(y)}. \tag{22}$$

Equation (22) can be also obtained, without the need for equation (21), by noting that equation (20) is simply Fisher's equation with (i) a modified growth term (11), which after linearization leads to a modified initial growth rate $\tilde{a} = a(1 - m(y))$, and (ii) an advection velocity $v = 2D \frac{\partial m / \partial y}{1 - m(y)}$. Thus, the speed of front solutions to equation (20) must be Fisher's, namely $2\sqrt{\tilde{a}D}$, minus the advection velocity, in agreement with equation (22). Moreover, the front speed obtained from the linear analysis described above is a lower bound to the front speed c. However, it is easy to apply variational analysis [14] and derive an upper bound with the same result, so equation (22) is the exact front speed for equation (20).

From equation (22), we see that if the Mesolithic population density increases with y, then the front speed decreases because of two effects: (i) the higher the gradient of the reduced Mesolithic density m, the higher the correction on the front speed; (ii) the speed also changes if there is less available space for the Neolithic population, i.e. for lower values of $s = (1 - m(y))$ (if $s = 1$, this second effect disappears).

To see the actual behavior of the front speed, equation (22), we need an expression for the variation of the Mesolithic population density M with y. However, the precise function $M(y)$ is unknown because published data on Mesolithic settlements are scarce and restricted to very specific local areas, and also because the estimation of population densities from archaeological data relies on assumptions that are difficult to test and cause important methodological problems [15]. However, as explained in the introduction, we do know that the Mesolithic
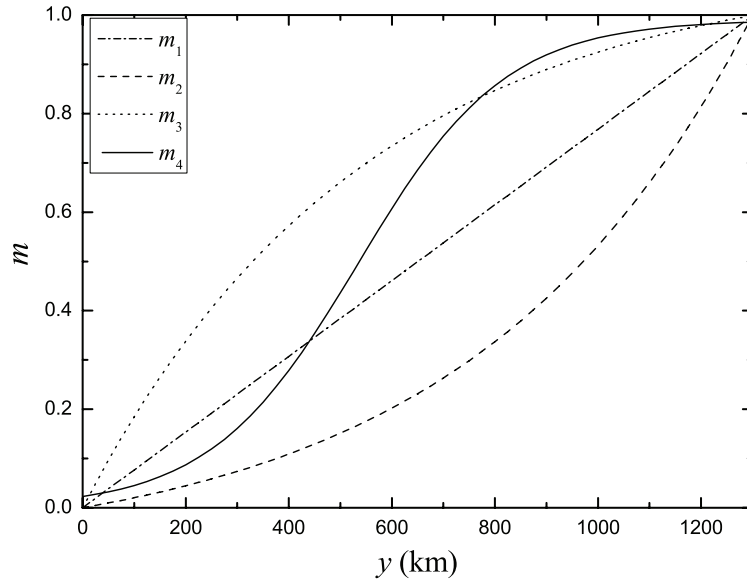
IOP Institute of Physics Φ DEUTSCHE PHYSIKALISCHE GESELLSCHAFT

Figure 2. Test functions used for the increase of the reduced Mesolithic population density ($m = M/M_{max}$) along the y-direction. $A_1 = 0.999/1300$, $B_1 = 0$; $A_2 = -0.1 = -B_2 = A_3 = B_3$, $\tau_2 = -\ln(10.99)/1300 = -\tau_3$; $A_4 = 0.99$, $B_4 = 42$, $\tau_4 = 1/0.007$.

density did increase at northern latitudes [7]. Thus, we apply equation (22) to four different test functions for the reduced Mesolithic density $m(y) = M(y)/M_{max}$ (see figure 2),

$$m_1 = A_1 y + B_1,$$
$$m_2 = A_2 + B_2 \exp(y/\tau_2),$$
$$m_3 = A_3 - B_3 \exp(-y/\tau_3), \tag{23}$$
$$m_4 = \frac{A_4}{1 + B_4 \exp(-y/\tau_4)}.$$

To estimate the anthropological parameters a and D appearing in equation (22), we apply that the initial growth rate for preindustrial populations has a mean value of $a = 0.028\,\text{year}^{-1}$ [10], the mean-squared jump distance is $\langle \Delta^2 \rangle = 1531\,\text{km}^2$ [8] and the mean generation time is $T = 32$ years [16][2]

As we expected from equation (22), we see in figure 3 that each of the four test functions leads to a decrease in the front speed along the y-direction. To better compare the results with archaeological data, in figure 3 we have plotted c/c_{max}, where the maximum speed from equation (22) is given by Fisher's value [11],

$$c_{max} = 2\sqrt{aD}. \tag{24}$$

In fact, this should be corrected due to a time-delay effect [8]. This would further complicate our equations, so we will not include this effect because, rather than comparing to the absolute

---

[2] For the estimation of the generation time $T = 32$ years, see note [24] in this reference.
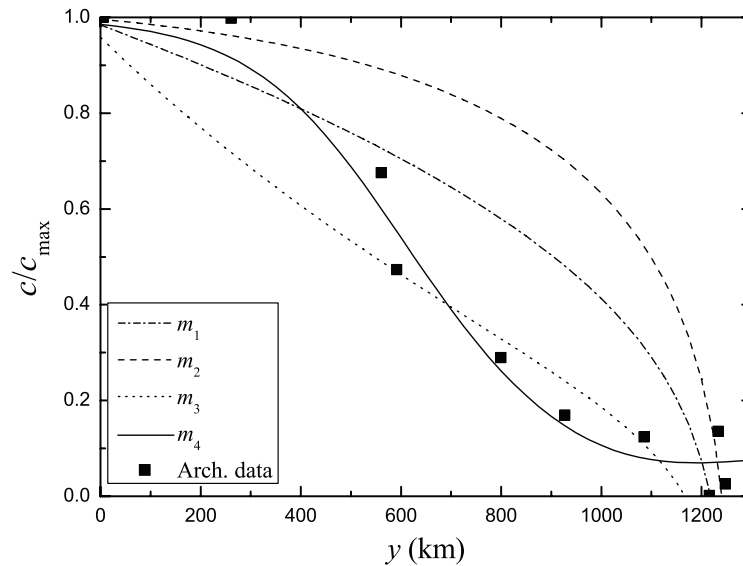
Figure 3. Curves: relative Neolithic front speed predicted by a model with the dispersion and growth processes dependent on the presence of Mesolithic populations, equation (25). Symbols: observed front speeds calculated from archaeological data [9].

value of the maximum front speed (which we already analyzed in [8]), here we are interested in focusing our attention on the slowdown effect. This is simpler by considering the relative speed from equation (22),

$$\frac{c}{c_{max}} = \sqrt{1 - m(y)} - \sqrt{\frac{D}{a}} \frac{\partial m/\partial y}{1 - m(y)}. \tag{25}$$

In figure 3 we compare the results obtained from equation (25) (curves) with Neolithic front speed data (symbols). The latter was obtained by computing the areas within isochrones separated 250 years inside the rectangle in figure 1 (such isochrones are shown in figure 1 every 500 years for clarity)[3].

Comparing the results from equation (25) to those from archaeological data in figure 3, we see that, even though none of the four test functions reproduce exactly the behavior of the archaeological data (which is not surprising for such a complex phenomenon), they do give a good approximation to the general behavior (especially m_4). Thus, a simple physical model can explain qualitatively the decrease in the front speed during the Neolithic expansion range in Europe. Therefore, physical models are useful to explain not only the average Neolithic front speed [8], but also its gradual slowdown in space.

The reaction–diffusion model presented in this paper could be applied to many examples of invasion fronts in which the indigenous population and the invasive one compete for space in a single biological niche, both in natural habitats [17, 18] and in microbiological assays [12, 19].

---

[3] In figure 3, we compare only the speed data calculated for latitudes above 45°, since for lower latitudes there is an important effect due to sea travel. The sites and dates used in our interpolations are those in [9].

IOP Institute of Physics ⦿ DEUTSCHE PHYSIKALISCHE GESELLSCHAFT

Acknowledgments

References

 [1] Steele J 2009 *Hum. Biol.* **81** 121
 [2] Vlad M O and Ross J 2002 *Phys. Rev.* E **66** 061908
 [3] Davison K, Dolukhanov P, Sarson G R and Shukurov A 2006 *J. Archaeol. Sci.* **33** 641
 [4] Fedotov S, Moss D and Campos D 2007 *Phys. Rev.* E **78** 026107
 [5] Ammerman A J 2003 *The Widening Harvest. The Neolithic Transition in Europe: Looking Back. Looking Forward* ed A J Ammerman and P Biagi (Boston, MA: Archaeological Institute of America) p 21
 [6] Coward F, Shennan S, Colledge S, Conolly J and Collard M 2008 *J. Archaeol. Sci.* **35** 42
 [7] Price T D 2003 *The Widening Harvest. The Neolithic Transition in Europe: Looking Back. Looking Forward* ed A J Ammerman and P Biagi (Boston, MA: Archaeological Institute of America) p 280
 [8] Fort J and Méndez V 1999 *Phys. Rev. Lett.* **82** 867
 [9] Pinhasi R, Fort J and Ammerman A J 2005 *PLoS Biol.* **3** 2220
[10] Isern N, Fort J and Pérez-Losada J 2008 *J. Stat. Mech.: Theor. Exp.* P10012
[11] Murray J D 2002 *Mathematical Biology* 3rd edn vol 1 (Berlin: Springer)
[12] Gause G F 1934 *The Struggle for Existence* (Baltimore, MA: Williams and Wilkins)
[13] Fort J and Pujol T 2008 *Rep. Prog. Phys.* **71** 086001
[14] Méndez V, Fort J and Farjas J 1999 *Phys. Rev.* E **60** 5231
[15] Zimmermann A, Hilpert J and Wendt K P 2009 *Hum. Biol.* **81** 357
[16] Fort J, Jana D and Humet J 2004 *Phys. Rev.* E **70** 031913
[17] Reynolds J C 1985 *J. Anim. Ecol.* **54** 149
[18] Shigesada N and Kawasaki K 1997 *Biological Invasions: Theory and Practice* (Oxford: Oxford University Press)
[19] Kloster M 2005 *Phys. Rev. Lett.* **95** 168701

Bibliography

[1] Smith BD. The Emergence of agriculture. New York: Scientific American Library; 1995.

[2] Childe VG. The Dawn of European Civilization. London: Kegan, Paul, Trench & Trubner; 1925.

[3] Childe VG What happened in history. Harmondsworth (UK): Penguinbooks; 1942.

[4] Clark JGD. Radiocarbon dating and the spread of farming economy. Antiquity 1965; 39: 45–48

[5] Clark JGD. Radiocarbon dating and the expansion of farming culture from Near East over Europe. Proc Prehist Soc 1965; 31: 58–73.

[6] Ammerman AJ, Cavalli-Sforza LL. Measuring the rate of spread of early farming in Europe. Man (NS) 1971; 6: 674–688.

[7] Fort J, Méndez V. Time-delayed theory of the Neolithic transition in Europe. Phys Rev Lett 1999; 82: 867–870.

[8] Gkiasta M, Russell T, Shennan S, Steele J. Neolithic transition in Europe: the radiocarbon record revisited. Antiquity 2003; 77: 45–62.

[9] Pinhasi R, Fort J, Ammerman AJ. Tracing the origin and spread of agriculture in Europe. PLoS Biol 2005; 3: e410.

[10] Ammerman AJ, Cavalli-Sforza LL. A population model for the diffusion of early farming in Europe. In: Renfrew C, editor. The explanation of culture change. London: Duckworth; 1973. p. 343–357.

[11] Fort J, Jana D, Humet J. Multidelayed random walks: theory and application to the Neolithic transition in Europe. Phys Rev E 2004; 70: 031913.

[12] Davison K, Dolukhanov P, Sarson GR, Shukurov A. The role of waterways in the spread of the Neolithic. J Archaeol Sci 2006; 33: 641–652.

[13] Fort J, Pérez-Losada J, Isern N. Fronts from integrodifference equations and persistence effects on the Neolithic transition. Phys Rev E 2007; 76: 031913.

[14] Fort J, Pérez-Losada J, Suñol JJ, Escoda L, Massaneda JM. Integro-difference equations for interacting species and the Neolithic transition. New J Phys 2008; 10: 43045.

[15] Fedotov S, Moss D, Campos D. Stochastic model for population migration and the growth of human settlements during the Neolithic transition. Phys Rev E 2008; 78: 026107.

[16] Patterson MA, Sarson GR, Sarson HC, Shukurov A. Modelling the Neolithic transition in a heterogeneous environment. J Archaeol Sci 2010; 37: 2929–2937.

[17] Ammerman AJ, Cavalli-Sforza LL . The Neolithic transition and the genetics of populations in Europe. Princeton, NJ: Princeton University Press; 1984.

[18] Fisher RA. The wave of advance of advantageous genes. Ann Eugen 1937; 7: 355–369.

[19] Skellam JG. Random dispersal in theoretical populations. Biometrika 1951; 38: 196–218.

[20] Kolmogorov A, Petrovsky I, Piscounoff N. A study of the diffusion equation with increase in the quantity of matter, and its application to a biological problem. Moscow Univ Bull Math 1937; 1: 1-25.

[21] Murray JD. Mathematical Biology. 3rd ed. Berlin: Springer-Verlag; 2002.

[22] Birdsell JB. Some population problems involving Pleistocene man. Cold Spring Harb Symp Quant Biol 1957; 22: 47-69.

[23] Roberts DF. Genetic effects of population size reduction. Nature 1968; 220: 1084-1088.

[24] Lotka AJ. Elements of mathematical biology. New York: Dover; 1956. p. 64-69.

[25] Fort J, Pujol T, Cavalli-Sforza LL. Palaeolithic populations waves of advance. Camb Archaeol J 2004; 14: 53-61

[26] Stauder J. The Majangir: Ecology and Society of a Southwest Ethiopian People. Cambridge: Cambridge University Press; 1971.

[27] Cavalli-Sforza LL, Bodmer WF. The Genetics of human populations. New York: Dover; 1999.

[28] MacDonald D, Hewlett B. Reproductive Interests and Forager Mobility. Curr Anthropol 1999; 40: 501-524.

[29] Sellen D, Mace R. Fertility and Mode of Subsistence: A Phylogenetic Analysis. Curr Anthropol 1997; 38: 878-889.

[30] Fort J, Méndez V. Wavefronts in time-delayed reaction-diffusion systems. Theory and comparison to experiment. Rep Prog Phys 2002; 65: 895-954.

[31] Benguria RD, Depassier MC. Speed of fronts of generalized reaction-diffusion equations. Phys Rev E 1998; 57: 6493-6496.

[32] Méndez V, Fort J, Farjas J. Speed of wave-front solutions to hyperbolic reaction-diffusion equations. Phys Rev E 1999; 60: 5231-5243.

[33] Press WH, Teukolsky SA, Vetterling WT, Flannery BP. FORTRAN numerical recipes. 2nd ed. Cambridge (UK): Cambridge University Press; 1992.

[34] Davison, K. The Neolithic of Europe: Mathematical Modelling and Radiocarbon Data [PhD thesis]. Newcastle (UK): Newcastle University; 2008.

[35] van Saarloos W. Front propagation into unstable states. Phys Rep 2003; 386: 29-222.

[36] Fort J. Fronts from complex two-dimensional dispersal kernels: Theory and application to Reid's paradox. J Appl Phys 2007; 101: 094701.

[37] Méndez V, Pujol T, Fort J. Dispersal probability distributions and the wave-front speed problem. Phys Rev E 2002; 65: 041109.

[38] Fort J, Pujol T. Time-delayed fronts from biased random walks. New J Phys 2007; 9: 234.

[39] Vlad MO, Ross J. Systematic derivation of reaction-diffusion equations with distributed delays and relations to fractional reaction-diffusion equations and hyperbolic transport equations: Application to the theory of Neolithic transition. Phys Rev E 2002; 66: 061908.

[40] Méndez V, Ortega-Cejas V, Campos D. Front propagation in population dynamics with dispersive variability and delayed growth. Physica A 2006; 367: 283-292.

[41] Fort J, Pujol T. Progress in front propagation research. Rep Prog Phys 2008; 71: 086001.

[42] Merikoski J, Maunuksela J, Myllys M, Timonen J, Alava MJ. Temporal and spatial persistence of combustion fronts in paper. Phys Rev Lett 2003; 90: 024501.

[43] Fort J, Méndez V. Time-delayed spread of viruses in growing plaques. Phys Rev Lett 2002; 89: 178101.

[44] Fedotov S, Iomin A. Migration and Proliferation Dichotomy in Tumor-Cell Invasion. Phys Rev Lett 2007; 98: 118101.

[45] Hamilton MJ, Buchanan B. Spatial gradients in Clovis-age radiocarbon dates across North America suggests rapid colonization from the north. Proc Natl Acad Sci 2007;104:15625-15630.

[46] Méndez V, Campos D, Fort J. Speed of travelling fronts: Two-dimensional and ballistic dispersal probability distributions. Europhys Lett 2004; 66: 902-908.

[47] Weseloh RM. Short and Long Range Dispersal in the Gypsy moth (Lepidoptera: Lymantriidae) Fungal Pathogen, Entomophaga maimaiga (Zygomycetes: Entomophthorales). Environ Entomol 2003; 32:111-122.

[48] Kot M, Mark A, Lewis P, van der Driessche P. Dispersal data and the spread of invading organisms. Ecology 1996 Oct. 1996; 77: 2027-2042.

[49] Clark JS. Why Trees Migrate So Fast: Confronting Theory with Dispersal Biology and the Paleorecord. Am Nat 1998; 152: 204-224.

[50] Fix AG. Migration and colonization in human microevolution. Cambridge, U.K.: Cambridge University Press; 1999.

[51] Brunet E, Derrida B. Shift in the velocity of a front due to a cutoff. Phys Rev E 1997; 56: 2597-2604.

[52] Currat M, Excoffier L. The effect of the Neolithic expansion on European molecular diversity. Proc R Soc B 2005; 272: 679-688.

[53] Harris S. Traveling waves with dispersive variability and time delay. Phys Rev E Stat Nonlin Soft Matter Phys 2003; 68: 031912.

[54] Gálfi L, Rácz Z. Properties of the reaction front in an $A + B \rightarrow C$ type reaction-diffusion process. Phys Rev A 1988; 38: 3151-3154.

[55] Gradshteyn IS, Ryzhik IM. Table of integrals, series and products. 5th ed. San Diego: Academic Press; 1994.

[56] Isern N, Fort J, Pérez-Losada, J. Realistic dispersion kernels applied to cohabitation reaction-dispersion equations. J Stat Mech - Theor Exp 2008; 2008: P10012.

[57] Steele J. Human dispersals: Mathematical models and the archaeological record. Hum Biol 2009; 81: 121-140.

[58] Ammerman AJ. Looking Back. In: Ammerman AJ, Biagi P, editors. The Widening harvest: the Neolithic transition in Europe : looking back, looking forward Boston: Archaeological Institute of America; 2003. p. 3-23.

[59] Coward F, Shennan S, Colledge S, Conolly J, Collard M. The spread of Neolithic plant economies from the Near East to northwest Europe: a phylogenetic analysis. J Archaeol Sci 2008; 35: 42-56.

[60] Price TD. The Arrival of Agriculture in Europe as Seen from the North. In: Ammerman AJ, Biagi P, editors. The Widening harvest: the Neolithic transition in Europe : looking back, looking forward Boston: Archaeological Institute of America; 2003. p. 273-294.

[61] Gause GF. The Struggle for Existence. Baltimore: The Williams & Wilkins Company; 1934.

[62] Zimmermann A, Hilpert J, Wendt KP. Estimations of Population Density for Selected Periods Between the Neolithic and AD 1800. Hum Biol 2009; 81: 357-380.

[63] Reynolds JC. Details of the Geographic Replacement of the Red Squirrel (Sciurus vulgaris) by the Grey Squirrel (Sciurus carolinensis) in Eastern England. J Anim Ecol 1985; 54: 149-162.

[64] Shigesada N, Kawasaki K. Biological invasions: theory and practice. Oxford: Oxford University; 1997.

[65] Kloster M. Analysis of Evolution through Competitive Selection. Phys Rev Lett 2005; 95: 168701.

[66] Isern N, Fort J. Anisotropic dispersion, space competition and the slowdown of the Neolithic transition. New J Phys 2010; 12: 123002.

[67] Fort J, Méndez V. Reaction-diffusion waves of advance in the transition to agricultural economics. Phys Rev E 1999; 60: 5894-5901.

[68] Steele J, Adams J, Sluckin T. Modelling Paleoindian dispersals. World Archeol 1998; 30: 286-305.